α-synuclein amyloid accumulation and its interaction with prion protein

Thesis submitted for the degree of "*Philosophiæ Doctor*"

in Functional and Structural Genomics

SISSA- International School for Advanced Studies

Candidate:

Suzana Aulić

Supervisor:

Prof. Giuseppe Legname

Academic year 2014-2015

"Beyond the horizon of the place we lived when we were young

In a world of magnets and miracles

Our thoughts strayed constantly and without boundary

The ringing of the division bell had begun…."

-Pink Floyd

α-Syn amyloid accumulation and its interaction with prion protein

AKNOWLEDGMENTS

I would like to thank my supervisor Prof. Giuseppe Legname for supporting me, and to express my deepest gratitude for his guidance, motivation, patience and for providing me with an excellent atmosphere for doing research. Especially, thanks for helping me to develop my background in cell biology and biochemistry, since it was a completely new field for me.

Besides my supervisor, special thanks go to Prof. Goedert and Prof. Zanusso, who were willing to participate in my final defense committee.

I would like to thank Joanna, Paola, Lara, Irene, and Maura who were always willing to help and give their best suggestions. Big thanks to all of Prion lab mates, the new ones and especially to those who left the lab, Gabriele and Lisa. I would also like to thank Kate, who patiently corrected my writing.

Last but not the least, I would also like to thank my mum and my sister. They were always supporting me and encouraging me with their best wishes. You two are the loves of my life!!!

Finally, I would like to thank my husband, Erik. He was always there cheering me up and stood by me through the good times and bad. Family is everything!

α-Syn amyloid accumulation and its interaction with prion protein

ABSTRACT

α-Synuclein (α-syn) plays a central role in the pathogenesis of neurodegenerative disorders collectively known as "synucleinopathies" that include Parkinson's disease (PD), dementia with Lewy bodies (DLB) and multiple system atrophy (MSA). Understanding the underlying molecular mechanisms of neurodegenerative diseases is indispensably important because of the prevalence of these devastating conditions in the elderly population. Several findings from cell culture and *in vivo* experiments suggest intercellular transfer of α-syn aggregates. The concept of intracellular α-syn pathology spread was recently extended by the discovery of propagation of α-syn aggregates throughout PD brains. The resulting concept of cell-to-cell propagation of α-syn pathology comprises of its release, uptake, and subsequently seeding of intracellular α-syn aggregation in recipient cells.

In this PhD thesis the methodology used to obtain synthetic mammalian prions has been used to obtain recombinant human and mouse α-syn amyloids in order to characterize whether synthetic material can promote prion-like accumulation of its soluble counterpart in neuronal cell lines *in vitro* and in wild type (WT) mice *in vivo*. To address these hypotheses, in the first part of the work the human neuroblastoma SH-SY5Y cell line and WT CD-1 mice were used. A single exposure to human α-syn amyloid fibrils was sufficient to induce aggregation of endogenous α-syn in SH-SY5Y cells. Remarkably, endogenous WT α-syn was sufficient for aggregate formation and overexpression of the protein was not required. Our results provide compelling evidence that endogenous α-syn can accumulate in cell culture after a single exposure to exogenous α-syn short amyloid fibrils. Importantly, using α-syn short amyloid fibrils as seed, endogenous α-syn aggregates and accumulates over several passages in cell culture. We further analyzed this phenomenon *in vivo* in WT CD-1 mice, where intracerebral inoculation of synthetic α-syn short amyloid fibrils induced the formation of phosphorylated α-syn aggregates in CNS regions distinct from the injection site.

After this observation, further studies were performed in order to understand the mechanism of internalization of α-syn amyloids. Indeed, while the function of the cellular prion protein (PrP^{C}) is still under debate, several reports indicate that PrP^{C} interacts with amyloid form proteins, Aβ oligomers and PrP scrapie (PrP^{Sc}) fibrils. In order to investigate

this, we used the same technique as in the first part of our study, working on mouse α-syn protein. Here, we explored the uptake of α-syn amyloids in a neuroblastoma cell line: N2a cells which endogenously express PrP^{C} (N2a), cells knocked out for PrP^{C} (N2a KO), N2a KO where the PrP^{C} was re-introduced using transfection protocol (N2a PrPFL), and scrapie infected N2a (ScN2a) cells. Our results show that the uptake of α-syn amyloids is lower in N2a KO compared to control cells (N2a), raising the possibility that PrP^{C} mediates the uptake of α-syn amyloids within cytoplasm of N2a cells. Subsequently, biochemical characterization of this putative interaction through the use of two distinct cross-link molecules has been investigated.

In the prion replication model, direct interaction between PrP^{Sc} and endogenous PrP^{C} is required for the formation of further infectious prions. In fact, molecules that specifically bind cellular PrP^{C} may interrupt the production of prions. To further analyze the effect of the addition of recombinant α-syn amyloids to scrapie infected cells, residual PK-resistant levels of PrP were investigated. ScN2a cells exposed to recombinant α-syn amyloids displayed drastically reduced levels of PK-resistant PrP^{Sc}. This observation supports the hypothesis that cell surface PrP^{C} might directly bind α-syn amyloids as previously suggested.

Finally, further work was required to validate the importance of this interaction in disease progression *in vivo*. Thus, stereotaxic injections of α-syn amyloids in substantia nigra pars compacta and striatum in FVB PrPWT and FVB PrPKO mice were performed.

In conclusion, our findings suggest a role for PrP^{C} in the regulation of α-syn uptake, thus evidencing a link between the two neurodegeneration associated proteins. Moreover, this study presents new insight on the possible implication of the prion protein in Parkinson's disease.

LIST OF PUBLICATIONS

All the work reported here arises from my own experiments and data analysis performed in SISSA or as a result of joint collaborations with other groups. This thesis is based on the following original publication, in addition to new un-published data that are going to be presented here:

Aulić S *, Le TT *, Moda F, Abounit S, Corvaglia S, Casalis L, Gustincich S, Zurzolo C, Tagliavini F, Legname G. Defined α-synuclein prion-like molecular assemblies spreading in cell culture. BMC Neurosci. 2014 Jun 4;15:69.

Other publications:

Staderini M *, **Aulić S***, Bartolini M, Tran HN, González-Ruiz V, Pérez DI, Cabezas N, Martínez A, Martín MA, Andrisano V, Legname G, Menéndez JC, Bolognesi ML. A Fluorescent Styrylquinoline with Combined Therapeutic and Diagnostic Activities against Alzheimer's and Prion Diseases. *ACS Med Chem Lett*. 2012 Dec 28; 4(2):225-9

Aulić S, Bolognesi ML, Legname G. Small-molecule theranostic probes: a promising future in neurodegenerative diseases. *Int J Cell Biol*. 2013;2013:150952

Le NT, Narkiewicz J, **Aulić S**, Salzano G, Tran HT, Scaini D, Moda F, Giachin G, Legname G. Synthetic prions and other human neurodegenerative proteinopathies. *Virus Res*. 2014 Oct 31. pii: S0168-1702(14)00437-7

Bolognesi M. L., Bongarzone S., **Aulić S**., Ai Tran H. N., Prati F., Carloni P., and Legname G. Rational approach to discover Prion recognition motif -metal chelator hybrid as multifunctional antiprion compound with multiple mechanisms of action. *Future Med Chem. 2015 Oct 29.*

Moda F*, Le TT*, **Aulić S**, Bistaffa E, Campagnani I, Virgilio T, Indaco A, Palamara L, Andréoletti O, Tagliavini Fand Giuseppe Legname "Synthetic prions with novel strain-specified properties". PlosPathogens. (*under review*)

Contribution to the chapter of a book "THE PRION PHENOMENA IN NEURODEGENERATIVE DISEASES NEW FRONTIERS IN NEUROSCIENCE", Nova Science Publishers, Inc.

"*" means that the authors contributed equally to the work.

LIST OF ABBREVIATIONS

Aβ	Amyloid-β
NFTs	Neurofibrillary tangles
AD	Alzheimer's disease
α-syn	α-synuclein
PD	Parkinson's disease
SOD1	Cu/Zn superoxide dismutase
TDP-43	TAR DNA-binding protein 43
ALS	Amylotrophic lateral sclerosis
PrP^{Sc}	Misfolded, pathogenic form of PrP^{C}, also known as prion
TSEs	Transmissible spongiform encephalopathies
PrP^{C}	Cellular prion protein
ThT	Thioflavin-T
APP	Aβ precursor protein
BH	Brain homogenates
Tg	Transgenic animals
EC	Entorhinal cortex
CTE	Chronic traumatic encephalopathy
PSP	Progressive supranuclear palsy
CBD	corticobasal degeneration
FTD	Frontotemporal dementia
MPTP	1-methyl-4phenyl-1,2,3,6-tetrahydro-pyridine
LBs	Lewy bodies
SN	Supstantia nigra
DLB	Dementia with Lewy bodies
MSA	Multiple System Atrophy
DMV	Dorsal motor nucleus of the vagus nerve
ENS	enteric nervous system
ThS	Thioflavin-S
WT	Wild type
AFM	Atomic force microscopy
EM	Electron microscopy
MCNSCs	Mouse cortical neuronal stem cells
PFFs	Preformed fibrils
p-Ser129	Phosphorylated Serine-129
CNS	central nervous system
BBB	blood-brain barrier
CJD	Creutzfeldt-Jakob disease
GSS	Gerstmann-Sträussler-Scheinker
FFI	Fatal familial insomnia
BSE	Bovine spongiform encephalopathy
CWD	Chronic wasting disease

TME	transmissible mink encephalopathy
PK	Proteinase K
PrP^{res}	Resistant PrP fragment
SDS-PAGE	Sodium Dodecyl Sulphate – Poly Acrylamide Gel Electrophoresis
PRNP	PRioN Protein gene
sCJD	Sporadic Creutzfeldt-Jakob disease
WB	Western blot
PNS	Peripheral nervous system
SNCA	Synuclein, alpha gene
NAC	Non-Aβ component
SEC	Size exclusion chromatography
SNCB	Synuclein, beta gene
BCSG1	Breast cancer-specific gene 1
Tyr	Tyrosine
Met	Methionine
CK-1	Casein kinase 1
CK-2	Casein kinase 2
VAMP	Vesicle-associated membrane protein
SV-2	Synaptic vesicle protein 2
p65	Synaptic vesicle protein p65
Thr	Threonine
SUMOs	Small ubiquitin-like modifiers
Lys	Lysine
Gln	Glutamine
NatB	N-terminal acetyltransferase B complex
GPI	Glycosylphosphatidylinositol
OPR	Open reading frame
ER	endoplasmatic reticulum
^{Ctm}PrP	C-terminal transmembrane PrP form
^{Ntm}PrP	N-terminal transmembrane PrP form
Asn	Asparagine
recPrP	Recombinant prion protein
aa	Amino acid
OR	octapeptide-repeat region
FTIR	Fourier transform infrared spectroscopy
Cys	Cysteine
HD	hydrophobic domain
PBMC	Peripheral blood mononuclear cell
KO	Knock out
Dpl	Doppel
Prnd	Prion-like protein doppel gene
CRISPR	clustered regularly interspaced short palindromic repeat
PKA	protein kinase A
MAPK	mitogen-activated protein kinases

PKC	protein kinase C
PI 3-kinase	phosphoinositide 3-kinase
BACE1	β-secretase
ASA	Amyloid seeding assay
MoSP1	Mouse Synthetic Prion Strain 1
MoSP2	Mouse Synthetic Prion Strain 2
PMCA	Protein Misfolding Cyclic Amplification
SHa	Syrian Hamster
qPMCA	Quantitative Protein Misfolding Cyclic Amplification
RT-QuIC	Real-Time Quaking Induced Conversion
vCJD	Variant Creutzfeldt-Jakob disease
CSF	Cerebrospinal fluid
HSPGs	Heparan sulfate proteoglycans
TNTs	Tunneling nanotubes
LTP	Long term potentiation
mGluR5	Metabotropic glutamate receptor 5
SPR	Surface plasmon resonance
EPR	Electron paramagnetic resonance
MTT	3-(4,5-dimethylthiazol-2-yl)-2,5-diphenyltetrazolium bromide
BCA	bicinchoninic acid protein
HRP	horseradish–peroxidase-conjugated
FA	formaldehyde
DSG	disuccinimidyl glutarate

TABLE OF CONTENTS

α-Syn amyloid accumulation and its interaction with prion protein

CHAPTER I

Introduction

Neurodegeneration is a key aspect of a large number of diseases that are commonly defined as "neurodegenerative diseases". These age-related pathologies have high societal costs and lead to a dramatic loss of quality of life. Nowadays, 45 million people worldwide are affected by some form of neurodegeneration, and in 2030 the affected are expected to reach 76 million. These conditions have in common the aggregation of distinct proteins depending on neurodegenerative disease type: amyloid-β (Aβ) and tau as neurofibrillary tangles (NFTs) in Alzheimer's disease (AD), α-synuclein (α-syn) in Parkinson's disease (PD), Cu/Zn superoxide dismutase (SOD1) and TAR DNA-binding protein 43 (TDP-43) in Amyotrophic lateral sclerosis (ALS), prions (PrP^{Sc}) in prion diseases, also known as Transmissible Spongiform Encephalopathies (TSEs), and others.

This chapter covers all relevant findings that provide insights into neurodegenerative disease types and in particular focuses attention on amyloid forms of α-syn protein and its currently known mechanism of accumulation and spreading. In addition, a detailed overview of cellular prion protein (PrP^{C}) and of PrP^{Sc} forms is presented here.

1.1. Neurodegenerative diseases

Different neurodegenerative diseases are characterized by the accumulation of clumps of protein in brain cells, including AD, PD, ALS, and TSEs. Over the past decade, reports that address the propagation of amyloidogenic proteins implicated in these neurological diseases as a prion-like phenomena are increasing [1, 2]. The prion-like distribution of amyloids contributes to the progression of the above mentioned pathologies (**Table 1.1**). In each of

these conditions aggregated forms of a characteristic protein act as a template or as a seed that efficiently recruit the endogenous counterparts into elongating fibrils. The *in vitro* (in cell culture) and/or *in vivo* studies (in living animal models) have revealed important insights of possible mechanisms of aggregation of these proteins. Here we sum up several *in vitro* and *in vivo* reports that outline evidence for prion-like spreading, focusing more attention on the two proteins, α-syn and prion protein, the topic of this PhD thesis work.

Table 1.1. List of important neurodegenerative disorders and the proteins involved in the diseases.

Disease	Clinical features	Protein involved
Alzheimer's	Progressive dementia	Aβ and tau
Parkinson's	Movement disorder	α-syn
Amyotrophic lateral sclerosis	Movement disorder	SOD1
Transmissible spongiform encephalopathies	Dementia, ataxia, psychiatric problems, insomnia	Prion protein

1.1.1. Aβ and tau in Alzheimer's disease (AD)

AD is the most common degenerative dementia condition characterized clinically by a slow decline in cognitive function, such as progressive loss of memory, task performance, recognition of people and objects. Neuropathologically the disease is marked by the specific neuron loss (particularly in the basal forebrain and hippocampus) and synapse loss, in addition to the hallmark findings of neurofibrillary tangles and senile plaques [3]. Senile plaques are heterogeneous lesions principally composed of highly insoluble Aβ peptide (in the form of extracellular deposits), whereas neurofibrillary tangles are made of fibrillary tau protein (that are placed intracellularly) [3, 4]. The Aβ aggregates are composed of a β-sheet rich structure that can be labeled using the typical amyloid dyes such as Congo red and Thioflavin-T (ThT) [5]. More than 90% of AD cases arise sporadically, however there have also been identified rare familial forms and relative genetic mutations, some of which are associated with mutations in the Aβ precursor protein (APP), and in presenilins, which are responsible of the cleavage of APP [6, 7].

In the early 1980s several *in vivo* seeding studies were performed using brain homogenates (BH) from AD patients and non-human primate host animals were

intracerebrally injected (*Callithrix jacchus*) [8]. From these studies emerged that several years (6-7 years) after incubation the amount of senile plaques was increased, although the inductive agent remained uncertain. Only in the mid-1990s, with the use of transgenic (Tg) animal mouse models that express mutant APP it was established that these AD-like neuropathological alterations can be induced by the prion-like seeding of Aβ aggregation. Later, it was showed that this process is inducible using both brain derived Aβ [9] as well as aggregates of pure synthetic Aβ [10, 11]. Nonetheless, as in the case of synthetic prions, the seeding capacity of aggregated synthetic Aβ is much lower than that of comparable amounts of brain-derived Aβ. This led to the supposition that, most probably, some cofactors present in BH can enhance the seeding potential of Aβ seeds. Several reports describe that Aβ can also form prion-like variants *in vitro* [12-17] and *in vivo* [18-22].

The intracellular aggregates of hyperphosphorylated microtubule-associated tau protein are also found in AD [3, 4, 23, 24]. Tau aggregates initially affect the large projection neurons that connect the memory-linked neural system (neurons in the layer II of the entorhinal cortex (EC) link the cerebral cortex with the hippocampus) [25] and then spreads to the hippocampus and cerebral cortex [25-29]. These accumulates are also present in a number of less common neurodegenerative diseases, such as chronic traumatic encephalopathy (CTE), progressive supranuclear palsy (PSP), corticobasal degeneration (CBD), Pick's disease, and frontotemporal dementia (FTD), in the absence of neuritic plaques. The NFTs, in different diseases, have some distinctive morphological features and may exhibit a distinct composition of tau isoforms that differs from AD [30]. The intracerebral injections of BH from different human tauopathies into mice induce corresponding human disease, which is suggestive of the existing proteopathic tau strains [31-33]. Tauopathy, however, contributes importantly to the cognitive deficits distinctive of AD. Tau is known as a natively unfolded protein that stabilizes and promotes the assembly of microtubule filaments in cells [34]. As in other neurodegenerative diseases, also this protein assumes a β-sheet rich structure in its insoluble form, and several cell culture studies have shown that tau pathology can be induced exposing cells to the synthetic tau fibrils, leading to the accumulation of soluble protein [35-40]. Moreover, *in vivo* studies showed that the intracerebral injection of synthetic material into WT mice can induce tauopathology [38]. This seeding phenomenon leads to the formation of aggregates that resemble those of NFTs in AD and FTD. Tauopathy more often can occur as a nonspecific response of neurons to a number of different insults, and in AD it is considered a critically important reaction to the Aβ abnormalities in the amyloid cascade event.

1.1.2. α-Syn in Parkinson's disease (PD)

PD is the second most common neurodegenerative disorder in humans, after Alzheimer's disease; it affects ~1% of people over 65 years of age [41], with a higher prevalence in men. It is an essentially sporadic neurodegenerative disease whose pathogenesis remains still unknown, but it can also have genetic (familial forms) [42-45] and environmental origin (like exposure to the environmental toxin 1-methyl-4phenyl-1, 2, 3, 6-tetrahydro-pyridine, MPTP, herbicide paraquat and the pesticide rotenone) [46, 47]. PD is characterized by the deposition of the α-syn protein in an aggregated form [48, 49]. α-Syn is one of the most abundant proteins in the brain, and it has a propensity to misfold and generate oligomers and fibrils which are characterized by the β-sheet-rich structure. A role for α-syn in PD was fueled by the discovery that it is the major component of filamentous intracellular aggregates termed Lewy bodies (LBs). These particular forms deposit as cytoplasmic inclusions, and cause widespread neuronal damage in human brains. α-Syn is also present in aggregated form in other neurodegenerative diseases which are collectively known as "syucleinopathies", where the accumulation occurs at different levels, such as in: the *substantia nigra* (SN) of patients with PD in a form of brainstem-type LBs, cortical LBs in the temporal lobe of patients with dementia with Lewy bodies (DLB), and in the pontine base of patients with multiple system atrophy (MSA) forming glial cytoplasmic inclusions. In PD, the α-syn amyloid-like structure is directly related to symptomatology and neuronal damage. LBs formed in the SN are spread throughout the brain in the course of the disease, subsequently appearing in distinct brain areas. In 2003Braak and colleagues proposed a model of propagation of α-syn aggregates via interconnected brain pathways [50, 51]. According to this model (**Figure 1.1**) the disease process begins in the lower brainstem in the dorsal motor nucleus of the vagus nerve (DMV), and in anterior olfactory structures. Afterwards, the pathology ascends rostrally from the DMV through the medulla, pontine tegmentum, midbrain, and basal forebrain, reaching finally the cerebral cortex. As the pathology arises from the brainstem, both the harshness and the clinical signs of the disease exasperate [52]. This progressive neurodegeneration in PD finally results in motor symptoms because of the death of dopamine-generating cells in the SN. Clinically, the most obvious symptoms involve alteration of the ability to control movements and are characterized by tremor at rest, bradykinesia (slow movements), rigidity or absence of voluntary movement, postural instability and freezing (involving parts of the body and/or the ability of speech). Also, some pre-motor symptoms have been observed, such as, olfactory dysfunction, sleep abnormalities, constipation and pain [53]. Depression is also

common in PD patients, together with cognitive and behavioral problems, further they become passive or withdrawn with lack of initiative.

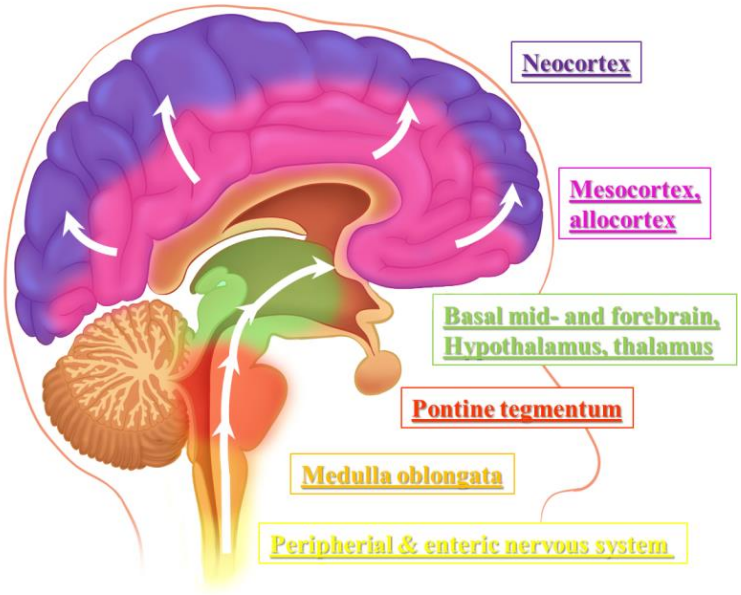

Figure 1.1. The six stages of α-syn pathology progression in PD according to the Braak hypothesis. The hypothesis proposes that α-syn pathology begins, due to unidentified insult, within enteric epithelium. Supposedly the insult can be also of the environmental origin. From the periphery, the α-syn deposits travel retrogradely via the axons of enteric nervous system (ENS) neurons to their somata reaching the spinal cord and then to the DMV in the medulla. Thereafter, it is able to reach the pons and SN and, further than, forebrain (amygdala) and the cerebral cortex (reaching finally neocortical structures).

Braak's model describes the progressive, stereotypic spread of the pathology from one affected brain region to the neighboring regions. This progression of the pathology was suggesting that the deposits might spread between neurons, though the molecular evidence was not identified until the discovery that grafted neuros in PD patients acquired α-syn aggregates. Indeed, this finding suggested that α-syn spread may be mediated in a prion-like fashion. This similarity in spreading with prion diseases was observed from four separate case reports that show that 11-16 years after fetal mesencephalic dopaminergic neurons transplantation patients developed α-syn-positive LBs in grafted neurons [54-56]. The α-syn inclusions were positively stained for Thioflavin-S (ThS), a dye that binds to the β-sheet rich structures, indicating the presence of amyloidogenic forms. They were also stained by the anti-ubiquitin [48, 57] and anti-α-syn phosphorylated at serine129 antibodies [58], which are other typical hallmarks of PD. Moreover, the affected transplants showed reduced levels of dopamine transporter and tyrosine hydroxylase. All this strongly indicated the presence of disease-related, post-translationally modified and aggregated α-syn typical of PD pathology.

1.1.2.1. *In vitro* studies

In vitro evidence shows that the monomeric α-syn incubated at 37°C under certain conditions (buffer, pH, and shaking conditions) converts into β-sheet rich fibrils reminiscent of those contained in LBs of PD [59-61]. Several factors can affect the fibrillation kinetics of this protein; one of which is the missense genetic mutations present in familial forms of PD (responsible for early onset of the disease) such as A53T, E46K, and A30P, can have implications on the time of fibril formation (also denoted as lag phase) [62-66]. Recently, another pathogenic mutation (H50Q) has been discovered by two independent groups [45, 67]. Mutations, A53T and E46K accelerate the *in vitro* fibrillation compared to wild type (WT) 3protein [68]. A53T fibrils were of about 5-14 nm in width and 100 nm in crossover spacing, also the E46K mutant was varied between 5 and 14 nm, but the fibrils were shorter in crossover spacing since they were of about 43 nm. As with WT protein, these α-syn mutants also form intermediates with pore-like activity [69-71]. On the contrary, the A30P mutation has unclear behavior, since different studies reported disaccording findings. In the first study done by Narhi et al. [72], the authors reported that this mutant is able to form the fibrils at a much greater rate if compared to the WT α-syn protein; while other groups found that this mutation increases the lag phase of the fibril formation [69, 73]. Moreover, some data have shown that A30P fibril morphology was similar to WT protein, while this was not true for the other two mutants, since they presented two-filament twisted morphology [59, 74]. The H50Q mutation, described in 2013, fibrillates more rapidly than WT α-syn form, but more slowly than A53T and E46K [67]. Atomic force microscopy (AFM) and electron microscopy (EM) analysis confirmed that while the morphology of H50Q was similar to WT, there was an abundance of shorter fibrils [67]. The importance of the use of *in vitro* methodologies to study the mechanism of fibril formation is crucial since it has been shown that the fibrils formed *in vitro* are very similar to those extracted from PD patient brains, or as reported, they reflect at least a subpopulation of fibrils formed during the disease [62].

Several studies have explored whether α-syn fibrils, obtained from recombinant protein, may be internalized by cells and ultimately recruit endogenous α-syn and initiate a PD-like pathological response. Growing indications show that misfoled α-syn aggregates may be taken up and propagated among cells in a prion-like manner and induce pathology features in healthy cells [75-78]. Desplats and coworkers [77] have shown that α-syn aggregates are transmitted via endocytosis to neighboring neurons and neuronal precursor cells, forming LBs-like inclusions. In this study they used mouse cortical neuronal stem cells (MCNSCs) which were incubated with media containing Alexa-Fluor-488-labeled α-syn aggregates, and

showed that exogenous fibrils can be internalized by cells by simple addition into cultured medium. Moreover, from the co-culturing experiments they show that the α-syn aggregates released from neuronal stem cells can be directly transferred to MCNSCs cells.

Straight after Luk et al. [75] reported that recombinant α-syn fibrils (denoted as PFFs, preformed fibrils) were delivered into QBI-293 cells that overexpress monomeric α-syn protein (QBI-WT-Syn cells). The aggregates were delivered into the cytoplasm of these cells, using a cationic-liposome transduction reagent. About 40% of PFF-transduced QBI-WT-Syn cells presented LB-like pathology. On the contrary, cells that were transduced with monomeric α-syn did not present a similar pattern, concluding that only the exogenous α-syn fibrils were able to induce intracellular inclusion formation. Most importantly, the inclusions presented all characteristic posttranslational modifications typical of PD disease, such as phosphorylation at the serine 129 and ubiquitination. Moreover, they showed that the exogenous α-syn fibrils seed intracellular inclusion formation through the recruitment and conversion of soluble endogenous cytoplasmic α-syn in different cell lines overexpressing soluble α-syn protein. In this thesis in "Results" chapter (see CHAPTER III) we report that the overexpression of endogenous α-syn is not a *condicio sine qua non* for the α-syn inclusion formation after incubation with exogenous fibrils.

The same group also tested whether exogenously added PFFs could induce aggregation of endogenous α-syn in primary cells not overexpressing the protein [79]. Here, the addition of PFFs for 14 days to hippocampal neurons derived from WT C57BL6 mice, developed PD-like inclusions. No LB pathology was observed in primary neurons obtained from mice that do not express the α-syn protein endogenously. The PFF-induced aggregates were resistant to detergent treatments (1% Triton X-100), while the monomeric protein was solubilized. Moreover, the isolated aggregates were hyperphosphorylated and ubiquitin positive, assessing in this way their analogy with LBs in PD. As a consequence of inclusion formation some synaptic protein levels decreased (i.e. synaptic vesicle-associated SNARE proteins, Snap25 and VAMP2, cysteine-string protein α), connectivity and neuronal excitability were impaired, eventually leading to neuronal loss.

Another important study [80] performed on mixed neuronal-glial cultures from P0 C3HBL/6 mice showed that WT and mutant recombinant α-syn fibrils were able to recruit endogenous α-syn into morphologically distinct inclusions in neurons, affirming that the mechanism by which this process occurs is a prion-like self-templating mechanism. Similarly to other reported studies, the aggregates formed were partially ubiquitinated, phosphorylated

(p-Ser129) and stained by ThS dye. Additionally, the study provided the evidence that the PD-like pathology can be passaged in primary astrocyte cultures.

In conclusion, these cell culture systems may give important indications for understanding the exact mechanism of PD pathology formation, as well as the underlying mechanism of cell-to-cell spread of the pathology (described in the paragraph 1.5.1).

1.1.2.2. *In vivo* studies

Together with *in vitro* findings, several recent *in vivo* studies have reported that intracerebral injection of recombinant α-syn fibrils into transgenic or WT mice lead to the formation of PD-like pathology. The α-syn aggregate formations were predominantly found in brain regions anatomically connected to the injection site [81, 82]. To corroborate the cell culture work, Desplats and coworkers [77] showed that grafted MCNSCs cells take up α-syn from the host brain when grafted into the hippocampus of a Tg mice overexpressing human α-syn (line 61). These mice spontaneously develop the α-syn pathology typical of PD [83, 84]. Seven days after stereotaxic intra-hippocampal injection, about 2.5% of the grafted MCNSCs were positive for the human α-syn immunostaining whereas the MCNSCs injected into non-Tg mice were not.

Another study has shown that injections of BH from symptomatic mouse or recombinant PFFs into still asymptomatic Tg mice overexpressing the human mutant (A53T) α-syn led to PD-like pathology and significantly reduced the survival time of these animals [81]. The pathology spread to distal central nervous system (CNS) areas, precisely in areas that project to or receives input from the inoculation sites, suggesting once again that the propagation process occurs between associated neuronal populations. Injections of *in vitro* formed fibrils in the SN in non-Tg-mice have induced the LB-like pathology after three months post inoculation, whereas, the soluble monomeric form did not [76].

Sacino et al. [80] observed that bilateral cerebral injection in neonatal C57BL6/C3H mice of α-syn fibrils induced the LB-like pathology after 8 months post injection. Equivalent density and distribution of α-syn deposits was seen bilaterally, and most importantly they were stained with the anti-p-Ser129 antibody. Whereas the neonatal injections in Tg mice (line M20) which overexpress by 5 times α-syn than the WT mice, induced the formation of α-syn inclusions in a higher rate, 8 months after injection (12 of 12 mice show abundant and widely distributed PD-like brain pathology) [85].

An additional significant *in vivo* study has shown that α-syn strain conformation and seeding propensity lead to distinct histopathological and behavioral phenotypes [86]. The

different strain conformations were first observed *in vitro*, and subsequently, after detailed characterization in cell culture system [87], the stereotaxic injections were performed [86]. In the former *in vitro* preliminary study two different strains of α-syn fibrils were described. Other important *in vivo* reports show the existence of α-syn strains [88, 89]. Briefly, starting from recombinant full-length human α-syn protein, under tightly controlled *in vitro* conditions, Melki and collaborators identified two polymorphs, denoted as "*fibrils*" and "*ribbons*". These two different strains faithfully propagate their intrinsic structure *in vitro*; they are taken up at different rates by the cells (*fibrils* bind to and permeabilize cell membranes at a faster rate), which consequently implies diverse toxicity (*fibrils* are more toxic than *ribbons*), and most importantly they seed aggregation of endogenous α-syn protein in different amounts (*fibrils* had higher aggregate-induction activity). Notably, the accumulated cytoplasmic α-syn was persistent after 60 days in culture in the case of exposure to *fibrils*, while the exposure to the *ribbons* led to the loss of the small punctuate aggregates after 30 days of maintenance in cultures. These findings suggest that endogenous α-syn aggregation that is seeded by different strains maintains a persistent and heritable phenotype. The stereotaxic injection of these highly purified preparations into the SN of rats expressing normal levels of α-syn led to the formation of LB-like inclusions after four months [86]. Also, *in vivo* the different strains induced dissimilar phenotypes, as the injection of *ribbons* led to the formation of predominantly hyperphosphorylated deposits, while the *fibrils* induced mainly the filamentous phenotype that was positive for the aggresome marker p62. Indisputably these effects were more evident in rats that overexpress α-syn protein. Although the injection of *ribbons* induced major phosphorylation of deposits, the *fibrils* imposed the largest neurotoxic load on the striatonigral pathway as well as major motor impairments in the rats. Intravenous injection in non-Tg rats revealed the α-syn deposits in the CNS after four months (in cortical neurons, spinal cord), indicating that the peripheral injection leads to the crossing of the blood-brain barrier (BBB). In this PhD thesis we will describe un-published data from stereotaxic injections in CD1 WT mice using the recombinant human α-syn fibrils (see **CHAPTER III**, section 3.1.5. *In vivo* studies).

However, Virginia's Lee group in 2013 [90] showed that distinct α-syn strains are able to induce aggregation of endogenous tau protein, leading to the hypothesis that not only one aggregated protein accumulates in patients with neurodegeneration. This is not the first report of molecular interplay between neurodegeneration-associated proteins; similarly, other groups showed that in brains of patients diagnosed with sporadic and genetic CJD (mutation E200K) the PrP^{Sc} was accumulating in close proximity to α-syn protein, Aβ, and tau protein [91, 92].

Aβ and α-syn aggregates are found mixed in many diseases, including AD, DLB, and MSA. In addition, distinct morphologies between disease-linked α-syn filaments have been described [93], providing a link between MSA and LB disorders.

1.1.3. SOD1 and TDP-43 in Amyotrophic lateral sclerosis (ALS)

ALS is another neurodegenerative disease where the prion-like mechanism is hypothesized as a mechanism of pathology propagation; here, the two misfolded proteins are SOD1 and TDP-43. The pathology is characterized by degeneration of lower motor neurons in the spinal cord and upper motor neurons of the cerebral cortex, resulting in progressive motor weakness [94].

Misfolded SOD1 was the first identified protein to be implicated in familial ALS (in 20% of familial ALS patients). Later studies describe it as a common prime candidate for all forms of ALS (familial and sporadic) where it may play a key role in disease pathogenesis. SOD1 aggregation can occur in several different ways, through a mechanism by which the native intrinsically stabile SOD1 homodimer gets disordered, producing misfolded monomer intermediates that can be incorporated into growing fibrillary structures. More than 180 genetic mutations have been identified [95-97]; oxidation or post-translational modification of WT SOD1 can also be a cause of aberrant folding and subsequent misfolding [98-100]. The mechanisms by which aggregated SOD1 contributes to ALS pathology are not yet completely understood. Experimentally, all Tg mice expressing SOD1 mutants develop intracellular aggregates in motor neurons and accessory neural cells that parallel with the onset of motor neuron disease and increase in dimension and amount during the course of disease evolution [101, 102]. Denaturation of WT and mutant SOD1 forms can induce aggregate formation *in vitro* [103]; it has also been shown that the relative tendency for aggregation is mutant variant-dependent [104]. *In vivo* formation of SOD1 aggregates has been observed in Tg mice expressing mutant protein [100, 105]. A hypothesis of prion-like mechanism for ALS is supported by the finding that, in a cell-free system, the WT SOD1 can be converted into misfolded conformer by mutant SOD1 alone; thus, eliminating the need for any extraneous protein or any other co-factor that may promote the aggregation process.

Furthermore, the TDP-43 has been identified in the majority of sporadic cases of ALS, as a major protein in ubiquitin-positive inclusions. Interestingly, TDP-43 has also been observed in inclusions found in Huntington's disease [106], PD [107], and approximately 20% of AD cases [108], which link this protein to a wide range of neurodegenerative disorders.

Functionally, TDP-43 is an important regulatory protein in the nervous system: it binds over 6,000 pre-mRNAs, affects the splicing patterns of 965 mRNAs and affects expression levels of another 600 mRNAs [109]. The pathological TDP-43 translocates from the nucleus to the cytoplasm where it gets accumulated and hyperphosphorylated. It is unclear whether pathology is caused by a loss-of-function due its nuclear depletion or by a toxic gain-of-function due to cytoplasmic mislocalization, or a combination of the two. As with SOD1, a growing body of evidence demonstrates prion-like behavior of TDP-43. It is firmly established that TDP-43 and its derived fragments have a high tendency to form β-sheet amyloid fibrils *in vitro* [109, 110] and pathological mutations expressed within the protein can enhance this property [109, 111, 112]. In a recent study [113], isolated TDP-43 aggregated from the brains of ALS and frontotemporal lobar degeneration patients were exogenously applied to cell culture (human neuroblastoma cells) and were able to seed the self-propagation of TDP-43 inclusions (that were both, ubiquitinated and phosphorylated). This was also true for synthetic material where, Furukawa and co-workers have demonstrated that exogenously applied recombinant detergent-insoluble aggregates of TDP-43 can be taken up by human embryonic kidney cells, and act as seeds for the aggregation of endogenous TDP-43 [110]. These induced aggregates were similar to that observed in ALS patients. Analogous mechanisms have been found in several other prominent neurodegenerative proteinopathies, such as prion diseases [114], AD [20, 115] and PD [75].

1.1.4. PrP^{Sc} in Transmissible spongiform encephalopathies (TSEs)

TSEs are unconventional animal and human forms of neurodegeneration that have been defined as transmissible diseases in early 1930s. Originally, this transmissibility hypothesis was considered as an unorthodox hypothesis. The latter hypothesis states that the infectious agent in TSEs is composed solely of an abnormally folded protein, called prion protein. TSEs include Creutzfeldt-Jakob disease (CJD), Gerstmann-Sträussler-Scheinker (GSS), fatal familial insomnia (FFI), and Kuru in humans; bovine spongiform encephalopathy (BSE) in cattle, scrapie in sheep, chronic wasting disease (CWD) in deer and elk, and transmissible mink encephalopathy (TME). The etiology of prion diseases can be spontaneous, genetic or infectious (**Table 1.2**). In humans, prion disorders manifest as rapid, progressive dementias with clinical visual signs that can vary between and within different syndromes [116]. Characteristic neuropathological alterations include vacuolation of the neuropil in the gray

matter, synaptic alterations, considerable neuronal loss, abundantly reactive astrogliosis and accumulation of PrP^{Sc} aggregates (reviewed in [117]).

A crucial experiment that showed the infective property of these pathologies was performed by Cuille and Chellè (reviewed in [118]), showing incontrovertible transmissibility of scrapie to goats. Afterward, Griffith speculated that a protein alone could be the infectious moiety responsible of the disease [119], and finally Dr. Stanley Prusiner experimentally demonstrated this postulate and defined a "prion" as a "proteinaceous infectious particle" [120, 121].

Table 1.2. Human and animal prion diseases.

Species	Disease	Sporadic	Genetic	Infectious
Humans	Creutzfeldt-Jakob disease (CJD)	√	√	√
	Gerstmann-Sträussler-Scheinker (GSS)		√	
	Fatal Familial Insomnia (FFI)		√	
	Variant CJD (vCJD)			√
	Kuru			√
Cattle	Bovine Spongiform Encephalopathy (BSE)	√	√	√
Sheep	Scrapie	√	√	√
Cervids	Chronic Wasting Disease (CWD)	√	n.d.	√
Mink	Transmissible Mink Encephalopathy (TME)	√	n.d.	n.d.
Feline	Feline Spongiform Encephalopathy (FSE)	√	n.d.	n.d.

n.d.: not determinated [122]

The pathogenic protein is the result of post-translational conversion of cellular prion protein (PrP^{C}) into a form called prion or PrP^{Sc}. This postulate, called "protein-only hypothesis" remained controversial for years, but recent studies have showed that infectious material can be generated *in vitro* [123-126], in the absence of genetic material, by replication of the protein misfolding process, and transmitted *in vivo*. Thus, prions exhibit the typical characteristics of *bona fide* infectious agents. In particular, the replication progress necessitates exposure to small amounts of PrP^{Sc} present in the infectious material, to trigger the autocatalytic conversion of host PrP^{C} to PrP^{Sc}. More precisely, the PrP^{Sc} growth occurs by the recruitment of monomeric PrP^{C} into the growing PrP^{Sc} polymer (aggregates) that finally form PrP-amyloid plaques within the CNS. Indeed, a key step in prion replication is a breakage of large PrP^{Sc} aggregates into many smaller seeds that amplify the prion replication

process, resulting in the exponential accumulation of PrP^{Sc} [127] . Different models of prion replication have been proposed (the latter, denoted as "nucleated polymerization" and "template directed misfolding" model [128, 129]); however, the available experimental data indicate that the aggregation process follows the seeding-nucleation mechanism. As mentioned above, this process initiates with the slow interaction between cellular prion protein in its monomeric form and a seed to create a stable seeds (oligomeric nucleus) around which a faster phase of growing occurs (forming protofibrils), reaching finally to the last saturation phase in which the elongation arises with the PrP^{Sc} amyloid formation (**Figure 1.2**).

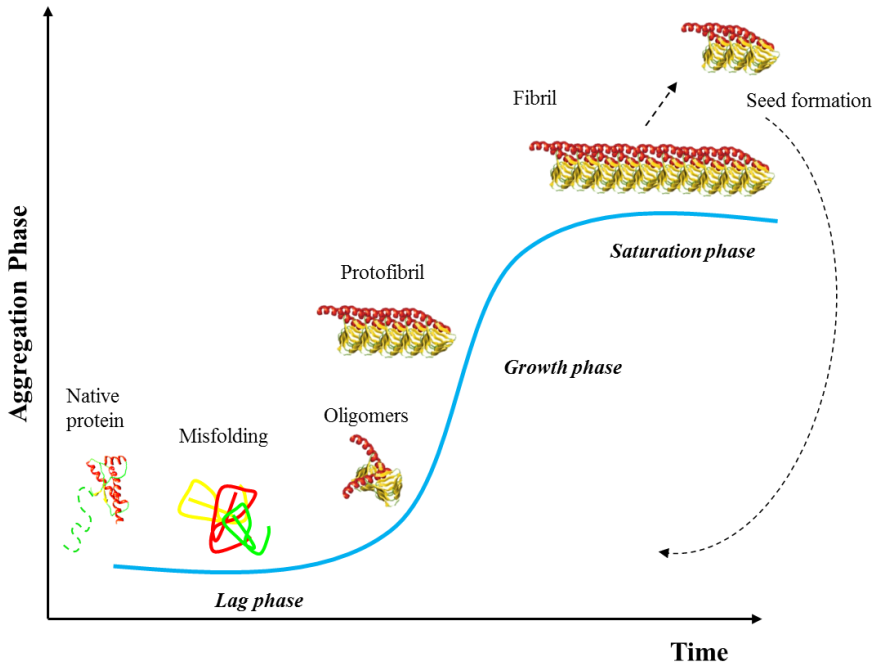

Figure 1.2. Scheme of nucleation-dependent fibril formation process. Amyloid formation consists of several steps: (i) a nucleation phase or *lag phase*, in which native protein undergoes conformational change and form oligomers, (ii) a growth phase, in which the nuclei rapidly grow by further addition of native protein (monomer) and form greater fibrils until the saturation phase (iii). The 'nucleation phase', is thermodynamically unfavorable and occurs gradually (slower phase), whereas 'growth phase', is much more favorable process (faster phase). Thus, kinetics of amyloid formation can be represented by a sigmoidal curve (blue curve) with a lag phase followed by rapid growth phase. The rate-limiting phase is the formation of critical amount of PrP^{Sc} to form a *"seed"* for the polymerization of PrP^{Sc}. The addition of seeds reduces the length of the lag phase and induces faster aggregate formation. Thus, fibril formation can be greatly accelerated by the addition of preformed seeds (nuclei).

A number of recent discoveries have provided experimental evidence for prion-like mechanisms of pathological transmission in several other common neurodegenerative diseases. As in the abovementioned proteinopathies, the aggregated form of prion protein is

present in its β-sheet rich conformation. Nevertheless, because of the insolubility of PrP^{Sc} and its infective nature, all the structural studies have yet failed to demonstrate its structure at the atomic level. In the absence of direct experimental data, two models have attempted to determine the putative PrP^{Sc} structure: the "β-helical" and the "spiral" models. The first originates from the combination of cryo-electron microscopy data and structural modeling, and proposes that PrP^{Sc} forms β-sheets which are rearranged in left-handed β-helices [130]. While in the "spiral" model the proposed PrP^{Sc} structure is derived from an all-atom explicit solvent molecular dynamic simulation [131, 132]. According to this model, during prion conversion the two native β-sheets elongate in a longer single β-strand, which forms intermolecular β-sheets with other PrP molecules leading to polymerization. From the experimental point of view, several biochemical, biophysical and structural approaches have been used in order to elucidate the PrP^{C} → PrP^{Sc} mechanism of conversion. A defining feature of PrP^{Sc} is its unusual high resistance to degradation by proteolytic enzymes such as Proteinase K (PK). The final proteolysis product of PrP^{Sc} is a smaller C-terminal PK-resistant fragment (PrP^{res}) composed of approximately 142 residues starting from the residue ~90, also denoted as PrP27-30 (because of its electrophoretic mobility) or PrP^{res} (**Figure 1.3**) [133].

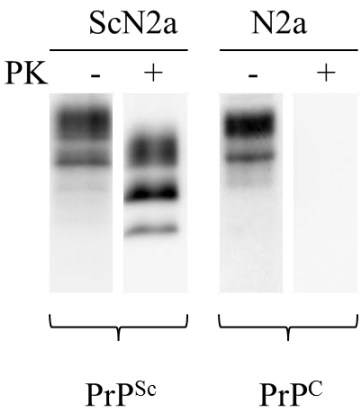

Figure 1.3. **Proteinase K (PK) resistance profile of prion protein in its two distinct conformations (PrP^{C} and PrP^{Sc})**. A Sodium Dodecyl Sulphate-Poly Acrylamide Gel Electrophoresis (SDS-PAGE) electrophoresis of cellular lysates immunoprobed with W226 antibody to detect PrP. In the PrP^{Sc} conformation the electrophoretic profile distinguishes three characteristic bands of PrP (i.e. un-, mono- and di- glycosylation pattern); whereas after PK digestion it is shifted to lower molecular weight. These are the N-terminally truncated forms of PrP^{Sc}, also called PrP27–30 that is fully infectious. The SDS-PAGE profile of the cellular PrP protein also distinguishes three characteristic bands that disappear completely after PK digestion.

Although it is extremely difficult to explain the strain phenomenon in prion diseases, different biochemical properties are associated with distinct stains. Indeed, using the enzymatic digestion as a tool, different molecular strains have been identified based on

differences in the fragment size and glycosylation site occupancy of PrP^{res}. In accordance with this, diverse subtypes of human prion disease can be classified using PrP^{res} molecular profiles in combination with the existence of mutations and polymorphisms in the prion protein gene (*PRNP*). For example, in sporadic CJD (sCJD) six molecular subtypes have been established that combine the *PRNP* codon-129 genotype polymorphism (MM, MV or VV) with the apparent molecular mass of the unglycosylated PK-resistant fragment of PrP^{res} on western blots (WB) which is either 21 kDa (type 1) or 19 kDa (type 2A), as showed by nomenclature defined by Parchi and Gambetti [134]. Moreover, additional PrP^{Sc} fragments have been linked to other human prion diseases, e.g. GSS with the P102L mutation in *PRNP*, in which either type 1 PrP^{res} or a low molecular mass ~8 kDa PrP^{res} fragment can prevail [135]. The section 1.4. "Strain phenomenon in neurodegenerative diseases" focuses more attention on the existence of strains in neurodegenerative disorders.

As previously mentioned, the generation of synthetic prions is one of the most important recent advances in prion biology that showed that PrP^{Sc} is the principal causative agent of TSEs, providing the definitive proof for the prion hypothesis.

For all neurodegenerative-involved proteins, the mechanism of intramolecular conversion is still under debate, nevertheless for the prion protein conversion more and more experimental evidence show the importance of template directed misfolding process.

1.2. Physiological roles of neurodegenerative-involved proteins

The physiological roles of either PrP^C or α-syn are not well elucidated yet, but are beginning to be clarified in recent findings. Actually, several roles in CNS and peripheral nervous system (PNS) have been attributed to both proteins. This section summarizes the structural features of the natively folded forms together with their physiological roles. In addition, several post-translational modifications on endogenous proteins that lead to the conformational changes are listed and described below.

1.2.1. α-Syn protein

A role for α-syn in PD was first established in 1997 by the identification of the mutation A53T in the *SNCA* gene [48]. α-Syn is a natively unfolded 140 amino acid protein widely expressed in the brain, found predominantly in presynaptic terminals [136-138]. As stated below, this protein is genetically and neuropathologically linked to PD [48, 49, 60], though abnormal α-syn pathology characterizes not only PD patients, but also patients with other neurodegenerative conditions collectively termed "synucleinopathies" [139, 140].

1.1.2.1. Structural features of α-syn protein

Despite the original definition as a natively unfolded protein, recent findings suggest that α-syn form α-helical structures that bind to negatively charged lipids [141, 142]. Structurally, the protein is characterized by three different regions:

- Residues 1-60: an N-terminal part of the protein that contains apolipoprotein lipid-binding motif, that contains seven highly conserved repeats consisting of 11 residues (**Figure 1.4**) [143-145]. All of the disease-related mutants (A30P, E46K, A53T, and the more recently discovered G51D and H50Q) are localized within this part of the protein sequence.
- Residues 61-95: a central hydrophobic region, termed non-Aβ component (NAC), confers the β-sheet potential. This fragment was first purified from AD patients [146]. As previously mentioned, several studies have shown that α-syn contributes to the AD pathology and other neurodegenerative disorders. *In vitro* and cell culture studies showed that the deletion of this segment leads to decreased fibril formation, indicating the essential role of this segment for α-syn aggregation.
- Residues 96-140: a C-terminal part is highly negatively charged, and it is prone to be unstructured [145]. Calpain is an enzyme that can process the C-terminal domain leading to the formation of fragments that are prone to fibrillation [147]. Importantly, the major

phosphorylation site (Ser129) is present in this region [58]. This post-translational modification is a main hallmark in DLB, MSA, and PD brains, since it is significantly elevated in α-syn deposits [58, 148, 149].

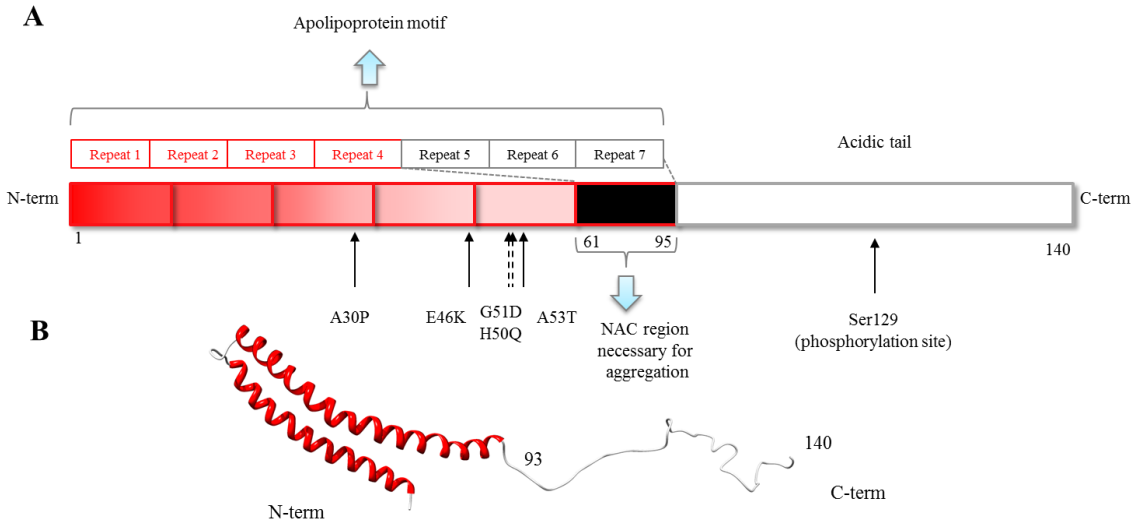

Figure 1.4. Human α-syn primary amino acid sequence (A) and 3D-structure of the protein (B) when bound to small unilamellar lipid vesicles (PDB code: 1XQ8). **A)** Different domains of the primary sequence of α-syn are indicated in red, black, and grey. Structurally, α-syn is composed of three modular domains; the N-terminal amphipathic region of α-syn (residues 1-60), that harbors 7 amino acid repeats with consensus sequence (XKTKEGVXXXX) analogous to the apolipoproteins (in red). The PD-linked mutations are placed in this area as well. N-terminal part is represented in red and PD-linked mutations are indicated below; the middle hydrophobic NAC (residues 61-95) comprises the highly amyloidogenic domain (in black); and the C-terminal tail (residues 96-140) remains free and unfolded (in grey).

Several studies performed using different biochemical and biophysical methods showed that α-syn purified from *E.coli* under native or denaturating conditions exists in a partially unfolded state. However, it has also been reported by one study that natively cell-extracted α-syn may be present in a tetramer form, characterized by α-helical folded monomers [150]. The α-syn extracted from patients and analyzed in non-denaturing gels or by size exclusion chromatography (SEC) columns were present as 57-60kDa proteins, but in denaturing conditions they were captured as 14kDa proteins. Together, these findings suggest that native α-syn exists in equilibrium between different conformational states, and it has been shown that several factors can modulate this equilibrium in order to disturb this balance. These factors include post-translational modifications, oxidative stress, proteolysis, concentration of lipids and metal ions. Nevertheless, the human brain analysis has recently confirmed that the

α-syn is almost entirely in its monomeric state [151]; however, these extensive biochemical studies still did not reveal its exact conformation.

1.2.1.2. Role of α-syn protein in neurotransmitter release

As mentioned above, α-syn is abundantly expressed in the nervous system, representing 1% of total cytosolic protein. In addition to its cytosolic localization, the use of anti-α-syn antibodies permitted its detection also at the nuclear level, accounting for the designation *"sy-nuclein"*. Numerous other subsequent studies confirmed the α-syn expression in the nucleus [152-154]. Additional two closely related isoforms of α-syn, named β- and γ-synucleins [137], have been identified (with 63% and 55% homology, respectively). The triple knock-out experiment suggests a different role for these proteins [155]. Indeed, β- and γ-syn are assumed to have a neuroprotective role by inhibiting α-syn aggregation and toxicity [156, 157]. The β-syn is encoded by the *SNCB* gene, it is highly homologous to the α-syn isoform, and as such is mainly expressed in brain. However, β-syn does not fibrillate when incubated under the same conditions as α-syn. On the contrary, the γ-syn is expressed in the peripheral nervous system, in ovarian tumors [158, 159], in the olfactory epithelium [160], and it is also detected in brain [161]. The normal cellular function of γ-syn is still poorly understood, but exogenous expression of the protein increased the invasive and metastatic potential of breast tumors, in fact it was first identified as a breast cancer-specific gene 1 (BCSG1) [158]. The β- and γ-syn proteins are not found in LBs, but both are related with hippocampal axon pathology in PD and DLB [34]. However, most of the experimental evidence links the α-syn isoform as a most abundant protein that is aggregated within LBs in synucleinopathies.

Its localization at presynaptic levels, the association with synaptic vesicles and the deficits in α-syn null-mice in dopaminergic system suggest that α-syn has a role in the regulation of neurotransmission, synaptic function, and plasticity [138, 162, 163]. Tg mice that overexpress human α-syn show reduction in synaptic vesicle and neurotransmitter release [164]. This was confirmed both in rodent models of PD and in the PC12 stable cell line that overexpress α-syn protein. These Tg mice show a number of behavioral changes, including olfactory loss, different gastrointestinal motility, and deficits in motor activity [165-168]. Moreover, using these α-syn overexpressing models it has been shown that this excess of protein induces a decrease in dopamine reuptake in dopaminergic terminals [169], and inhibits intersynaptic mobilization of vesicles, leading to a smaller reserve pool of vesicles [170].

Recent findings report that α-syn can act as a chaperone protein for the presynaptic SNARE complex by controlling the degradation and affecting the association, maintenance

and distribution of this complex, which is directly involved in the release of neurotransmitters, including dopamine. The initial study [171] could not detect a direct interaction between the two proteins, but a subsequent work performed by Burré and collaborators [172] identified a direct biochemical interaction of α-syn hydrophilic C-terminal domain and v-SNARE synaptobrevin 2. Several other α-syn interactors have been identified that might govern its activity (at least 30 proteins), including synphilin that appears to promote the α-syn aggregation process; tubulin that interacts with the multimeric form of α-syn, thus influencing microtubule cytoskeleton; and GTPaseRab3a that has been proposed to regulate the α-syn binding to the membrane evidencing the role of α-syn in the synaptic vesicle cycle [173-177].

1.2.1.3. Post-translational modifications and mutations of α-syn protein

As cited before, several factors might perturb the equilibrium between the monomeric and multimeric form of α-syn, leading to accumulation and a subsequent LB-like plaques formation. Among these, the most relevant are the post-translational modifications like phosphorylation (Ser87, Tyr125, and Ser129), lysine modification (ubiquitination), oxidative modifications (tyrosine and methionine oxidation), and others.

Phosphorylation

Phosphorylation modification is the most common and probably the most important post-translational modification. Recently it was established that the C-terminal part of the α-syn protein contains the major phosphorylation site positioned at residue Ser129, while the second phosphorylation site was identified at Ser87, located in the NAC domain [178]. Two casein kinases denoted as CK-1 and CK-2, are the two enzymes that catalyze this reaction, in addition to a third kinase, called G-protein-coupled receptor kinase [178]. Importantly, latter localizes to the synaptosome, and it has been shown to phosphorylate numerous synaptic vesicle proteins such as VAMP, SV-2, and p65 [179-181]. It has been estimated that only 4% of native α-syn gets phosphorylated in normal conditions, while in PD brains this percentage increases to approximately 90%, suggesting that this extensive post-translational modification is an important pathogenic event [58, 148]. The effect on α-syn aggregation was studied by expressing S129A and S129D, mutants that were incapable of phosphorylation and mimic phosphoserine, respectively [182-184]. Thus, the authors showed that the α-syn phosphorylation at this residue enhanced the formation of aggregates confirming the findings

observed *in vivo*. On the contrary, the phosphorylation of the Ser87 expands the structure of protein, increasing its conformational flexibility, and blocking its aggregation *in vitro*. Similarly, when the Thr125 is phosphorylated it attenuates the conversion of α-syn to toxic oligomers [185, 186]. From these findings it is evident that the position of the modification is important.

Ubiquitination and SUMOlation

Auxiliary to the phosphorylation, mono- or di-ubiquitination of the α-syn has been shown to occur. Ubiquitin is a small protein that can be attached to lysine (Lys) residues of target proteins that have to be proteolytically degraded by proteasome complex. Indeed, α-syn contains 15 lysine residues, of which only Lys6, Lys10, and Lys12 were shown to be involved *in vivo* [187]. Though ubiquitination is not required for the degradation of monomeric α-syn, it appears that it occurs only after α-syn aggregation [188, 189]. As with the phosphorylation, also in the ubiquitination process the position of the modified residues is important; for example, the modification of Lys6 induced a slower aggregation if compared to the un-ubiquitinated protein [190], while the multiple lysine modification led to the formation of an aggregated toxic form [187].

Aa additional novel protein modification that recently has been implicated in the pathogenesis of different neurodegenerative disorders is performed by small ubiquitin-like modifiers called SUMOs [139, 191-196]. This highly dynamic and reversible process modifies protein-protein interactions, affects sub-compartmental localization, and might antagonize the proteasome pathway by competing with ubiquitin [197]. Only one unidentified Lys residue located at the N-terminal part of α-syn protein was shown to be modified by SUMO1, promoting α-syn aggregation and a decrease its toxicity in COS-7 cells [198].

Oxidative modifications

Oxidative modifications can highly alter the aggregation processes of α-syn; some of the most important include tyrosine (Tyr) and methionine (Met) oxidation responsible for the formation of cross-linked α-syn oligomers. A non-covalent interaction with dopamine and its oxidation products form adducts with α-syn protein that inhibit its fibrillation and stabilize the oligomer's formation [199-201]. The α-syn primary sequence contains four tyrosine residues that can be nitrated, comprised of Tyr39, Tyr125, Tyr133, and Tyr136, all of which have been detected in LBs of PD patients. It has been shown that also *in vitro* all four tyrosines of α-syn are subject to nitration [202-206], though only the Tyr39 nitration hinders its ability to bind

lipid membranes [205]. However, nitrated α-syn was unable to form fibrils by itself (probably due to the oligomer formation), but its presence accelerated the fibril formation of unmodified protein [205]. Furthermore, the formation of cross-linked oligomers can be observed after treatment with oxidative agents. Indeed, tyrosine cross-linking promotes the oligomerization process and inhibits its transition to fibrils [205, 207, 208].

The same number of Met residues is present in the α-syn sequence and it can be oxidized to two final products (methionine sulfoxide and the further oxidized product, methionine sulfone). The four methionines are located at codons 1, 5, 116, and 127, and are highly susceptible to oxidation to methionine sulfoxide *in vitro* [209-212], leading to the formation of a more polar product that destabilizes the α-syn protein, but makes it less prone to oligomerization and fibrillation process. The methionine-oxidized protein is also able to inhibit the fibrillation of the non-modified α-syn protein [211]. Two independent studies have proposed that oxidation of Met disrupts *"end-to-end association"* of α-syn necessary for fibril growth and thus guides its aggregation toward less structured, non-toxic oligomers [200, 213].

Others

Several other minor modifications involve the α-syn protein sequence having an impact on its conformation. Aldehydes produced by sugar reducing reactions and lipid peroxidation can form Schiff base adducts with α-syn protein that has been shown to promote its cytotoxic β-sheet rich oligomer formation at the expense of fibrils [214-219] . The N-terminal region of the protein is greatly involved in the cross-linking reaction catalyzed by transglutaminase [220], where the glutamine residues have been found to serve as cross-link acceptors (Gln79, Gln99, Gln109) and Lys60 as a cross-link donor. As with the two previously mentioned aldehyde-mediated reactions, also these cross-linked products promote the oligomer formation [221, 222]. Another common post-translational modification that involves the N-terminal domain of α-syn protein is the acetylation, which is catalyzed by the N-terminal acetyltransferase B complex (NatB). Yet, the exact role of this modification is still poorly understood.

Point mutations in α-syn protein

A30P, E46K, and A53T are the three PD-linked point mutations of α-syn protein that have been found to alter its secondary structure and promote its aggregation [42-44]. Soon after the identification of these pathological mutations several groups have tried to verify whether these modifications might have an impact on the overall structure of the protein. Wrongly, using a combination of low-resolution approaches they found that these

modifications do not have an impact on the structure of α-syn monomer [66, 68, 223]. Only with the use of high-resolution techniques such as NMR spectroscopy it has been revealed that the A30P substitution strongly attenuates the helical propensity in the N-terminal region [224]. A slightly modest effect on structural conformation was observed in the A53T mutation, resulting in a slightly enhanced preference for extended forms in a region around the site of modification [224]. The E46K substitution leads to minor structural changes in the monomeric protein [71] and enhances the contacts between N- and C-terminal parts of the protein [225]. Bertoncini et al. [226] suggest that these mutations tend to modify long-range transient structure in α-syn, even though this conclusion remains under debate [227]. Nevertheless, PD-linked point mutations were shown to accelerate α-syn aggregation *in vitro*; more precisely, A30P mutation promoted α-syn oligomer formation, while A53T and E46K mutations promoted fibril formation [62, 66, 68, 72, 74, 223, 228-230].

1.2.2. Cellular prion protein

The cellular form of the prion protein, denoted as PrP^{C}, is a glycosylphosphatidylinositol (GPI)-anchored protein present on the outside leaflet of the cellular membrane of most cell types in mammals. The gene that encodes for PrP^{C} is called *PRNP* in humans and *Prnp* in other species, it comprises two (in human, hamster etc.) or three (in rat, mouse, sheep, and cattle) exons, but its open reading frame (OPR) is located in a single exon [219, 220]. Studies performed by Weissmann's group showed that both the infective protein component of scrapie PrP^{Sc} and the non-infective cellular form PrP^{C} share the amino acid sequence and are encoded by a single-copy gene [219, 221]. Although the PrP^{C} is highly preserved among species, its physiological function has not been well defined yet. Indeed, the main challenge in the Prion Biology is to clarify its biological function, which in turn will help to comprehend why the post-translational modifications lead to its misfolding into a scrapie form.

1.2.2.1. Structural features of cellular prion protein

The human prion gene encodes a 253-amino acid precursor protein, also denoted as a "pre-pro-protein". This precursor protein contains the signal sequence (first 22 N-terminal residues) that targets the endoplasmic reticulum (ER) in which is cleaved in the lumen. In this sub-cellular compartment other post-translational processing occurs, including the N-linked glycosylation, single disulfide bond formation, and the cleavage of the last 23 C-terminal residues with the subsequent attachment of the GPI moiety. The latter process leads to the

formation of mature PrP^C that in this form consists of 208 amino acids [231]. Remarkably, PrP can be synthesized with three topologies in the ER: a secreted form that reflects the main pathway for PrP synthesis *in vivo*, and ^{Ctm}PrP and ^{Ntm}PrP that have their -COOH or $-NH_2$ terminus in the ER lumen, respectively [232]. The role of the ^{Ctm}PrP and ^{Ntm}PrP isoforms is still not completely elucidated but may be related with neurotoxicity and cellular death, especially in case of inherited prion diseases [233]. As mentioned above, after maturation in the ER and Golgi apparatus, the PrP^C is attached to the cell membrane by its GPI anchor at its C-terminus. The mature protein contains two N-linked glycosylation sites (Asn181 and Asn197 of human PrP; asparagine residues 180 and 196 of mouse PrP) thus, it can be present in its un-, mono-, of diglycosylated form, and it is predominantly localized to detergent-resistant microdomains [234]. A glycosylation profile varies according to distribution through the CNS, since a rather large variety of N-glycans are found attached to both full-length and truncated PrP^C [235, 236]. The role of glycosylation implicated in PrP^C function is less known, but it was suggested that it might regulate susceptibility to conformational conversion [231]. However, molecular dynamic simulations suggest that some attached N-glycans may modulate PrP^C stability [237-239], although experimental evidence is still lacking [240].

The majority of the structural data of PrP^C comes from recombinant bacterially expressed PrP (recPrP). Despite the lack of post-translational modifications, recPrP is structurally equivalent to brain-derived physiological PrP^C. The NMR [241-250] and X-ray crystallography [251, 252] studies have shown that the full-length PrP has a unique 3D organization: a structurally well-defined C-terminal part and flexible N-terminal part (**Figure 1.5**). The protein has a long N-terminal unstructured tail (residues 23–128), while the structured, or globular domain consists of three α-helices (aa 144–154, 173–194, and 200–228), and a two stranded antiparallel β-sheet (aa 128–131 and 161–164) flanking the first α-helix. This flexible N-terminal tail is present in most of the animal species studied, except deer and elk [253], and contains a series of four or five octapeptide-repeat regions (OR) of eight amino acids (PHGGGWGQ). This region does not seem to be a part of a β-sheet rich core of the PrP^{Sc} form, and there is no defined experimental evidence for its role in prion infectivity [254]. However, the insertion of one extra octapeptide-repeat region is linked to inherited forms of prion diseases [255, 256], suggesting that it might play a role in modulating the conversion of the protein into the pathogenic form. Within the OR, histidine and tryptophan residues were found to be essential for the coordination of copper and other bivalent metals, suggesting a role for PrP^C in regulating the homeostasis of these cations. Indeed, several studies reported the existing interaction between PrP^C and copper, postulating

that the protein might act as its transporter, or a scavenger for Cu^{2+}-generated free radicals [257]. Additional histidines at residues 96 and 111 are also involved in Cu^{2+} binding [258]. This region seems to be critical for prion conversion, raising the possibility that the binding of this bivalent metal could modulate the conversion of $PrP^{C} \rightarrow PrP^{Sc}$. However, animals treated with excess of copper [259] or with metal chelators [260] in both cases showed a late onset of disease symptoms. Together, these data indicate that currently there is no consensus and, often, contrasting results regarding the specific physiological function of copper binding, as well as the implication of this metal in developing prion diseases.

As mentioned above, globular domain of the prion protein is a structurally well-defined region encompassing residues ~124-228, consisting of the three α-helices (α_1, α_2, and α_3) and two very short β-strands which form an antiparallel β-sheet (β_1 and β_2). The α-helices have been show to undergo a vast structural rearrangement into β-sheets in the pathogenic form. Indeed, Fourier transform infrared spectroscopy (FTIR) experiments show that the α-helix content of PrP^{C} passes from 48% to ~24% in the pathogenic form, while the β-sheet content increases from 8%, in the physiological condition, to ~50% in PrP^{Sc} form [261, 262]. Helices α_2 and α_3 form the bulk of the structure and are covalently linked by a single disulfide bond using the two cysteine residues (Cys179 and Cys214) (**Figure 1.5 B**). Data reported by Knaus et al. [263], using a crystallography technique, showed that the breaking and reforming of the disulfide bridge might explain the intermolecular rearrangements that occur during transition (oligomerization) that lead finally to the pathogenic PrP^{Sc} isoform formation. However, it is not clear whether these interactions really occur *in vivo*, or if the structures observed might just be an effect of the crystallization process. Nevertheless, the fact that another recent study reported an analogous finding, working on PrP fragments, is encouraging and might shed light on the $PrP^{C} \rightarrow PrP^{Sc}$ conversion process.

Another important structural feature of the PrP^{C} is the presence of a hydrophobic domain (HD, residues 111-134), which is mainly found between the short β-sheet β_1 that wraps around helix α_1. The HD contains the palindromic alanine-rich sequence AGAAAAGA, that lies within the so called "*toxic peptide*" [264]. It has been shown that peptides corresponding to the palindrome are important in the conversion of PrP^{C} to PrP^{Sc}; indeed, deletion of this region prevents conversion of PrP into pathogenic form [265, 266], and interferes with *in vitro* formation of protease-resistant PrP [267].

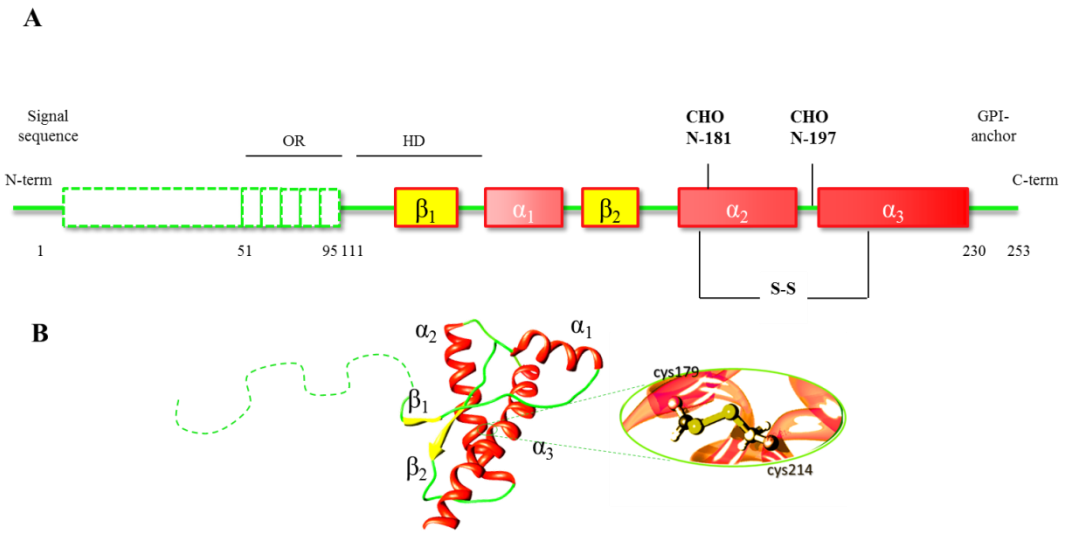

Figure 1.5. Human PrP primary amino acid sequence (A) and 3D-structiure of the C-terminal fragment huPrP(90-230) (PDB code: 1QM0) (B). **A**) A primary structure of the cellular prion protein including post-translational modifications, like the two glycosylation sites (N-18 and N197), the di-sulfide bond (between cysteins 179 and 214, evidenced in (**B**)); B) Tertiary structure of the cellular prion protein shows the structurally well-defined C-terminal fragment (consisting of three α-helices showed in red and two antiparallel β-strains represented in yellow), whereas the N-terminal flexibly disordered "tail" is represented with the green broken line.

1.2.2.2. The PrP^C localization and its physiological roles

The cellular prion protein is highly expressed within both the CNS and the PNS; its content varies among different brain regions, between various cell types, and among cells with distinct phenotypes. However, the fact that the protein is highly expressed in neuronal cells indicates that PrP^C has a singular significance in neurons. Notably, the high concentration has been observed at the synapse level [268]. Nonetheless, conflicting results were reported concerning its exact synaptic localization, since it is still under debate whether it is expressed in pre-, post- synaptic level, or both [269-271]. In line with this, several findings report that PrP^C could play a role in synaptic structure, function or its maintenance [272, 273]. In an elegant experiment Kanaani et al. [273] incubated cultured rat hippocampal neurons with recPrP and showed that in these conditions the prion protein induces a rapid increase of axons and dendrites, and increases the number of synaptic networks. This observation indicates that PrP^C might regulate the synapse formation.

Similarly, considerable amounts of PrP^C have been found in peripheral tissues, including various cellular components of the immune system, bone marrow, and blood (**Table 1.3**), suggesting different physiological roles also in the PNS.

Table 1.3. Expression and distribution of prion protein (modified from [274]). T cells, T lymphocytes; NK, natural killer cells; DC, dendritic cells; B cells, B lymphocytes; PMN, polymorphonuclear leukocytes; PBMC, Peripheral blood mononuclear cells.

Species	Organ/tissue	Cellular type
Central Nervous System		
Hamster	Brain (hippocampus, septum, caudate nucleus, thalamus)	Neuron cell bodies, intracellular, presynaptic
		Manly along axon tracts
	Developing brain	
		Presynaptic
	Hippocampus	Pre- and postsynaptic
	Cerebellum	
Mouse	Brain, olfactory bulb	Neurons, intracellular, neuronal processes
		Neurons
	Embryonic brain, spinal cord	
Rats	Cerebellum	Neuron and glial cell bodies and processes
		Retinal precursors and differentiating neurons
	Neonatal retina	
Human	Brain,	Presynaptic, not in cell bodies
	Hippocampus	Presynaptic
	Cerebellum	Neurons
Peripheral Nervous System		
Hamster	Blood, heart, skeletal muscle, lung, gut, spleen, testis, ovary, and others	Both in neuronal cell bodies and neuropil
	Stomach, intestine, lung, kidney	Secretory globules
	Muscle	Subsynaptic sarcoplasm, not postsynaptic plasma membrane
Mouse	PNS, bone marrow, lymphoreticular system, gut, lung, kidney, testis, skin, not liver	Peripheral axons, neuron cell odies, not glia; hemopoietic progenitors, megakaryocytes, monocytes, not granulocytes in bone marrow; dendritic cells, pericytes, intraepithelial lymphocytes in various tissues
		Submucosa, muscularis mucosa
	Intestine	
		Subsynaptic sarcoplasm, not postsynaptic plasma
	Muscle	membrane, myoblast cell lines
Human	Stomach, kidney, spleen, enteric nervous system	Secretory globules, enteric glia
	Olfactory mucosa	Olfactory epithelium
	Skin	Keratinocytes
	Muscle	Subsynaptic sarcoplasm, not postsynaptic plasma membrane
	Blood	Lymphocytes and lymphoid cell lines, monocytes, not erythrocytes, not mature granulocytes monocytes, T cells, NK cells, B cells, $CD34^+$ cells, megakaryocytes, platelets
Bovine	Spleen, lymph nodes, blood	Follicular DC, B cells, lymphocytes, monocytes, PMN
Sheep	Blood	B cells, T cells, monocytes, not granulocytes, not erythrocytes, PBMC, platelets, not granulocytes

Although mRNA and protein levels usually correlate well, one specific study reported marked disparity within the CNS between mRNA and protein levels of PrP^C [275]. Here, in situ hybridization and immunohistochemistry experiments showed a big discrepancy between the PrP mRNA, and PrP^C protein levels, respectively. The non-radioactive *in situ* hybridization mRNA analysis displayed a high PrP mRNA content within dopaminergic neurons of the SN, olfactory glomeruli, and locus coeruleus, while the immunoblot analysis was PrP^C-negative. Also, within the deep cerebellar nuclei, all neurons expressed high levels of PrP mRNA, but only interneurons contained high protein levels of PrP^C. The motivation for this discrepancy between PrP mRNA and protein levels within the CNS is still unclear. It has been reported that the PrP^C expression depends on both maturation and cellular activation in different cell types [276-282]. The overall evidence for heterogeneous, cell type specific, and regulated expression of PrP^C is relevant both for the understanding of pathogenesis and of physiological functions of PrP^C. The previously mentioned study conducted by Ford and collaborators [275], failed to localize PrP^C within dopaminergic neurons, in contrast to the more recent work which addressed this question, showing a localization of PrP^C in dopaminergic neurons and in dopaminergic synapses in the striatum [283]. This work demonstrated that PrP^C can be considered as an important modulator of the dopaminergic neurotransmitter system. This observation was supported by the *in vivo* behavioral and neurochemical studies on PrP null-mice which indicate that PrP^C deletion disrupts the homeostasis of the dopaminergic system.

Since PrP^C has been strongly conserved throughout evolution in mammals, there was great expectation that ablation of *Prnp* gene would reveal a physiological function of this puzzling protein [284]. Nevertheless, the first created PrP-null mice, in general had no obvious phenotype; including no anatomical abnormalities in the brain, nor in peripheral tissues, speculating that either PrP^C is not necessary for normal development, or its absence is compensated by a redundant protein which maintains an important phenotype [285, 286]. Importantly, these mice were not susceptible to the PrP^{Sc} infection and pathology transmission, supporting the hypothesis that the expression of the PrP^C is an absolute requirement for development of TSEs [285]. Although the original reports on the *Zurich* and *Edinburgh* PrP-null mice reported no phenotype, many subsequent studies have shown that *Prnp* knocked-out (KO) mice have a number of phenotypes, some of which have been questioned and many of which are not obvious. In contrast to these mice lines, old PrP^C KO mice (*Nagasaki*), developed ataxia and Purkinje cell degeneration. These mice were generated by replacement of *Prnp* ORF, 0.9 kb of intron 2, 10 bp of the 5'-noncoding region, and 0.45

kb of the 3'-noncoding region by a neo cassette [287]. However, the reintroduction of *Prnp* abolished the observed phenotype, leading to the assumption that it was due to the lack of PrP^C [288]. Later it was determined by several groups that these different phenotypes observed in three mice lines was due to the upregulation of a Doppel (Dpl), a protein encoded by a *Prnd* gene, which is positioned 16kb downstream of *Prnp*. Indeed, the deletion strategy used in *Nagasaki* mice fused PrP's promoter to Dpl, driving expression of Dpl in the brain, where it is not normally expressed [289, 290]. Thus, showing that only the ectopic expression of Dpl, rather than the absence of PrP^C, was the cause of the neurodegeneration observed, precluding an association of these differences with the lack of PrP^C expression. Importantly, many roles have been attributed to PrP^C using also studies in cell culture [291, 292], not only Tg animals.

To overcome the problem of *Prnp* deletion approach, recently Schmitt-Ulms' group describe the generation of PrP knock-out clones in cell culture using a novel genome-editing technology, CRISPR/Cas9 (clustered regularly interspaced short palindromic repeat) [293]. This technique uses RNA, rather than peptides, to distinguish its target site in the genome and does not even need drug resistance cassettes. The authors used the aforementioned technology to ablate PrP expression in N2a neuroblastoma cells, C2C12 myoblasts and NMuMG epithelial cells. Following the removal of PrP^C in NMuMG cells, a global proteome analysis revealed changes in ~120 protein levels that contribute to the organization of extracellular matrix, and are involved in regulation of the cell junction or the cytoskeleton organization, strongly indicating a role of PrP in cellular adhesion and differentiation. Although the changes observed were modest for a majority of these proteins, and did not exceed a three-fold change, the analysis used here permitted the conclusion that even smaller levels of up-/downregulation were real and not an artifact of the method.

The use of cell culture, in particular of these cell clones, should facilitate efforts to study the cellular biology of PrP^C together with the identification of its role in TSEs and other neurodegenerative diseases like AD and PD. Ideally, their use could ease the studies of signaling pathways downstream of PrP. Indeed, several roles in signaling have been attributed to the cellular prion protein, including: PrP^C-mediated signal transduction, signaling dependent on PrP^C-caveolin interaction; moreover, evidence that PrP^C mediates activation of the cAMP/protein kinase A (PKA) pathway could be studied in depth. Other physiological roles ascribed to the PrP^C protein are, involvement in MAP kinases pathway since expression of PrP^C affects the basal level of Erk activity, and phosphorylation of non-receptor tyrosine kinases (Syk and Pyk2, and adaptor protein Cbl). Associatios between the cellular prion

protein and calcium-mediated cellular events, the activation of Protein Kinase C (PKC), and with phosphoinositide 3-kinase (PI 3-kinase)/Akt Pathway have also been reported.

1.2.2.3. Post-translational modifications and mutations of prion protein

Normally, the mature prion protein undergoes some post-translational modification, such as glycosylation at the two Asn residues (N181 and N197, **Figure 1.5**). Other modifications that influence PrP^{C} structure, however, have been identified. For example, it has been reported that deposits of PrP^{Sc} associate with the presence of oxidative stress in TSEs, indicating that these conditions might influence the normal conformation of PrP^{C} leading to the disease. Oxidative stress causes a harsh condition since reactive oxygen and/or nitrogen species modify cellular components resulting in lipid peroxidation, nitration and/or cross-linking of proteins and nucleic acid mutations. One important *in vitro* study reports that under such conditions the secondary structure of recPrP assumes a structure similar to that reported for PrP^{Sc} [294]. Importantly, the physical and biochemical features of the prion protein found in these environments are associated to disease-linked forms, raising the possibility that such modifications of PrP^{C} structure might have a role in the onset of PrP^{Sc} formation and could contribute to the development of prion plaques *in vivo*. Several other types of modifications, chemical and enzymatic, have been detected in the prion protein (e.i. aspartate deamination, aldehyde adducts, proline hydroxylation).

Aside from GPI-anchor attachment and N-linked glycosylation, PrP^{C} undergoes further post-translational modifications including two proteolytic cleavage events termed α- and β-cleavage that produces N-terminal (N1 and N2) and C-terminal (C1 and C2) fragments respectively [295, 296]. This processing has been shown to regulate its physiological function generating biologically active fragments that can even modulate the course of prion progression.

The effect of chemical modifications on the secondary structure is similar to those of point mutations; which also influence the susceptibility to conformational changes that could be dramatic for the disease progression [297]. Indeed, as for PD, TSEs also can be genetic and a large pool of *PRNP* mutations has been identified in humans. About 10 to 15% of prion disease cases are related to the presence of an autosomal dominant mutation of the prion protein gene. Also the common polymorphic codon 129 (M/V129) of *PRNP* plays an important role in risk and phenotype of sporadic and genetic prion diseases [298, 299]. Studies suggest that phenotypically different familial prion diseases might depend on this polymorphism. However, this variant does not independently promote disease, but it seems that the homozygosity at the codon might increase disease susceptibility. Other point

mutations can occur on the *PRNP* gene: D178N, V180I, E200K, V210I, V203I for CJD and P102L, P105L, A117V, F198S for GSS [300]. Interestingly, only one haplotype seems to cause FFI, the D178N mutation in the presence of normal variant M129, whereas the combination with V129 causes fCJD [301]. Somehow, these mutations influence the protein conformational arrangement, cellular processing and/or interactors or its localization, such that the conversion of PrP^{C} to PrP^{Sc} and the aggregation process is promoted, resulting in neurodegeneration and ultimately in death [302-304].

1.2.2.4. A role for prion protein in AD

As previously mentioned, PrP^{C} might be implicated in the pathogenesis of AD, more precisely it may have two roles: a role in the physiological regulation of APP processing, and a role in the pathological progress of AD by mediating Aβ toxicity through the binding Aβ-oligomers. Indeed, in 2007 Hooper and co-workers [305] reported an interaction between the PrP^{C} and the β-secretase (BACE1), the enzyme that regulates the production of Aβ, from APP. This initial cleavage of APP by the β-secretase releases a soluble N-terminal fragment, sAPPβ, while the remaining membrane fragment C99 gets further processed by γ-secretase into the amyloidogenic Aβ peptide and AICD. Therefore, the interaction of the PrP^{C} and BACE1 decreases the amyloidogenic processing of the APP with the consequent decrease of Aβ levels, leading to the hypothesis that PrP^{C} might be protective against AD. On the contrary, Lauren et al. [306] recently reported that Aβ-oligomers bind to full-length PrP^{C} and additional analysis indicated that PrP^{C} has high affinity and selectivity for these oligomers. More detailed review will be given in the section *"1.6. Cellular prion protein as a receptor for amyloid form proteins"*. Strittmatter's team also confirmed these results in brain slices taken from mice that were knocked-out for the prion protein, and found that Aβ did not cause defects in long-term potentiation, which is important for long-term memory formation [307]. In addition, using an antibody that blocks the PrP^{C} also prevented damage caused by the Aβ peptides. Taking all these findings together, they might have some important implication in developing therapies for neurodegenerative disorders.

1.3. Strategies for amyloid generation and detection

In the past few years, considerable progress has been made in our understanding of prion diseases, through the development of several approaches for producing amyloid fibrils starting from recombinant PrP. Indeed, in the prion field important *in vitro* techniques have been developed to reproducibly form synthetic fibrils. The *in vitro* aggregation methods are potent molecular tools for studying the mechanisms of neurodegeneration, and it could be useful to transfer them also to the α-syn field. In this section we recapitulate all relevant studies and experimental data that have led to the generation of fibrils of PrP and α-syn using different *in vitro* methods. The most important *in vitro* fibrillation techniques for both, α-syn and PrP^{C} proteins, are:

1.3.1. Amyloid Seeding Assay (ASA)

Prusiner and co-workers defined "amyloid seeding assay" (ASA) as the *in vitro* method for amyloid fibril formation that uses preformed PrP^{Sc} as seeds. For instance, the partially purified prion strain preparation may act as a seed for the polymerization of recPrP in amyloid fibrils. This method is able to detect PrP^{Sc} (both PK sensitive and resistant) from different human or animal infected samples [308, 309]. An additional characteristic is the possibility to shake the sample in order to enhance the interaction between recPrP and the seed (amyloids from recPrP or purified PrP^{Sc} from infected samples) and promote the production of multiple seeds. Moreover, the unfolding of recPrP is enhanced by the low denaturant concentration (usually GndHCl). This *in vitro* process is monitored simply by the ThT dye. Once ThT is added to recombinant prion proteins, it becomes incorporated when polymerization occurs causing an increase in fluorescence over time. When used in conjunction with multi-well plates and automated fluorescence plate readers, the ThT represents a feasible, highly sensitive, high-throughput approach to detect conformational changes of proteins. In the presence of amyloid, ThT undergoes an increase of fluorescence and a spectral shift in the excitation/emission maxima that is measured.

Legname *et al*. reported a production of infective synthetic prions via the *in vitro* conversion of recPrP into PrP^{Sc} [123]. The same authors reported in their previous work [310] that depending on the reaction conditions, two misfolded forms were adopted: at low pH (3 to 5) and in the presence of partially denaturating conditions (urea 4-5M) a β-oligomer PrP^{Sc}-like form is obtained with no further aggregation, while under the neutral or slightly acidic pH and low concentration of urea (1-2M) the longer fibrillar amyloids were obtained. The

polymerization process was monitored using ThT as an amyloid dye which showed strong increase of fluorescence upon binding to β-sheet rich structures. Notably, in this work the authors discovered that the addition of a seed of pre-folded amyloid to the fresh reaction reduces the time of fibrillation process (lag phase), demonstrating that recPrP fibrils can be induced by seeding process. With the following work published in 2004 [123], it was assessed that the conversion after polymerization of recPrP(89-230) into amyloid fibrils is sufficient for generation of infectivity once these get injected into mice. Indeed, the pre-folded amyloid fibrils (defined as "unseeded") and the seeded were intracerebrally injected into mice that overexpress MoPrP(89-230) protein, the Tg9949 mice. After injection, seeded amyloid fibrils induced shorter incubation time (382 days) and PK resistance if compared to unseeded fibrils (473 days and PK sensitivity). This survival time and biochemical profile differences were accompanied by diverse neuropathological features; such as vacuolation and gray matter PrP^{Sc} deposition. This is indicative of two different prion strains that were subsequently denoted as MoSP1 (Mouse Synthetic Prion Strain 1, from seeded PrP fibrils) and MoSP2 (Mouse Synthetic Prion Strain 2, from unseeded PrP fibrils). The serial passages of MoSP1 BH into FVB-WT mice and different Tg mice shortened the incubation period and showed the infective property of the material. Also, the conformational stability measured (Gnd HCl) was very high (~4.5M) compared to naturally occurring prion strains, and it confirmed that a novel synthetic prion strain had been obtained. Combining these findings it was demonstrated that the length of incubation time in mice is directly proportional to the conformational stability of the prion strain [308, 311]. Consistent with this hypothesis, studies with other amyloid-prone proteins (tau, α-syn, Aβ) showed that less stable fibrils have a higher tendency to break, and create new seeds for the conversion.

1.3.2. Protein Misfolding Cyclic Amplification assay (PMCA)

PMCA was developed by Soto's group, and it consists in multi-round sonicated reactions with healthy brain-derived PrP^{C} as a substrate with an extremely low titer of PrP^{Sc} derived from infected material [312]. This method mimics the PrP^{Sc} autocatalytic amplification by which as little as 1 ag of infected material can be detected [313]. The sonication step is necessary to break down the aggregates and to generate multiple smaller PrP^{Sc} nuclei that will function as a seed in the subsequent amplification phase. The products are then diluted in new healthy BH for further amplification cycles. To confirm the presence of scrapie product, different biochemical assays, such as immunoblotting after PK digestion, insolubility in non-ionic detergent have to be performed. Notably, the PMCA-derived PrP^{Sc} was shown to be

infectious when intracerebrally injected into WT Syrian Hamster (SHa). The same group established that the PMCA can be modified to generate *de novo* prions, starting from normal BH in the absence of any PrP^{Sc} seed. *De novo* generated PrP^{Sc} was infectious when inoculated into WT SHa, producing a new disease phenotype with distinctive clinical, neuropathological and biochemical characteristics [312]. Recent findings show that RNA and lipids are potentially important cofactors that facilitate the PrP conversion *in vitro*, and thus might promote the *de novo* prion formation. Indeed, Wang et al. used the PMCA to produce synthetic prions staring from recombinant PrP (mouse full-length) in the presence of both lipid (the synthetic phospholipid POPG) and RNA (total RNA isolated from mouse liver). Afterwards, they performed the intracerebral injection in WT CD-1 mice and showed that the PMCA generated material was able to cause *bona fide* prion disease; about 150 days post infection animals developed classical neuropathological traits of prion diseases. Furthermore, infected BH was able to propagate the disease to recipient WT mice. Additionally one modification of PMCA was reported by Chen and colleagues, called quantitative PMCA (qPMCA), in which PrP^{Sc} content is estimated by the number of PMCA rounds necessary for a positive response [314]. Using this approach the authors were able to quantify the PrP^{Sc} concentration in different tissues of diseased animals, including brain, spleen, blood and urine. Taking together these findings, the PMCA technique has contributed to elucidate the mechanism of prion conversion, the nature of the infectious agent and the detection of tiny quantities of PrP^{Sc} in biological samples [315].

Importantly, Herva *et al*. [316] reported the use of this technique to form *de novo* α-syn fibrils. This study showed that the PMCA-derived α-syn amyloids biochemically possess the same characteristics of α-syn aggregates present in PD patients' brains. These *in vitro*-formed aggregates were able to chronically infect the neuroblastoma SH-SY5Y cell line (the aggregates were maintained up to 10 divisions after the initial exposure), and could be used to screen anti-aggregating agents for PD. Indeed, the authors validated this *in vitro* model using some already proven anti-amyloid drugs. One additional study reported the use of adopted PMCA for the amplification of chimeric α-syn homologous protein with an inducible dimerizing portion (denoted as $\alpha\text{-syn}^{Fv}$) [317]. More specifically the $\alpha\text{-syn}^{Fv}$ aggregates were used as a seed for the amplification of α-syn amyloids in modified PMCA [317, 318]. However, the use of this technique for α-syn fibrillation requires high concentrations of protein, the presence of the seed and still the reaction times are quite long. Therefore, several adaptations still have to be performed to achieve satisfactory results in refining the reproducibility of recombinant α-syn seeds.

1.3.3. Real-Time Quaking Induced Conversion assay (RT-QuIC)

Researchers at Rocky Mountain Laboratories have developed a new prion seeding assay called Real Time Quaking Induced Conversion Assay (RT-QuIC) that gives end point quantitation for measuring the levels of prions in infected samples. This assay is a result of combination of the original QuIC assay and the ASA. In this assay, very small amounts of infectious prions are added to normal prion protein to seed, or cause the misfolding, of the prion proteins [319]. The assay is quantitated by measuring serial dilutions of the samples and determining the loss of seeding activity (SD_{50}, dilution at which 50% of the wells became ThT positive), which is the end point dilution. As in the ASA, the readout is based on 96-well plate format with the use of florescent ThT dye, which is a big advantage since it can be included in the mixture reaction directly. This method is analogous to that of end-point dilution titrations classically used in animal bioassays but with greatly reduced times and costs. For instance, the end-point RT-QuIC analysis afforded the detection and quantification of prion seeding activities in BH and CSF of 263K-infected hamsters, and in nasal lavages from TME-infected animals [320-322]. Moreover, analogous end-point dilutions of scrapie BH with both the animal bioassay and the RT-QuIC were achieved [319]. The authors argued that the lag phase might be considered analogous to the TSE incubation period between the injection and the near lethal stage of disease, since a clear dependence of the lag phase on the concentration of seed was observed.

Previous findings have shown that bank vole, and Tg mice expressing bank vole prion protein, are susceptible to a vast range of prions from different species [323, 324]. With this in mind, Caughey and co-workers have shown that bacterially expressed full-length recombinant prion protein from bank vole is an effective substrate for RT-QuIC detection of every type of prion that has been tested so far (humans, cattle, sheep, dear, elk, mouse and hamsters), including those that previously could not be detected using RT-QuIC or the PMCA [325]. Furthermore, this study shows that bank vole RT-QuIC-derived prions have strain-dependent PK-resistance banding profiles that could further facilitate prion strain discrimination. Moreover, using bank vole as a substrate in RT-QuIC it is possible to discriminate between the two bovine strains, classical and atypical L-type BSE. Therefore, using the bank vole prion protein as an apparently universal substrate for RT-QuIC might significantly improve the manageability, efficiency and cost-effectiveness of detecting and discriminating numerous prion strains.

Several improvements and adaptations have to be accomplished yet in order to develop protein aggregation assays for Aβ and α-syn using RT-QuIC technology.

1.4. Strain phenomenon in neurodegenerative diseases

Another peculiar aspect of neurodegenerative diseases is the existence of strains. In Prion Biology strains are encoded by diverse fibrillary structures that determine the incubation periods of disease and are thought to be responsible of various clinical symptoms and neuropathological profiles. Indeed, it has been confirmed that these different phenotypic TSE variants, once inoculated into distinct hosts, cause disease with reliable characteristics, such as incubation period, individual patterns of PrP^{Sc} distribution and spongiosis, and relative severity of the spongiform modifications within the CNS. Biochemically PrP^{Sc} can vary in its protease resistance, glycosylation profile, electrophoretic mobility, and sedimentation. Most importantly, it has been established that the injection of brain homogenates coming from ill animals maintained the same clinical and biochemical outcomes and could be maintained through several passages in models of prion diseases.

The prion strain phenomenon can be explained by the formation of different PrP^{Sc} conformers that can be stably and faithfully propagated in rodent animal models. Indeed, different biochemical, spectroscopy, and microscopy approaches confirmed the postulate that dissimilarities between prion strains lies in the PrP^{Sc} three-dimensional structure diversity [326-332]. Specific prion strains are able to affect specific brain regions generating differences in clinical signs, such as those observed in different syndromes. This has been shown for the first time in 1961 when Pattison and Millson infected goats with the same batch of infectious scrapie agent and the animals developed two different clinical phenotypes, which the authors defined, according to pathological manifestations, as "*scratching*" and "*nervous*" [333]. Nowadays there are different parameters used to differentiate and classify several prion strains, such as incubation period, histological damage profile and clinical signs (for the *in vivo* characterization studies) [334-336]. For example, injection of distinct prion strains typically results in distinct and reproducible incubation times [335, 337], while using a histological profile approach (also denoted as lesion profile) different mouse strains can be identified [338]. Likewise, a list of numerous clinical symptoms can be useful to differentiate strains since it has been demonstrated the correlation between the two features [339]. On the other hand, the biochemical profile can specifically distinguish various prion forms (i.e. SDS-PAGE mobility after PK digestion [134, 340, 341], glycosylation pattern [134, 341, 342], extent of PK resistance [340] and denaturation by chaotropic agents [326, 340], and sedimentation [340]). To date a number of prion strains have been identified [343].

Important of note is the existence of phenomenon defined as "species barrier", which is the ability to infect some species and not others. More specifically, in some species PrP^{C}

conformation does not permit conversion by prions coming from other species. This has been observed in rabbit, an animal that has been unable to be infected by various sources of prions. However, this notion has been withdrawn by a recent use of PMCA technique with which it has been showed that also these animals are both susceptible to and capable of developing clinically transmissible prion disease [344]. One opposite example is given by the bank vole, which is considered an universal acceptor for prions from multiple other species [324]. This rodent lacks the species barrier, and it can be considered also as an universal substrate for RT-QuIC-based detection and for discrimination of prion strains [325]. However, the existence of the strain phenomenon is not only a scientific challenge, but it also denotes a serious risk for public health [345]. In fact, interspecies prion transmission from cattle to human is the most significant problem that has an impact on public health [346-348]. There is now strong experimental evidence that the agent responsible for the occurrence of BSE in cows is the same agent responsible for the outbreak of vCJD in humans. Differences like clinical manifestation of the disease, the profile of brain damage and the biochemical features of PrP^{Sc} have been observed between vCJD and sCJD, which develops spontaneously [349]. Most importantly, two different subtypes of PrP^{Sc} in CJD brains have been distinguished, such as type 1 and 2 in sCJD and type 2b in vCJD, according to the biochemical profile after PK digestion [350, 351]. In addition, vCJD type 2b has a marked similarity to the strain of PrP seen in BSE. Nevertheless, it still has to be explored whether these PrP^{Sc} forms are illustrative of distinct prion strains. Additionally, the human polymorphism at codon 129 (Met or Val) can influence the CJD type and the course of the disease [298, 299], since it has been reported that it might influence protein conformation. Moreover, BSE has been found in two diverse molecular forms defined as atypical BSE: higher (H)-type which is characterized by the PK-resistant fragment that is higher than classical BSE, or lower denoted as (L)-type [352]. Importantly Legname et al, verified the transmissibility of distinct synthetic prion strains, denoted as MoSP1 and MoSP2 [353], that were obtained using seeded and unseeded protocols, respectively [123]. The same laboratory showed, in a subsequent work [354], that serial passages in mice are necessary for the adaption of the prion strain that finally exhibit common physicochemical features.

However, not only PrP^{Sc} is characterized by the existence of different strains. Similarly, Melki and co-workers reported the existence of α-syn strains obtained *in vitro* using two different reaction conditions characterized by two distinct fibrillary structures [87]. In a recent work the authors confirmed that the two different polymorphs behave differently once injected in WT and α-syn overexpressing rats [86]. Indeed, the *fibrils* and *ribbons* (the two

distinct strains) presented different neuropathological features, and PK resistance profiles once injected within SN and stratum. Most importantly, the injection of *ribbons* caused a distinct histopathological phenotype displaying PD and MSA traits accompanied by the deposition of insoluble α-syn in oligodendroglial cells, leading to the notion that distinct α-syn strains might be responsible for different synucleinopathies in humans. Two other independent recent studies reported by Prusiner's and Vila's group showed that the α-syn aggregates isolated from MSA and PD patients, respectively, and injected into mice led to development of MSA and PD-like neuropathologies in recipient hosts [88, 89]. Distinct α-syn structures have been observed in human brains of PD patients where it has been found that LBs in the midbrain were morphologically different from those found in the cortical regions [49]. Analogous advancement in the field of α-syn strains has recently been described for synthetic fibrils produced from recombinant protein, whereby serial passage *in vitro* resulted in the conversion of one strain of α-syn fibrils into the other [90]. After injection of newly formed or repeatedly seeded α-syn fibrils in animals, the authors observed different lesion profiles and differential induction of tau aggregation by the two kinds of preparations. More precisely, the seeded α-syn fibrils were able to induce a major aggregation of endogenous tau protein in both Tg and non-Tg neurons, where it co-localizes with these neuritic α-syn inclusions. In fact, in patients with distinct synucleinopathies the relationship between tau and α-syn accumulates are frequently observed supporting direct cross-seeding between the two diseases [355-357]. Taken altogether the existence of different α-syn strains could be behind the remarkable diversity of synucleinopathies among different individuals [358].

The initial studies performed in 2005 showed that $A\beta_{40}$ fibrils obtained from *in vitro* fibrillation, subjected to or not to the agitation step, exhibit different neurotoxicity in cell culture [17]. This finding closely parallels prion strains since different structures have been attributed to these two preparations. Moreover, Aβ plaques extracted from two different AD patients that had distinct neuropathology and clinical history were used to seed the Aβ fibrillation *in vitro*. Electron microscopy and solid-state NMR techniques confirmed that the brain extracts from two different patients seeded the formation of two structurally distinct Aβ forms [19]. Additional evidence for the presence of Aβ strains came from the use of strictly controlled *in vitro* fibrillation conditions of synthetic $A\beta_{40}$ and $A\beta_{42}$ [11]. The same group established that at least two distinct strains are present in AD patient brains and that these Aβ strains are serially transmissible during serial passages in mice [359].

Evidence of the existence of distinct strains of tau protein has also been reported. A detailed study conducted by Sanders and co-workers [31] showed that, when the cells

expressing truncated tau protein,are exposed to fibrils of truncated tau they develop tau clusters that have different shapes (that the authors define as clones). The pattern of these clones is stably passaged over generations and transmissible to naïve cells. Subsequently, the authors injected distinct cell lysates into Tg animal models, and as in cell culture studies the distinct neuropathological patterns were stably propagated through various generations of mice. Other recent findings associate the existence of tau strains with distinct tauopathies [33, 360, 361]. Indeed, it has been found that the inoculation of Tg human tau mice (line ALZ17) and non-Tg mice with BH from patients with different tauopathies induces certain neuropathological features of the diseases [33]. A range of distinct filamentous morphologies have been identified in brains of patients with human tauopathy [362] and distinct conformers of accumulated tau may cause distinct tauopathies, based on specific brain regions and cell types involved in the disease [33].

1.5. Prion-like spreading of α-syn pathology

A number of recent experimental findings suggest that protein aggregates, which are the hallmarks of major neurodegenerative diseases, spread in a prion-like manner [363, 364]. Although the majority of reported *in vivo* findings have focused on Aβ, tau, α-syn and PrP^{Sc} it is tempting to hypothesize that the same mechanism could be characteristic of all neurodegenerative proteinopathies spreading. Studies are currently ongoing to verify how common this pathogenic mechanism is among the diseases. In fact, several lines of evidence suggest that transmission of accumulated α-syn occurs in a prion-like manner. As previously mentioned the α-syn protein is a key player in the pathophysiology of PD and other diseases, collectively defined as "synucleinopathies".

The first evidence that PD pathology uses a prion-like mechanism for spreading was shown in patients that recieved embryonic neuronal transplants as a therapeutic strategy. In the late 1980s, some patients with idiopatic PD received intrastriatal grafts of human fetal dopaminergic neurons, as a therapeutic strategy. Unfortunately, several years later (11-16 years) postmortem analysis have shown that LBs were present in the grafts, raising the possibility of aggregates' spread from diseased cells to the transplanted ones [54-56]. Since LBs were not present in all grafts further studies were necessary to understand what was happening at the cellular level and whether the host-to-graft transmission theory was correct. This theory assumes that α-syn could be exocytosed from living cells, or it could be released by dying cells into the surrounding extracellular space. Afterwards, grafted neurons could up-take this α-syn, although the exact mechanism has yet to be discovered (several mechanisms have been proposed, see **Figure 1.6**). Once within the cytoplasm of the grafted neurons, the exogenous aggregated α-syn could act as a template that promotes misfolding of soluble α-syn, eventually leading to the formation of LBs [54]. As in prion diseases where the PrP^{C} expression is required for the conversion into PrP^{Sc}, similarly endogenous expression of α-syn is necessary for the development of α-syn pathology *in vitro* [79] and *in vivo* [76]. Also the conversion mechanism might have the same molecular characteristics since for both, PrP^{Sc} and β-sheet rich α-syn, the seeded-nucleation elongation process has been confirmed [365, 366]. A previously mentioned Braak's model for α-syn spread is highly in agreement with the prion-like mechanism of transmission [50]. In fact this model has proposed that propagation of α-syn aggregates occurs via interconnected brain pathways, in a stereotypic, topographical manner [50] (also shown in **Figure 1.1**). The authors described the presence of α-syn in its pathological form in brain regions such as caudal raphe nuclei, coeruleus-subcoeruleus complex and SN. While, some groups have confirmed these findings [367-369], others were

not able to establish this theoretical caudo-rostral pattern of progression [370, 371]. There are still several open questions, but many experimental findings corroborate the idea that α-syn spread via a prion-like infectious progression is central to PD.

The findings from human samples suggest cell-to-cell transmission of α-syn aggregates, and are supported by different *in vitro* and *in vivo* studies [2, 54, 75, 77-79, 372-376]. Recent *in vitro* studies confirmed that recombinant α-syn fibrils could act as a seed for the recruitment of endogenous α-syn into a insoluble aggregated form in cells that overexpress α-syn protein [75, 79, 375]. As mentioned above (Section 1.1.2 α-syn in Parkinson's disease) the formation of these α-syn pathological species within host cells leads to modifications in synaptic functions, compromising neuronal excitability and connectivity, and finally ends in neuronal death. Desplats and collaborators [77] instead proved the α-syn cell-to-cell spread *in vivo* using GFP-labeled mouse cortical neuronal stem cells that were injected in the hippocampus of Tg human α-syn mice. After 4 weeks of injection, 15% of the grafted cells exhibited human α-syn deposits, and just a few of these had inclusion bodies in the cytoplasm. On the other hand, one additional study showed that only after 6 months post-transplantation, 5% of grafted neurons exhibited human α-syn immunoreactivity [375], confirming the transfer of human α-syn from host-to-graft *in vivo* in Tg animal models. The abovementioned transfer was also confirmed in WT animals, although at a different rate according to the site of injection, mouse strain, and preparation of recombinant α-syn fibrils [76, 78, 80]. Importantly, Recasens et al. [88] showed that this mechanism is valid also for species closer to humans, such as macaque monkeys. In this work the authors showed that the α-syn contained in LBs extracted from postmortem PD brains can spread from one cell to another and can trigger the conversion of endogenous α-syn in β-sheet-rich diseases-related form. Altogether, these studies reveal that the seeding process is a key step in α-syn spreading and it might be considered as a rate-limiting point for the initiation of the aggregation progression. The aforementioned series of *in vivo* experiments support the hypothesis of α-syn prion-like propagation, since the injections not only led to generation of α-syn pathology near to the injection site, but also resulted in a time-dependent spreading of pathology to synaptically connected distant brain regions. Indeed, different intracerebral injection sites have been tested including the striatum [78], the midbrain (SN) [76], the cortex and the hippocampus [80] and in all cases the delivery of the exogenous recombinant or brain extracted LBs/LNs-like fibrils induced the formation of pathogenic aggregated forms and promoted their spreading from the injected site to different interconnected brain structures. This, in turn, suggests that starting insult area can determine the brain region that will subsequently be affected. However, the

exact mechanism of what triggers the initiation process of conformational change from soluble into β-sheet rich insoluble forms is still an enigma and further studies have to be performed to understand this conversion process.

The use of synthetic prions has confirmed the "protein only hypothesis" claiming that the PrP molecule alone is the infectious agent that is transmitted *in vivo* [123, 353]. However, the synthetic fibrils are not as infectious as brain-derived PrP^{Sc} unless other cofactors are present (like RNA and lipids) [126, 377, 378]. As with prions, only high doses of synthetic α-syn fibrils are able to induce pathology with the same potency as small amounts of brain-derived α-syn aggregates, suggesting that the pathology-linked α-syn formed *in vivo* has higher templating efficiency [81]. Similar findings were observed for Aβ [10]. Indeed, the importance of cofactors in transmission progression is highly significant and their relevance to human pathologies still has to be explored.

All these findings are a step forward towards demonstrating that all neurodegenerative diseases might use mechanisms similar to prion propagation to spread within distinct brain regions.

1.5.1. Cell-to-cell propagation

A number of cellular events have to occur in order to permit a prion-like spread, including: the secretion, the uptake and the protein seeding by the releasing neurons. Unlike Aβ and prions, which are extracellular aggregates, the pathologic α-syn is accumulated intracellularly and it has to be secreted in order to reach other cells. The exact mechanism of α-syn secretion is still poorly understood. The hypothesis of secretion of α-syn was confirmed by its recent discovery in biological fluids such as blood plasma and cerebrospinal fluid (CSF) [379, 380]. In line with the latter findings, *in vitro* studies have confirmed that α-syn is secreted by primary rat cortical neurons and released into the surrounding cultured medium [381]. Before these discoveries it was though that this small protein was an exclusively intracellular protein [138].

Several reports showed that the secretion process is increased under protein misfolding stress and may occur using non-classic secretory pathways [382] that involve vesicle trafficking through exocytotic secretory vesicles [381] and exosomes [383]; lastly, the α-syn aggregates can also be released directly from dying or injured cells through membrane disruption or pore formation [384]. Once in the extracellular environment, α-syn has to access to the adjacent neurons via active process, such as endocytosis [77, 373, 385], exosomal

transport [383, 386], or internalization by a receptor-mediated process [373], or via direct penetration of the plasma membrane [385, 387, 388] (**Figure 1.6**). Entry and subsequent trafficking to the late endosomes may concentrate the endocytosed proteins, forming aggregates that might seed endogenous protein aggregation [389].

Indeed, it had been described for several neurodegenerative-involved proteins (like PrP^{Sc}, Aβ, tau, and SOD1 proteins), including also the α-syn protein, that the presence of the seed provides a template for the assembly of soluble protein and triggers the formation of highly ordered β-sheet rich structures. Besides, these findings confirm that the expression of a soluble monomeric counterpart is necessary for the pathogenesis process, suggesting that a sequence-specific templating is essential for the seeding process [31, 90, 390]. In fact, when cells overexpressing the α-syn that lacks its NAC domain (Δ71-82), which is crucial for the α-syn aggregation, were exposed to exogenous recombinant α-syn fibrils they did not form the intracellular inclusions, confirming the requirement of full-length protein for the sequence-specific templating. Somehow, the *in vivo* injection in the hippocampus of Tg human α-syn (line M20), of this form was able to induce the pathology-like inclusions in the brain although at a lower rate compared to the N-terminal truncated 21–140 α-syn fibrils (only 2 animals of total of 36) [80, 85]. This indicates that most probably other factors and/or molecules might also be involved in the initiation of the seeding process in the CNS.

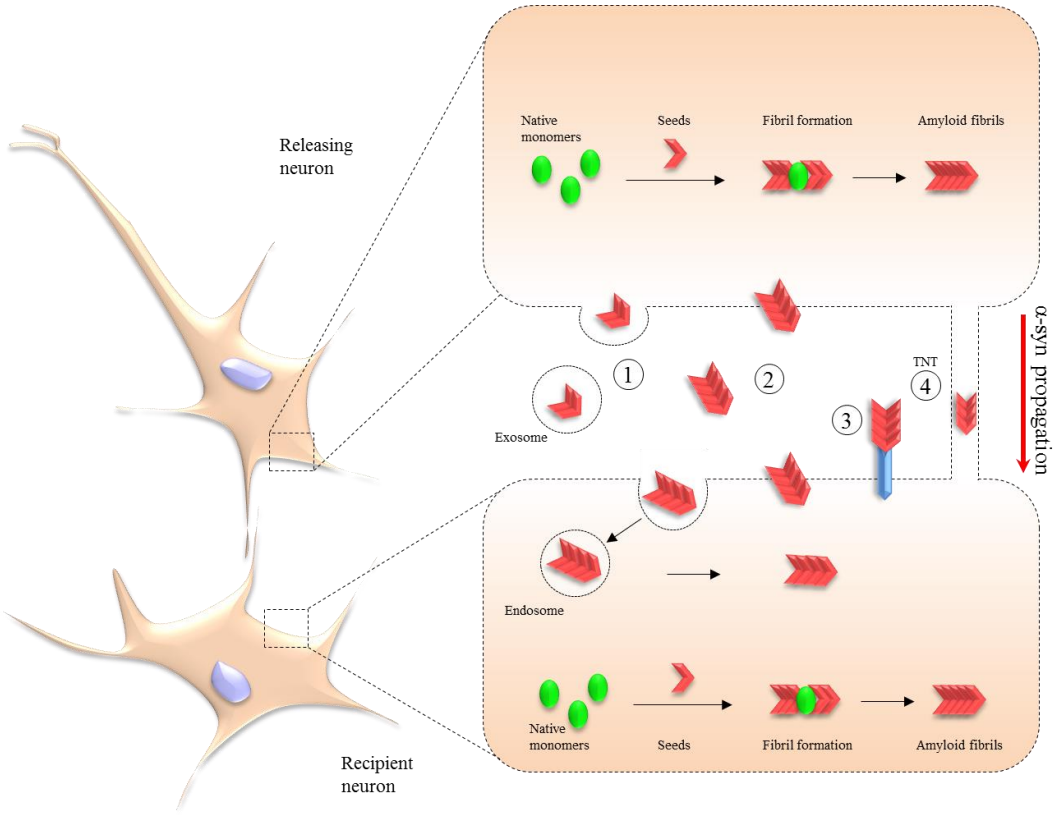

Figure 1.6. Possible cell-to-cell mechanisms of cytoplasmic protein aggregates transmission. Upper panel shows the formation of misfolded seeds within the cytoplasm of releasing neuron, where soluble native monomers are recruited into growing amyloid fibrils. The latter then can be released into the recipient cell (using different mechanisms 1, 2, 3, or 4), or it can generate more seeds through fragmentation or secondary nucleation. The seeds can use membrane formations such as exosomes (1) to be released from the releasing neuron and may fuse with the membrane of the recipient cell (forming the endosome); (2) or simply the free-floating seeds can penetrate the recipient cell membrane. The receptor-mediated endocytosis (3) was also suggested as a possible mechanism of cell-to-cell transmission. The formation of TNT structures (4) is indicative of spread of cytoplasmic aggregates. Taken-up seeds can nucleate the fibril formation of soluble monomers within the cytoplasm of the recipient neuron (lower panel).

As described above, the transcellular migration of cytoplasmic α-syn aggregates could arise forming the exosomal cell-derived vesicles, structures shown to be used for the propagation of PrP^{Sc} fibrils [386]. On the other hand, the aggregates might also be released in the extracellular space as free-floating fibrils without implication of any membrane-associated structures, a process shown for the transmission of tau fibrils [391]. Consequently, these free-floating seeds can directly enter the neighboring recipient neuron through the plasma membrane [392] or could enter by fluid-phase endocytosis, or more specifically micropinocytosis [35, 393, 394]. Another proposed internalization process described for both tau and α-syn aggregates and defined as adsorptive endocytosis, is an intermediate process between receptor-mediated and fluid phase endocytosis [37, 79]. Finally, several studies have

shown that α-syn aggregates penetrate the cells via receptor-mediated endocytosis that requires specific interactions between ligands and cell-surface receptors [77, 375]. Due to the dimensions of fibrils this seems unlikely to be a major mode of fibril internalization, leading to the hypothesis that other mechanisms have to occur in order to permit the uptake of aggregated forms of α-syn protein. As Holmes et al. [394] have shown in their recent study, heparan sulfate proteoglycans (HSPGs) can be considered as a receptor for cell uptake of tau and α-syn fibrils that subsequently seed intracellular fibril formation. Additional means of transcellular migration of protein aggregates might use structures denoted as tunneling nanotubes (TNTs), which are tunnel-like structures made of F-actin-based membranes that have been demonstrated to be involved in the spreading of PrP^{Sc} [395] and Aβ aggregates [396]. Although, for the α-syn spread this process has not been fully established, however, during my PhD thesis I spent my time in Chiara Zurzolo's laboratory at the Institute Pasteur, at Unité de traffic membranaire et pathogenèse, where we studied formation of TNTs structures following the exposure to exogenous α-syn fibrils. We observed an increase of 121 ± 3.70 % of TNTs in CAD cells, following the over-night exposure (16h) to exogenous α-syn fibrils (unpublished data).

However, the *in vivo* studies that showed pathology spreading along neuronal networks indicate the existence of the synaptic transmission of protein aggregates. This trans-synaptic spreading pattern was observed for tau and α-syn aggregates [28, 29, 397]. Moreover, α-syn is highly concentrated at the presynaptic terminals [138] which might privilege its intercellular transmission and might be considered as a crucial site for initiating template recruitment.

Important of note is also the finding that peripherally injected aggregated forms of neurodegeneration-involved protein, such as Aβ, PrP^{Sc}, and α-syn, were shown to induce pathology in CNS, preserving their seeding capability [86, 365, 398, 399]. This is in line with the recent discovery that suggests that α-syn in PD may initiate in the enteric nervous system (in the gut) and progressively ascend to the brain [400].

1.6. Cellular prion protein as a receptor for amyloids

Despite the fact that several physiological roles have been attributed to the cellular form of the prion protein, its exact function in CNS and PNS still have to be deciphered. Actually, one intriguing function for this GPI-anchored protein has been proposed from the time when it has been found to interact with β-sheet rich isoforms of several disease-correlated proteins [401-403]. Indeed, this cell surface protein could mediate the neurodegeneration process not only in prion disorders but also in other proteinopathies.

As widely described, the PrP^{C} expression is required for pathogenesis of prion diseases; moreover a critical feature for this process is a direct interaction of PrP^{C} with PrP^{Sc}. Using this sequence-dependent interaction process, PrP^{Sc} forces PrP^{C} to change its conformation subsequently leading to accumulation and disease progression. High sequence homology is not crucial for the simple interaction, but is necessary for the conformational shift from α-helix form to β-sheet rich structure, and its transmission. In fact, the transmission of prion diseases between different mammalian species is restricted by a barrier defined species or transmission barrier. However, it has been discovered that PrP^{C} can mediate toxic signaling of PrP^{Sc} without changing its cellular conformation; for instance, PrP^{C} from different species (hamster, human, cervid or bovine) was able to mediated toxic signaling of mouse PrP^{Sc} as efficient as mouse PrP^{C} [401]. In the same work the authors reported that β-sheet-rich isoforms of a completely different protein, like Aβ-peptide, can induce apoptotic signaling through PrP^{C}. This PrP^{C}-mediated toxic signaling was blocked using an oligomer-specific antibody (denoted as A11), which led to the hypothesis that different toxic β-rich isoforms share common structural features, which are recognized and bound by PrP^{C}. Considered together, these findings strongly indicate that PrP^{C} has an intrinsic capacity to bind β-sheet-rich forms independently of their primary amino acid sequence.

The first evidence that PrP^{C} might mediate the Aβ toxicity derived from experiments performed on hippocampal slices obtained from PrP-null mice that showed that the treatment with this preparation did not induce the suppression of long-term potentiation (LTP) as in slices from WT mice [306]. LTP is a widely used electrophysiological measure of synaptic plasticity related to learning and memory. Here, the calculated affinity (K_D) for Aβ oligomers and PrP^{C} was ~0.4 nM. Other *in vitro* and *in vivo* studies that have used anti PrP-antibodies prevented the Aβ oligomer-induced toxicity, confirming that the interaction with PrP^{C} leads to synaptic dysfunction [404-406]. Strittmatter's group provided more detailed molecular mechanistic understandings by showing that this interaction involves metabotropic glutamate receptor 5 (mGluR5), the tyrosine kinase Fyn, and phosphorylation of the NR2B subunit of

NMDA receptor, eventually dysregulating the receptor's function, excitotoxicity and dendritic spine retraction [306, 407]. Additionally, several studies reported the existence of PrP^C-Aβ complexes in the brains of AD patients [408-415]. However, not everybody was able to support these observed findings [408, 416, 417], arguing the existence and importance of this possible interaction. These divergences that appear from different studies may, at least in part, be explained by the fact that synthetic preparation obtained can differ from one laboratory to another [418, 419]. It has been speculated that probably only a definite conformation or size of synthetic oligomers functions over a PrP^C-mediated activity. However, due to these ambivalences, the role of PrP^C in mediating the synaptic toxicity of Aβ undoubtedly necessitates additional elucidation.

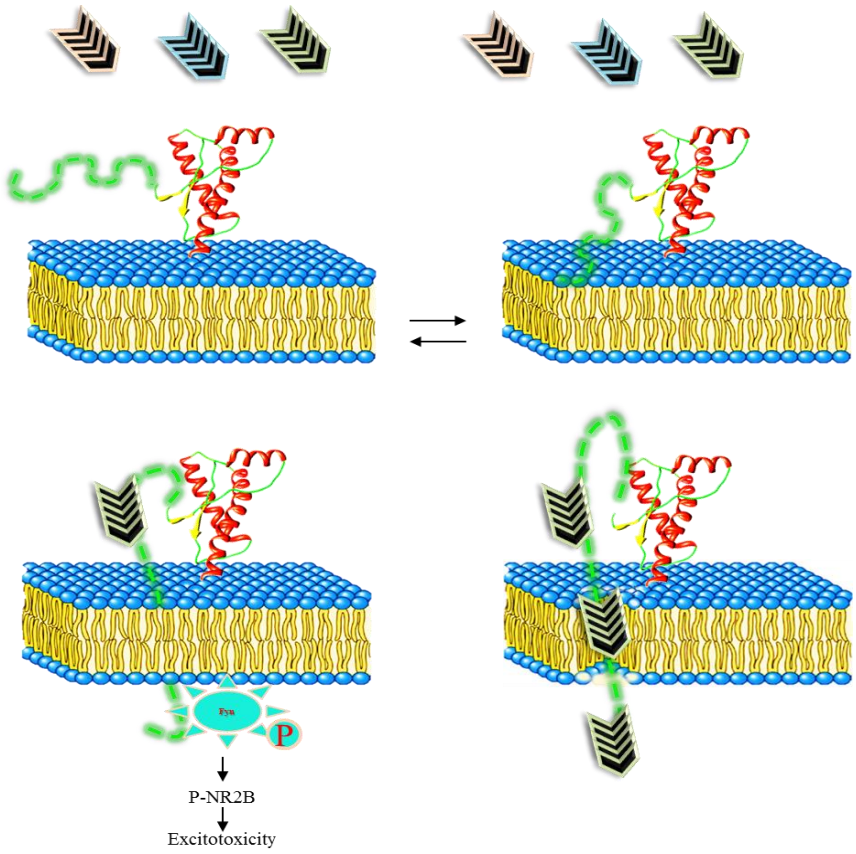

Figure 1.7. A hypothetical model of PrP^C transducing activity [420]. PrP^C at the cell surface can physically interact with different β-sheet-rich isoforms (PrP^{Sc}, Aβ, and others). In particular conditions the N-terminal part of the PrP^C can insert within the phospholipidic bilayer, activate Fyn kinase that activates the phosphorylation of the NR2B subunit of NMDA receptor, eventually causing excitotoxicity. Thus, this model suggests that PrP^C could directly transduce neurotoxic signals upon binding amyloids, or even permit their intracellular delivery through the lipid bilayer.

Several works aimed to establish specific regions of the prion protein involved in PrP^{C}-Aβ as well as PrP^{C}-PrP^{Sc} interaction at the biophysical level have identified three key segments: one in the C-terminal part (residues 136-158 mouse numbering) and two in the N-terminal part of the cellular prion protein (residues 23-33 and 98-110) [401, 411, 412, 421, 422]. Some of them used the antibody inhibition or deletion strategy, others more specific biophysical methods such as Surface Plasmon Resonance (SPR) and Electron Paramagnetic Resonance Spectroscopy (EPR) techniques. In all the cases the N-terminal part of the PrP^{C} sequence appeared to be of crucial importance for the interaction with β-sheet rich structures, such as PrP^{Sc} and Aβ oligomers. Indeed, the cluster of basic residues within the N-terminal 23–27 region of the prion protein (more precisely, the KKRPK sequence), together with the 92-110 sequence (GGGTHSQWNKPSKPKTNMK), has been shown as essential for effective binding to Aβ oligomers and the scrapie isoform. These two regions have important roles in the interaction of PrP^{C} with several cellular factors like those reviewed in [274], glutamate receptor subunits [423], glycosaminoglycans [235], and most importantly it has been shown that this N-terminal domain can penetrate lipid layers, functioning as a protein transduction domain [424, 425] (**Figure 1.7**). Under specific conditions, these polybasic regions could promote the transient insertion of the flexible domain into the plasma membrane, allowing the protein to enter in contact with the cytosol (similar to the ^{Ntm}PrP topology [232]). This model suggests also a mechanism by which the cellular prion protein might directly transduce toxic signaling of β-sheet rich aggregates, or even consent their uptake within the cytoplasmic compartment [420]. Another intriguing finding that might support the latter postulate is that the 23–27 region has been implicated in internalization of PrP [426, 427]. All of these findings emphasize a close link between the physiology of the prion protein and its implication in several neurodegenerative pathologies, not only in TSEs. In the near future this might have important therapeutic implications since molecules that bind to specific functional regions of PrP^{C} could modulate its activity and may delay the neurotoxicity of several kinds of pathogenic protein aggregates [403]. The intriguing question is whether PrP^{C} function or only its presence is involved in mediating the second most widespread neurodegenerative disease, specifically PD.

1.7. Aims of the research

Several *in vitro* and *in vivo* studies have reported that the LBs/LNs pathology spreads in a prion-like manner. Importantly, numerous evidences underline the importance of the use of synthetic amyloid preparations to gain some elucidations for the underling molecular mechanism of accumulation and spread. The addition of exogenous synthetic α-syn fibrils in cell culture is able to recruit the conformational conversion of soluble native monomeric α-syn into β-sheet rich insoluble isoform. Numerous independent studies reported that this is occurring in particular experimental conditions, more precisely, in cell culture and Tg mice models where the α-syn expression is higher (overexpression) than those in normal conditions.

More than a few cellular models have been developed over the last years to reproduce in culture the pathological features of PD. The first model was formed using the HEK293 cell line where the α-syn, WT or mutant, was overexpressed. This overexpression leads to the protein accumulation and aggregate formation, providing a cell model feasible for pathogenesis studies of α-syn aggregation, and thus, of PD [428-430]. However, this model has the major disadvantage of being kidney originated and therefore lacks some crucial neuronal features. To overcome this deficiency, the SH-SY5Y human neuroblastoma line with neural background was established for cell culture studies in the PD field. Similar to the abovementioned model, also in this one the α-syn is overexpressed. One important study, where the cell-to-cell transmission of α-syn aggregates was confirmed, used this cell culture model [77]. As it is easily expandable and reproducing phenotypic features of α-syn pathology, several other groups have used it for seeding and transmission studies [383, 431].

Here, we used both the SH-SY5Y cells that overexpress the human WT α-syn protein and those that have normal endogenous levels of α-syn. In order to gain insights into which form of α-syn fibrils is able to recruit at a higher rate the endogenous monomeric protein we first evaluated the uptake in human neuroblastoma SH-SY5Y of three different human α-syn fibrils which we defined oligomers, short amyloid fibrils, and long amyloid fibrils. Notably, we first characterized the three distinct synthetic preparations using biochemical and spectroscopy techniques. As reported by Volpicelli-Daley et al. [79], using primary cells, the overexpression of α-syn protein was not necessary to induce seeded PD-like inclusion formation. Here, we investigated this in a cell culture system to obtain a valid tool for studying aggregate formation which could possibly open new approaches to study PD.

As numerous reports state that cellular prion protein might bind β-sheet rich amyloid structures, such as Aβ and PrP^{Sc}, we focused our attention on whether this is also valid for α-syn aggregates. The section 1.6. *"Cellular prion protein as a receptor for amyloids"* describes in detail the findings relative to PrP^{C}-Aβ and PrP^{C}-PrP^{Sc} interaction. With this in mind, in the second part of the Thesis, we addressed the question of whether the PrP^{C} protein might have a role in mediating α-syn pathology. The first evidence for such a role came from the cell culture studies. Simply, we formed different α-syn amyloid preparations and we applied them to murine neuroblastoma N2a cells that express cellular prion protein (N2a) and to N2a cells where the expression of PrP was knocked out (N2a KO). After four days of incubation a significantly major uptake was observed in cells that express PrP^{C} endogenously (81.2 ± 3.1 % vs. 30.7 ± 4.4 %). Thus, we hypothesized that the direct interaction between the α-syn amyloids and PrP^{C} might occur. In order to verify this we used different biochemical and biophysical approaches.

These findings point towards a novel physiological function of PrP^{C} in regulating the internalization of α-syn amyloids.

CHAPTER II

Materials and methods

In vitro experiments

2.7. Human α-synuclein protein

2.1.1. Expression and purification of recombinant human α-synuclein

Expression and purification of recombinant human α-syn were performed in accordance with the method previously described [432]. Briefly, the human α-syn gene was cloned and expressed in pET11a vector using BL21 (DE3) E. coli strain. Expression of α-syn was obtained by growing cells in Luria-Bertani broth medium with 100 mg/mL ampicillin at 37°C until an O.D.600 of about 0.6, followed by induction with 0.6 mM isopropyl β-D-thiogalactoside (IPTG) for 5 hours. The protein was purified according to the method of Huang et al. [432].

2.1.2. Fibrillation of human α-syn

All solutions were sterilized by filtration through a 0.22-μm filter prior to each assay run. Reactions were prepared in a 96-well black plate (BD Falcon), and each well contained 200 μL of reaction solution [1.5 mg/mL recombinant human α-syn, 100 mM NaCl, 10 μM Thioflavin T (ThT) in 20 mM Tris–HCl pH 7.4]. Each sample analysis was performed in fifteen replicates. Each well contained one 3-mm glass bead (Sigma). The plate was covered with sealing tape (Fisher Scientific), incubated at 37°C under continuous shaking, and read on SpectraMax M5 fluorescence plate reader (Molecular Devices) by top fluorescence reading every 5 min at excitation of 444 nm and emission of 485 nm.

2.1.3. Cell lines

The GT1-1 cells were received from the laboratory of Professor Krister Kristensson, Department of Neuroscience, Karolinska Institutet Stockholm, Sweden, following an MTA agreement with Dr. Pamela Mellon of the University of California, San Diego, USA. This cell culture model is frequently used in the field of prion biology and it is established from gonadotropin hormone-releasing neurons immortalized by genetically targeted tumorigenesis in transgenic mice [433]. The SH-SY5Y cell line is a thrice-cloned sub-line of SK-N-SH cells, which were originally established from a bone marrow

biopsy of a neuroblastoma patient with sympathetic adrenergic ganglial origin [434]. GT1 cells were seeded in 10-cm plates containing 10 mL of Dulbecco's modified Eagle's medium (DMEM) culture media, supplemented with 10% fetal bovine serum (FBS) and 1% penicillin-streptomycin. SH-SY5Y normal cells were cultivated in 10-cm plates, containing 10 mL of minimal EMEM: Ham F12 (1:1) culture media, supplemented with 15% FBS, 1% non-essential amino acids, 0.5% L-glutamax, 1% penicillin-streptomycin and 1% G-418 (only for SH-SY5Y wild-type cells transfected for overexpressing α-syn). The cells were grown at 37°C in 5% CO2 to 95% confluence for 1 week before splitting at 1:10 for further cultivation.

2.1.4. Cytotoxicity assay

The cytotoxic effect of α-syn fibrils was assessed by measuring cellular redox activity with 3-(4,5-dimethylthiazol-2-yl)-2,5-diphenyltetrazolium bromide (MTT). Briefly, 100,000 SH-SY5Y and GT1 cells/well were cultured in a 96-well microtiter plate and treated with α-syn oligomers, short fibrils and long fibrils (suspended by vortexing). Following 24-h incubation, the cytotoxic effect was assessed by measuring cellular redox activity, following the manufacturer's (Sigma) instructions.

2.1.5. AFM analysis

AFM analysis was performed in accordance with the method previously described [435]. Three to five μL of fibril solution was deposited onto a freshly cleaved piece of mica and left to adhere for 30 min. Samples were then washed with distilled water and blow-dried under a flow of nitrogen. Images were collected at a line scan rate of 0.5-2 Hz in ambient conditions. The AFM free oscillation amplitudes ranged from 25 nm to 40 nm, with characteristic set points ranging from 75% to 90% of these free oscillation amplitudes. AFM data were analyzed with Gwyddion (gwyddion. net) and SPIPTM (www.imagemet.com) software.

2.1.6. α-syn amyloid solution for cell infection

The α-syn amyloid solution was transferred from the 96-well plate into a 1.5 mL Eppendorf tube and collected under sterile conditions. The solution was ultracentrifuged at 100,000 g for 30 min at 4°C (Beckman Coulter). Pellets were resuspended in 1X PBS and then sonicated (Branson 2510) for 5 min prior to adding to the cultured cell plate.

2.1.7. α-syn fibril infection in cell lines

Three hundred μg of α-syn amyloids was added to GT1 and SH-SY5Y cell plates (10 cm-plate) and exposed in the cell culture media for 7 days before the next splitting and media change. Cells were split and maintained for six additional passages. Cell lysates were collected at each passage for Western blotting and immunofluorescence studies. For immunofluorescence of amyloids internalization, cells were cultured in 12-well plates with coverslips; 30 μg of α-syn amyloids was added to the cell culture media and incubated for 7 days.

2.1.8. Detection of α-syn aggregates in treated cells and analysis by Western blotting

The total protein content of samples was measured by bicinchoninic acid assay (BCA) (Pierce). Fifty μg of cell lysates protein was used and 5X loading buffer was added in a 1:5 ratio. The samples were boiled for 5 min at 100°C, loaded onto a 10% Tris-Glycine SDS-PAGE gel, and transferred overnight onto Immobilon P PVDF membranes (Millipore). Membranes were blocked by 5% nonfat milk, incubated with 0.4 μg/mL rabbit polyclonal anti-α-syn antibody (Santa Cruz) followed by incubation with goat antirabbit IgG F(ab)2 fragment conjugated with horseradish peroxidase. Blots were developed with the enhanced chemiluminescent system (ECL, Amersham Biosciences) and visualized on Hyperfilm (Amersham Biosciences). To analyze α-syn aggregation in cell samples, cells were scraped in TBS buffer containing 1% Triton X100, protease cocktail inhibitors and phosphatase

inhibitor. After sonication (Sonicrep 150) with 10 amplitude microns for 3 times (30 seconds of sonication and 30 seconds intermediate stop) cells were centrifuged at 2000 RPM for 5 min before the protein was quantified. Fifty µg of sample was centrifuged at 100,000 g for 30 min. Supernatant (in term S-TX) was collected and the pellets were resuspended in 2% SDS. Samples in 2% SDS were centrifuged and supernatant (S) and pellet (P) were collected. All the fractions were added to loading buffer 5X in ratio 1:5 and prepared similarly for Western blotting.

2.1.9. Reverse transcribed–polymerase chain reaction

Total RNA was extracted from cultured cells using the Trizol Reagent (Life Technologies) extraction method. From 1 µg of total RNA, cDNA was synthesized using 200 units MoMuLV-reverse transcriptase (SuperScrip™ III RT; Life Technologies), oligo (dT) primers and 1 µl 10 mM dNTP Mix in a final volume of 13 µl. Ten microliters of the 25-fold diluted solution was subjected to quantitative PCR analysis. The following primer pairs were used for α-syn: Hu_Syn_FW 5′-ATGGATGTATTCATGAAA-3′, Hu_Syn REV 5′-TTAGGCTTCAGGTTCGTA-3′. PCR amplification was conducted using the PhusionW High-Fidelity DNA Polymerase protocol, under the following conditions: initial denaturation at 98°C for 30s, 10s at 98°C, 30s at 45°C and 30s at 72°C for 25 cycles, followed by 10 min at 72°C. After amplification, 10 µl aliquots were electrophoresed in 1.5% agarose gel, followed by photographic recording of the gel stained with ethidium bromide.

2.1.10. Immunofluorescence and ThS staining of α-syn fibril-treated cells

Cells on coverslips were washed with PBS and fixed with 4% paraformaldehyde, then washed twice, 15 min/time with PBS and blocked in blocking buffer [5% normal goat serum (NGS) in PBS + 0.3% Triton] for 1 hour. For Thioflavin S (ThS) staining, fixed cells were incubated with 0.025% of the fluorophore (Sigma) for 8 min and washed three times with 80% ethanol for 5 min each time, prior to the antibody incubations. Immunofluorescence was performed using the primary and secondary antibodies listed in **Table 2.1**. Primary antibodies were made up in 1% blocking buffer and PBS. After incubation, the cells were washed 5 times for 5 min/time with PBS; secondary antibodies were incubated in 1% blocking buffer and PBS form 45 min. Finally, cells were washed 5 times, 5 min/time with PBS, and counterstained with DAPI to reveal nuclei, then mounted in Vectashield Mounting Medium. Cell coverslips were stored at 4°C for confocal fluorescence microscopy. The fluorescence was measured in at least 10 randomly chosen observation fields for each experimental condition using Leica SP5 confocal laser scanning microscope. The increase in fluorescence was measured calculating CORRECTED TOTAL CELL FLUORESCENCE (CTCF) using the formula: CTCF = Integrated density – (Area of selected cell X Mean fluorescence of Background readings) using the ImageJ 1.47 Software (NIH). Quantification experiments were carried out independently at least three times; more than 150 cells were counted for each condition. Individual differences were assessed using individual student's t-tests in GraphPad Prism software (San Diego, CA). Data are shown as mean ± standard deviation (SD).

2.1.11. Immunofluorescence microscopy analysis of phosphorylated aggregates

All dopaminergic neuroblastoma SH-SY5Y cells were grown on ibidi dishes (Biovalley) for microscopy. After washing in PBS, cells were fixed using 4% (w/v) paraformaldehyde (Sigma) in PBS for 15 min and permeabilized with 0.01% Triton X-100 (Sigma) in PBS for 3 min, washed and blocked in 2% Bovine serum albumin (Sigma) in PBS for 20 minutes. Cells were immunostained using anti-α-syn (Santa Cruz Biotechnology, INC) and anti-phospho S129 α-syn (Abcam) followed by secondary antibody coupled to Alexa 488 (Invitrogen). Cells were mounted in Aqua Poly/Mount (Polysciences) and pictures were acquired using white field Axiovision microscope (Zeiss) with a 63x objective. Quantification experiments were carried out independently at least three times; more than 150 cells were counted for each condition. Individual differences were assessed using individual

student's t-tests in GraphPad Prism software (San Diego, CA). Data are shown as mean ± standard error of the mean (SEM).

In vivo experiments

2.1.12. Stereotaxic surgery - In collaboration with Prof. Fabrizio Tagliavini's group, NeuroPrion - Istituto Nazionale Neurologico Carlo Besta, Milan, Italy

- *First passage*

All surgical procedures were performed under sterile conditions. Six week-old CD1 mice (n=7) were anesthetized with tribromoethanol (100 µL/10 g) and placed in a stereotaxic instrument on a mouse and neonatal rat adaptor. Ten µL of (i) synthetic human α-syn monomers, (ii) synthetic human α-syn oligomers, (iii) synthetic human α-syn short fibers, (iv) synthetic human α-syn long fibers and (v) PBS was inoculated in the right substantia nigra pars compacta (SNpc) following these stereotaxical coordinates (- 3.28 caudal; + 1.5 lateral; 4.5 depth). Uninjected animals were used as negative controls.

- *Second passage*

Thirty µL of (i) α-syn brain homogenate, (ii) mock brain homogenate and (iii) PBS was inoculated in the right striatum following these stereotaxical coordinates (- 1 caudal; + 2 lateral; 3.5 depth). Uninjected animals were used as negative controls.

2.1.13. Brain homogenization

Ten percent brain homogenate (w/v) was prepared from a symptomatic animal previously injected with short fibers of synthetic human α-syn. Ten percent mock homogenate (w/v) was obtained from healthy CD1 mouse brain. Each homogenate was prepared using saline solution (NaCl, B. Braun 0.9%) with the addition of protease inhibitors (Roche).

2.1.14. Immunohistchemical analysis

Brains were fixed in Alcolin (Diapath), dehydrated and embedded in paraplast. Seven-µm thick serial sections were stained with haematoxylin-eosin (H&E) or immunostained with antibodies against: α-syn (monoclonal, clone 4D6, Signet), phosphorylated α-syn (rabbit polyclonal, Abcam), glial fibrillary acidic protein (rabbit polyclonal, GFAP, DakoCytomation) as marker of astrocytes, Iba1 (goat polyclonal, Abcam) as marker of activated microglial cells, tyrosine hydroxylase (rabbit polyclonal, Santa Cruz Biotechnology) as marker of dopaminergic neurons. To test for the presence of protease-resistant α-syn, some sections were post-fixed in formalin and treated for 5 min with proteinase K at different concentrations (5-30 µg/ml in 0.3% Brij-35). Immunoreactions were visualized using anti-rabbit or anti-goat biotinylated secondary antibody (1:100, Vector) and streptavidin-peroxidase complex (1:200, Vector). For mouse monoclonal antibodies, a specific streptavidin-biotin system (Animal Research Kit and Peroxidase, DakoCytomation) was applied. 3-3'-diaminobenzidine (DAB, DakoCytomation) was the chromogen used.

Table 2.1. Antibodies used in this study

Antibody	Source	Host	Dilution (IF)	Dilution (WB)	Dilution (ICC)
α-synuclein (C-20)-R	Santa Cruz	Rabbit	1:500	1:500	
α-synuclein [LB 509]	Abcam	Mouse	1:1000	1:1,000	
α-synuclein (D37A6)	Cell Signaling Technology	Rabbit	1:100	1:500	
α-synuclein (clone 4D6)	Signet	Mouse			1:1,000 (o/n)
α-synuclein (phospho S129)	Abcam	Rabbit	1:500	1:500	1:300 (o/n)
Glial fibrillary acidic protein (GFAP)	DakoCytomation	Rabbit			1:800 (o/n)
Iba1	Abcam	Goat			1:2,000 (o/n)
Tyrosine Hydroxylase	Santa Cruz	Rabbit			1:800 (o/n)
Monoclonal ANTI-FLAG® M2	Sigma	Mouse	1:1,000	1:10,000	1:300 (o/n)
Alexa 488 anti-mouse		Goat	1:500		1:800 (o/n)
Alexa 488 anti-rabbit		Goat	1:500		1:2,000 (o/n)
Alexa 594 anti-mouse		Goat	1:500		1:800 (o/n)
Alexa 594 anti-rabbit		Goat	1:500		

2.2. Mouse α-synuclein protein

In vitro experiments

2.2.1. Antibodies

Mouse anti-PrP mAb W226 (Petsch et al., 2011) from Kirsten Korth laboratory (Germany), N-terminal SAF34 mAb, α-synuclein Antibody (C-20)-R: sc-7011-R (Santa Cruz Biotechnology, Inc), β-actin HRP conjugated (Sigma-Aldrich), goat anti-mouse IgG-HRP, goat anti rabbit IgG-HRP (Life Technologies). Working dilutions are listed in **Table 2.3**.

2.2.2. Expression and purification of recombinant mouse α-synuclein

Recombinant α-synuclein (α-syn) protein was purified from *Escherichia coli* BL21(DE3) cells expressing mouse α-syn construct from the pET11a expression vector. *E.coli* cells were grown in minimal medium at 37°C in the presence of ampicilin (100 μg/ml) until OD600 of about 0.6, followed by induction with 0.6 mM IPTG for 5 hours. The protein was extracted from periplasm by osmotic shock as previously described (Huang et al, 2005), followed by boiling for 20 min and ammonium sulfate precipitation. The protein was next purified by anion exchange chromatography (HiTrap Q FF column, GE Healthcare) and fractions were analysed by SDS-PAGE. Finally, the protein was dialysed against water, lyophilized and stored at -80°C.

2.2.3. Fibrillation of mouse α-syn

Prior to fibrillization, the protein was filtered (0.22 µm syringe filter) and the concentration was determined by absorbance measured at 280 nm. Purified mouse α-syn (1.5 mg/ml) was incubated in the presence of 100 mM NaCl, 20 mM Tris-HCl pH 7.4 and 10 µM Thioflavin T. Reactions were performed in a black 96-well plates with a clear bottom (Perkin Elmer), in the presence of one 3-mm glass bead (Sigma) in a final reaction volume of 200 µl. Plates were sealed and incubated in BMG FLUOstar Omega plate reader at 37°C with cycles of 50 s of shaking (400 rpm, double-orbital) and 10 s of rest. ThT fluorescence measurements (excitation: 450 nm, emission 480 nm, bottom read) were taken every 15 min.

For *in vivo* and cell culture experiments, fibrillation of the protein was performed as described above, but in the absence of ThT. After fibrillization, the reaction mixtures were ultracentrifuged for 1h at 100 000g (Optima Max-XP, Beckman) and resuspended in sterile PBS.

2.2.4. Atomic Force Microscopy

Atomic Force Microscopy (AFM) was used in the present work to acquire high-resolution three-dimensional reconstructions of α-syn preparations. All AFM images were acquired using a commercially available microscope (Solver Pro AFM from NT-MDT – NT-MDT Co. – Moscow – Russia) endowed with a closed-loop scanner. Measurements were carried out in air at room temperature working in dynamic mode. Cantilevers, characterized by a resonant frequency of about 90 kHz and a force constant of about 1.74 nN/nm (NSG03 series from NT-MDT – NT-MDT Co. – Moscow – Russia) were used working at low oscillation amplitudes with half free-amplitude set-point. High resolution images of 10×10 μm^2 were 512×512 pixels frames acquired at 1 lines/second scan speed. All AFM data were analysed using Gwyddion [436], a free SPM data analysis software. Fibril length was evaluated as linear fibril's end-to-end distance and analyzed using commercial data analysis software (Igor Pro, Wavemetrics, US).

Samples for AFM imaging were prepared by drop deposition of fibril solution on a ultra-flat mica surface. Briefly, 20 µl of solution were spotted onto a freshly cleaved piece of mica (8×8 mm^2 side size) and left to adhere for 20 minutes. Subsequently a 60 µl drop of ethanol was placed on the sample to induce fibril precipitation for 5 minutes. Sample is thereafter blow-dried under a flow of nitrogen.

2.2.5. Cell culture

Mouse neuroblastoma N2a cells were kindly provided by Prof. Chiara Zurzolo (Unité de traffic membranaire et pathogenèse, Institute Pasteur, Paris, France). ScN2a cells are clones persistently infected with the RML prion strain as described by Prusiner's group [437]. Cells were grown and maintained at 37°C/ 5% CO_2 incubator in minimal essential medium (MEM) + glutamax (Thermo Fisher Scientific Inc.), supplemented with 10% fetal bovine serum, 1% non-essential aminoacids, and , 100 units/ml penicillin and 100 µg/ml streptomycin. 30000 cells/dish were cultured for treatments and subsequently sub-cultured for passages (#). N2aPrP KO cells were kindly provided by professor Gerold Schmitt-Ulms (Tanz Centre for Research in Neurodegenerative Diseases, University of Toronto, Toronto, Ontario, Canada), for which they used the CRISPR-Cas9-Based Knockout system to ablate the expression of PrP protein [293].

2.2.6. Stabile transfection

In the N2aPrP KO cells obtained with CRISPR-Cas9-Based Knockout system the PrP^C expression was re-introduced transfecting the cells with PrP full length using Effectene® Transfection Reagent (QIAGEN). To obtain the stably-transfected cell line a selection was performed using 1mg/mL G418 (Life Technologies) for 2 months and after that a lower amount of antibiotic was used for maintenance (0.5mg/ml of G418).

2.2.7. MTT assay

Cell viability was determined by 3-(4,5-dimethyl-2-thizolyl)-2,5-diphenyl-2H-tetrazolium bromide (MTT, Sigma Aldrich) assay following the manufacturer's instructions after 24 h treatment. 30.000 cells/well were treated with 2μM (30μg/ml) of α-syn fibrils in Costar™ 96-Well Plates (Thermo Fisher Scientific Inc.). Three independent experiments were performed in six technical replicas per condition (treated or un-treated). Water-insoluble colored formazan derivative was solubilized in DMSO : isopropanol (1 : 1). Absorbance of converted dye was measured at a wavelength of 570 nm. Viability was assessed in terms of % of control (untreated cells).

2.2.8. Western blotting

After 4 days of treatment with different α-syn preparations, medium was removed and the cells were washed twice with PBS 1X and lysed in lysis buffer (10mMTris-HCl pH 8.0, 150mMNaCl, 0.5% nonidet P-40, 0.5 % deoxycholate). Total protein content of cell lysates was measured using bicinchoninic acid protein (BCA) quantification kit (Pierce) and stored at -20°C until analysis. The total of 30 μg/ml of cell lysates were resuspended in Laemmli loading loading buffer, and boiled for 10 min at 95°C. Subsequenty the samples were loaded onto a 12% Tris-Glycine SDS-PAGE gel, and transferred onto nitrocellulose membrane (GE Healthcare), blocked using 5% non-fat milk (w/v) blocking solution for 1 h at room temperature with agitation followed by incubation with anti-PrP antibodies (W226, 1:1000; SAF43, 1:1000) or anti β-actin (1:50000, A3854 Sigma-Aldrich) diluted in blocking solution. Membranes were washed with TBST (0.1% Tween 20 in TBS), and incubated in horseradish–peroxidase-conjugated (HRP) goat anti-mouse secondary Ab (diluted 1:2000) for 1h. The membranes were washed in TBST and proteins were visualized following the manufacturer's instructions using Amersham ECL Western Blotting Detection Reagent (GE Healthcare) with UVITEC Cambridge. Quantitative densitometry analysis of proteins was performed using NIH Image software (ImageJ 1.50a, USA).

2.2.9. Proteinase K digestion

ScN2a cell lysates (500 μg/ml) were treated with 20 μg/ml of proteinase K (PK) for 1h at 37°C. The reaction of proteolysis was stopped by the addition of phenylmethyl sulphonyl fluoride (PMSF) in a final concentration of 2mM. Immediately after the termination of reaction the samples were centrifuged at 55 000 rpm, the surnatant was discarded and the remaining pellet resuspended in 2x loading buffer, boiled for 10 min, and resolved by 12% SDS-PAGE. Proteins were transferred onto nitrocellulose membrane (GE Healthcare), blocked using 5% non-fat milk (w/v) blocking solution for 1 h at room temperature with agitation followed by incubation with anti-PrP antibodies (W226, 1:1000; SAF43, 1:1000) or anti β-actin (1:50000, A3854 Sigma-Aldrich) diluted in blocking solution. Membranes were washed with TBST (0.1% Tween 20 in TBS), and incubated in HRP-conjugated goat anti-mouse secondary Ab (diluted 1:2000) for 1h. The membranes were washed in TBST and proteins were visualized using Amersham ECL Western Blotting Detection Reagent (GE Healthcare) with UVITEC Cambridge. Quantitative densitometry analysis of proteins was performed using NIH Image software (ImageJ 1.50a, USA).

2.2.10. PGNase F deglycosylation

30 μg/ml of cell lysates were denatured at 95°C for 10 min and incubated with peptide N-glycoside F (PNGase F kit, New England Biolabs) o.n. at 37 °C according to manufacturer's instructions. To stop the reaction the samples were heated at 75°C for 30 min, and re-suspended in loading buffer (2X). Prior to electrophoresis, samples were boiled and run in 12% SDS-PAGE gels. Proteins were transferred onto nitrocellulose membrane (GE Healthcare), blocked using 5% non-fat milk (w/v) blocking solution for 1 h at room temperature with agitation followed by incubation with anti-PrP

antibodies (W226, 1:1000; SAF43, 1:1000) diluted in blocking solution. Membranes were washed with TBST (0.1% Tween 20 in TBS), and incubated in horseradish–peroxidase-conjugated goat anti-mouse Ab (diluted 1:2000) for 1h. The membranes were washed in TBST and proteins were visualized using Amersham ECL Western Blotting Detection Reagent.

2.2.11. Total RNA extraction and RT-PCR analysis

The total RNA extraction was performed using a ready-to-use TRIzol® Reagent (Invitrogen) following the Manufacture's instruction. Briefly, the medium was removed from plates with control cells and those treated with different α-syn preparations and the cells were washed twice with PBS 1X. Subsequently, the cells were lysed using the TRIzol® Reagent. Following RNA isolation, a DNase I digestion was performed using 1 unit of enzyme per μg RNA for 10 min at room temperature, and RNA cleanup was implemented using RNeasy spin columns following the instructions. RNA concentration was determined using the NanoDrop system (Thermo Scientific). First-strand cDNA was synthesized using 4 μg of total RNA in a 20 μl reverse transcriptase reaction (RT^+ samples) mixture following the instructor manual. For each sample a negative control was carried along by omission of the reverse transcriptase (RT^- control).

The cDNA was diluted to 1ng/μL final concentration prior to Real-Time PCR reactions. Two ng RNA equivalent was added to the reaction mix including 2× iQ™ SYBR® Green Supermix (Bio-Rad Laboratories, Inc.), 400 nM of the corresponding forward and reverse primer (Sigma), and quantified in technical triplicates on an iQ5 Multicolor Real-Time PCR Detection System (Bio-Rad Laboratories, Inc.).

After initial denaturation for 3 min at 95°C, 45 cycles were performed at 95°C for 10 sec and 60°C for 1 min. Differential gene expression of was normalized to GAPDH and ACTB expression. RT^- controls were included in the plates for each primer pair and sample. The relative expression ratio was calculated using the ΔΔCT method [438, 439]. Significance was calculated with the unpaired student t-test ($p < 0.05$). The primers used for RTqPCR reactions are listed in Table 2.2.

Table 2.2. List of primers used for RTqPCR.

Gene	Chromosome	Primer sequence	Amplicon length (bp)
ACTB	3	F: GTTGCGTTACACCCTTTCTTG R: CTGTCACCTTCACCGTTCC	146
GAPDH	11	F: CCTGCACCACCAACTGCTTA R: CATGAGTCCTTCCACGATACCA	74
Prnp	2	F: GAGACCGATGTGAAGATGATGGA R: TAATAGGCCTGGGACTCCTTCTG	80

2.2.12. Immunofluorescence

30000 cells were cultured on coverslips and treated with α-syn fibrils, afterwards the cells were fixed with 4% formaldehyde in PBS for 30 min. Cells were then washed three times with PBS (1X) followed by blocking in 5% Normal Goat Serum (NGS, ab7481, Abcam)/0.3% Triton X-100 for 1h, at R.T. Cells were incubated with primary antibodies diluted in 1% of blocking buffer (anti-PrP Ab W226, 1:500, anti-α-syn Ab C-20, 1:1000), followed by three washings with PBS and secondary antibody incubation (goat anti-mouse A488, and goat anti-rabbit A595, Life Technologies). To ensure

that α-syn preparations were within the cell cytoplasm a specific dye that labels the entire cell was used (HCS CellMask™ dye). Cells were mounted in Aqua Poly/Mount (Polysciences), and images were acquired using Leica confocal microscope (Leica TCS SP2, Wetzlar, Germany).

2.2.13. Uptake quantification

The uptake quantification was performed in blind on more than 200 cells in four independent experiments. Random fields per coverslips at 63x magnification (zoom 3X) were captured using Leica confocal microscope (Leica TCS SP2, Wetzlar, Germany). To observe internalized α-syn fibrils, the coverslips were double-labeled with anti- α-syn antibody and whole cytoplasmic dye CellMask. Cells considered α-syn positive were those in which the aggregates were found in perinuclear zone. The images were acquired as 20-30 z-stacks of 0.22 μm, 1024 × 1024, and analyzed using Orthogonal Views function in Image J (NIH). Data are represented as % of total cell counted.

2.2.14. Discrimination between PrP^{Sc} and PrP^{C} by immunofluorescence assay

Immunofluorescence discrimination was performed as previously described [440, 441]. 30000 cells/well in 24-well plates were seeded on glass coverslips (N2a or ScN2a). The following day the cells were rinsed twice with PBS 1X and subsequently treated with α-syn fibrils and left in incubation for four days. After indicated time of incubation the cells were fixed with freshly prepared 4% formaldehyde for 30 min R.T. Subsequently, the cells were washed twice with PBS 1X and in the case of ScN2a, a denaturation step with 6 M GdnHCl for 10 min followed. Afterwards the cells were blocked with 5% NGS/0.3% Triton X-100 in PBS 1X for 1h, at R.T. Cells were incubated with primary antibodies diluted in 1% of blocking buffer (anti-PrP Ab W226, 1:500, anti-α-syn Ab C-20, 1:1000), followed by three washings with PBS and secondary antibody incubation (goat anti-mouse A488, and goat anti-rabbit A595, Life Technologies). Cell cytoplasm and nuclei were stained with the specific dye that labels the entire cell, HCS CellMask™ dye (in PBS 1X for 30 min, at R.T.). Cells were mounted in Aqua Poly/Mount (Polysciences), and images were acquired using Leica confocal microscope (Leica TCS SP2, Wetzlar, Germany).

2.2.15. Protein Misfolding Cyclic Amplification assay (PMCA)

PMCA was performed as previously described [442]. Briefly, as a substrate, we used brain specimens obtained from outbred FVB animals. Brains were harvested after perfusion, and 10% homogenate was prepared in conversion buffer (PBS containing 150 mM sodium chloride and 1% Triton X-100) with the addition of protease inhibitors. Different concentrations of α-synuclein fibrils and α-synuclein monomers were added to the substrate. PBS was used as control for the reaction. To evaluate the inhibitory effect of α-synuclein (monomers vs fibrils) RML prion strain were spiked at different dilutions (from 10-5 to 10-9) and assessed by means of PMCA. The reaction mix were transferred in 0.2 ml tubes, positioned on an adaptor placed on the plate holder of a micros onicator (Misonix, Model S3000) and subjected to 96 cycles of PMCA. Each cycle (also referred as PMCA round) consisted of 29 min and 40 sec of incubation at 37/40°C followed by a 20 sec pulse of sonication set at potency of 260-270 Watt. After one round of PMCA, an aliquot of the amplified material was diluted 10-folds into fresh substrate and a further PMCA run performed following the same procedure. To increase PMCA efficiency, teflon beads (n=3) were added to the samples before each round of amplification. To avoid samples cross-contamination between each round, thorough decontamination of instruments and equipment was performed using 2N sodium hydroxide (NaOH) or 4M guanidinium-hydrochloryde.

2.2.16. Formaldehyde crosslinking

All steps were carried out at RT unless noted. Cells were washed twice with phosphate buffered saline (PBS), pH 7.2. Crosslinking occurred during 15-minute incubation in the presence of 1 to 5% (w/v) formaldehyde in PBS, pH 7.2. Fixative was removed and the crosslink reaction was quenched with 125 mM glycine in PBS, pH 7.2 for ten minutes. Cells were washed twice with PBS and proteins were extracted from crosslinked cells with ice-cold extraction buffer (10 mM Tris-HCl (pH 8.0), 100 mM NaCl, 0.5% NP-40, 0.5% DOC). Equal amounts of protein (determined using the BCA reagent) were precipitated with acetone. Protein pellets were resuspended in either SDS-loading buffer without subsequent boiling or in crosslink reversal buffer (2% SDS, 500 mM 2-mercaptoethanol, 250 mM Tris, pH 6.8) and heated for 1 to 30 minutes at 95. In both instances, samples were analyzed via immunoblotting.

2.2.17. Disuccinimidyl glutarate (DSG) crosslinking

A cross-linking protocol was adapted with some minor modifications [443, 444]. Briefly, fully confluent cell culture dish with N2a cells (controls and treated with α-syn fibrils) was collected by scraping, washed with PBS, and resuspended in 200 µl PBS with 1X Complete Protease Inhibitor Mixture, EDTA-free (Roche Diagnostics). Immediately before use, a 50 mM stock of the cross-linker disuccinimidyl glutarate (DSG) was prepared in DMSO. The samples were incubated with 1 mM DSG or DMSO for 30 min at 37°C in a shaking incubator. The cross-linking reaction was quenched by addition of 1 M Tris, pH 7.5, to 50 mM final concentration and incubated for 15 min at room temperature. Next, samples were lysed by 15 sec sonication (30% amplitude). Finally, the samples were ultracentrifuged (Optima TLX, Beckman) for 30 min at 200,000 x g to recover the cytosolic fraction from the supernatant. A total of 10 ug of protein was loaded on 4%–12% Bis-Tris gels (Thermo Fisher Scientific Inc, Life Technologies). After electroblotting, the PVDF membranes were incubated for 30 min in 0.4% PFA and rinsed twice with PBS [443, 445]. Blocking and immunodetection were performed as described above. The effectiveness of cross-linking was analyzed by immunoblotting with the monoclonal antibody C20 R (1:1000, Santa Cruz Biotechnology) for α-syn and W226 for the PrP protein.

In vivo experiments

2.2.18. Animals

Female FVB WT and FVB *Prnp*$^{0/0}$ mice were taken from a colony maintained at Scuola Internazionale Superiore di Studi Avanzati (SISSA), Trieste, while the original breeders were generously provided by George A. Carlson, McLaughlin Research Institute (Great Falls, MT) [446]. Mice were grouped-housed (3-4 mice per cage). Mice were housed with ad libitum access to food and water in the SISSA non-specific pathogen free (SPF) animal facility with 12 h dark/light cycles and controlled temperature and humidity. All efforts were made to minimize animal suffering and to reduce the number of animals used. All the experiments were performed in accordance with European guidelines for animal care [European Community Council Directive, November 24, 1986 (86/609/EEC)] and following SISSA Ethical Committee permissions and SISSA veterinary service.

2.2.19. Stereotaxic surgery

Two months old female FVB WT and FVB *Prnp*$^{0/0}$ mice were subdivided in groups composed of thirteen animals each and intraperitoneally anesthetized with a mixture of Xylazine (15mg/kg) and

Zoletil (15mg/kg). F. sonic α-syn short fibrils (15µg) were stereotaxically injected into the Substantia Nigra Pars Compacta of the right hemisphere of mice (coordinates from Bregma: AP -3.2mm, ML -1.2mm, DV -4.4mm beneath the Dura Mater). Control mice were injected with sterile phosphate-buffered saline (PBS) solution. The material was injected with a 10 µL Hamilton syringe at a rate of 3µl for 1 minute, 3 µl for 2 minutes, 4 µl for 5 minutes. The needle was left in place for a total of 13 minutes. After recovery from surgery, animals were monitored regularly and sacrificed at 9 months post injection (mpi) by overdose with Xylazine/Zoletil. For immunohistochemistry, brains were removed after transcardial perfusion with phosphate buffered 4% paraformaldehyde (PFA, pH 7.4) and underwent overnight postfixation in PFA. For biochemical studies, the transcardial perfusion was performed with the saline solution and brains were immediately frozen in liquid nitrogen after removal and stored at -80 °C until used.

2.2.20. Immunohistochemistry

Three out of 13 mice were sacrified 9 mpi. Fixed brains were cut with a Leica SR 2000R microtome as 30 µm-thick free-floating coronal sections and treated with 3% H_2O_2 and 10% methanol for 10 minutes to inactivate endogenous peroxidase. The reaction was inactivated in PBS. Slices were treated 30 min with 5µg/ml of Proteinase-K (PK) digestion to reveal α-synuclein aggregates. Blocking was performed in 0.05% Triton-X100, 5% normal goat serum (NGS, Sigma-Aldrich), 1% bovine albumin serum (BSA, Sigma-Aldrich) in PBS. Primary antibodies were incubated overnight at 4°C (see Table 2.3 for the list of antibodies used, working dilutions and pre-treating of slices). After incubation with the biotinylated-secondary antibodies (Sigma-Aldrich) and the VECTASTAIN® ABC Kit, sections were stained using 3'-diaminobenzidine (DAB; Sigma-Aldrich, SIGMAFAST™) as a chromogen. Sections were mounted on Superfrost glass slides (Menzel-Gläser Adhesion Slides SuperFrost® Plus) and dehydrated as follow: 1' in EtOH 50%, 1' in EtOH 70%, 1' in EtOH 90%, 1' in EtOH 100%, 1' in EtOH/Xilene (1:1), 2' in Xilene. Quantification of PK-resistant α-syn aggregates was performed with TMARKER v2.73 software [447].

2.2.21. Immunofluorescence

Free-floating sections were blocked in 0.05% Triton-X100, 5% normal goat serum (NGS, Sigma-Aldrich), 1% bovine albumin serum (BSA, Sigma-Aldrich) in PBS. Primary antibodies were incubated overnight at 4°C (see Table 2.1). Immunofluorescence reactivity was revealed with Alexa Fluor 488 or 594 conjugated fluorescent secondary antibodies (Life Technologies). Nuclei were counterstained with DAPI. For the detection of phosphorylated α-synuclein, the reaction was performed in Tris-buffered saline (TBS) solution.

2.2.22. Images acquisition and analysis

Bright images were captured by a Canon EOS 550D connected to Leika DM IL LED S40/0.45 microscope. Fluorescent images were captured using a C1 NIKON confocal. Quantification of PK-resistant α-syn aggregates was performed with TMARKER v2.73 software [447].

2.2.23. Behavioral analysis

A test battery was developed to assess the effects of short α-syn fibrils injections on the behavior of mice. For time-course analysis of the behavioral phenotype, tests were performed at 3 and 15 months post injection (mpi) on the same mice (**Figure 2.1**).

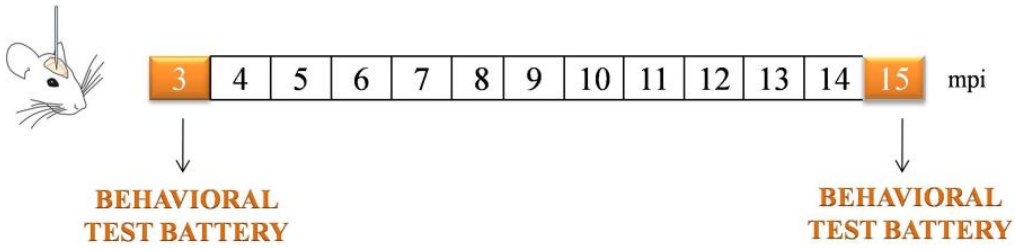

Figure 2.1. Scheme of study design

Tests within the battery were distributed along two weeks and ordered from least to the most invasive in order to allow the "recovery time" between tests and to decrease the probability that behavioral responses would be affected by previous testing experience. Please see **Figure 2.2** for summary of test battery. Behavioral tests were conducted during the light phase of the cycle, by a single researcher that was blind to treatment and genotype during experiment testing and data collection.

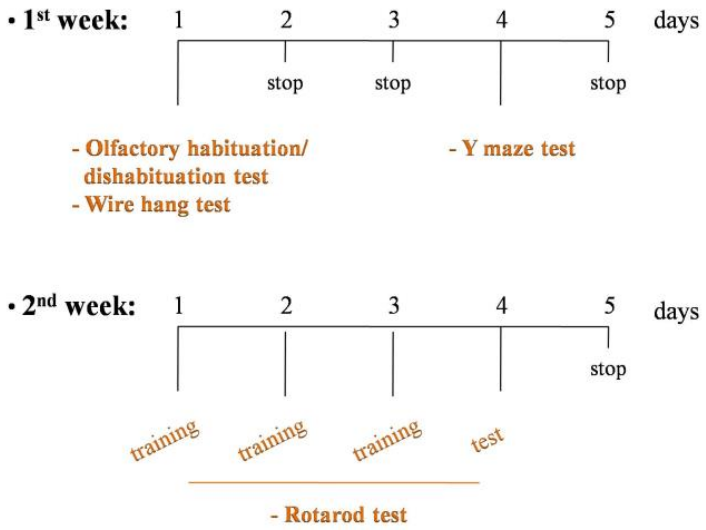

Figure 2.2. Behavioral test battery

2.2.24. Survival

Animals were examined weekly in order to determine the lifespan. Mice were considered dead when they no longer had a heartbeat. In this case they were removed and recorded immediately. Moribund animals were euthanized by CO_2 asphyxiation.

2.2.25. The olfactory habituation/dishabituation test

This test allowed to investigate ability of mice to discriminate different odors. It consisted of two phases: habituation and dishabituation. During the habituation, water is presented in three consecutive trials for duration of 2 minutes each, in order to progressively decrease the sniffing time towards a repeated presentation of the same odor stimulus. This phase was followed by dishabitution that consisted in vanillin presentation for 2 minutes to restore the olfactory investigation towards a novel odor. Parameter employed to evaluate olfactory ability was the ratio between the sniffing time towards the vanillin and the 3rd water presented.

2.2.26. Wire hang test

The wire hang test was performed by placing the mouse on a wire cage lid. The lid was gently shaken to allow the mouse to grip the wires, then turned upside down and suspended 20 cm above the cage floor to prevent the animal from easily climbing down. The latency to fall was recorded with a 60 seconds cut-off time. Mice that held on the lid for < 10 sec were provided a second trial.

2.2.27. Y maze test

Y maze apparatus (LE847, Panlab) consisted of 3 grey plastic identical arms (30 x 6 x 15 cm) that were at 120° angle one to the other, forming a Y shape. Each mouse was placed at the end of one arm (start arm) and was allowed to explore freely the maze for an 8 minutes session. The number of entries in each arm was counted visually and an arm entry was scored when the four paws of the animal were within that arm. Mice that did not leave the start arm were excluded from the data analysis. The parameters evaluated were the "Locomotor Activity" defined as the total number of arms entered and the "Spontaneous Alternation" calculated as following equation:

$$\frac{\text{Number of alternations (entries into 3 different arms consecutively)}}{\text{Total number of alternation opportunities (tot arm entries-2)}} \times 100$$

2.2.28. Rotarod test

Motor coordination and balance were assessed using the Rota-Rod apparatus (model LE8200, Panlab, S.L.U., Spain). Rotarod test was performed according to the protocol previously described by Nazor et al. [448]. Briefly, mice were pre-trained for three consecutive days, by placing them on the moving rotarod at 5 r.p.m. until they performed at this speed for 90 seconds. On the day of testing, the apparatus was set to accelerate from 4 to 40 r.p.m. in 180 seconds. The test consisted of three trials separated by 10 minutes inter-trial time and the latency to fall was recorded during each trial.

Table 2.3. Antibodies used in this part of the study

Antibody	Source	Antigen retrieval	Dilution (WB/IHC/IF)
W226	Kirsten Korth Lab		1:1000
SAF 34			1:500
β-actin	A3854 Sigma-Aldrich		1:50000
α-syn (C-20)-R	Santa Cruz, sc-7011-R	-	1:1000
Phosphorylated α-syn^{pSer129}	Biolegend	70% Formic acid, 30'	1:700

CHAPTER III

Results

The results presented here include the work on human and mouse α-syn protein. In **Part I** we present the initial study performed using human α-syn protein in which we show that the overexpression of endogenous human α-syn is not a *condicio sine qua non* that leads to accumulation of LBs/LNs-like amyloids in cell culture system. Whereas, in **Part II** we focus our attention on mechanisms of internalization of mouse α-syn fibrils, working with different mouse neuroblastoma N2a cells, in which the expression of the PrP isoform is dissimilar (PrP^{C} or PrP^{Sc} form) or eliminated (N2aKO cells).

Part I: Defined α-syn prion-like molecular assemblies spreading in cell culture

Part II: Cellular prion protein binds α-synuclein fibrils

Part I: Defined α-syn prion-like molecular assemblies spreading in cell culture

The assembly into filaments is a concentration-dependent process, therefore the increased expression of α-syn (either WT or mutant), due to saturation effects, appears to be the key pathogenic event in the α-syn aggregation process [449]. Indeed, the quantity of monomeric α-syn is an essential feature that determinates the kinetics of fibril formation *in vitro* [63-66, 432], while the overexpression of α-syn protein accelerates the aggregation process in cell cultures after exposure to exogenous fibrils [75, 77]. However, two independent studies showed that the overexpression of native WT or mutant α-syn protein is not necessary for stimulation of PD-like pathology in primary cells [79, 450]. Here, in order to set up a cellular system to attain α-syn aggregates, we used immortalized cell cultures of human neuroblastoma, SH-SY5Y. The reason we focused on immortalized cell lines is that they yield more homogenous cell preparations, harbor an adequate quantity of samples for biochemical analysis, and cultures can be maintained and sub-cultured for long periods. Undeniably, the drawback of employing primary cell culture models is that they have a limited use for transmission experiments. However, in this part of the work we wanted to exemplify whether the recombinant human α-syn amyloid preparations could acquire prion-like properties, once they are converted into a β-sheet-rich structure. Finally, we wanted to explore the possible similarities between the pathological mechanisms of TSEs and synucleinopathies *in vitro* and *in vivo*.

Results I

3.1.1. Preparation of human α-syn fibrils and structural characterization

We produced highly pure recombinant human α-syn protein either as WT sequence or with the FLAG-tag (marked in yellow, **Figure 3.1.1**), and established a protocol to make structured amyloid fibers as previously shown for the production of mammalian synthetic prions [123].

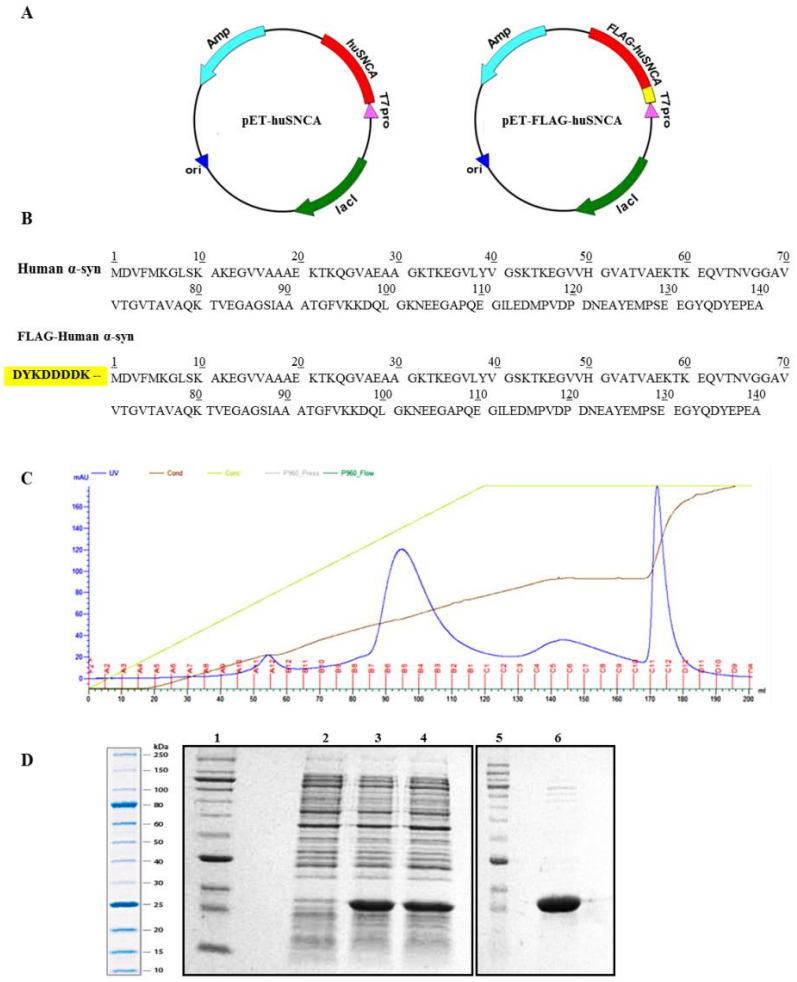

Figure 3.1.1. Plasmids used for expressing human α-syn and FLAG-human α-syn in E. coli BL21(DE)3. **(A)** Homology comparison between mouse α-syn and human α-syn, **(B)** highlighting amino acid substitutions. **(C)** Typical chromatogram obtained from human α-syn protein purification by anion-exchange chromatography with HiTrap Q Sepharose Fast Flow column. The protein was eluted with a 0–0.5 M NaCl gradient in 20 mM Tris pH8.0. Fractions B7-B2 correspond to purified protein. **(D)** Expression of recombinant human α-syn protein, 15% SDS-PAGE. Lane 1 and 5, molecular mass marker; lane 2, whole cell extract before IPTG induction; lanes 3 and 4, cell extract after IPTG induction: 5 hours (lane 3), overnight induction (lane 4); lane 6, purified α-syn protein.

Amyloid fibrillation is the *in vitro* method in which the recombinant soluble proteins misfold into β-sheet rich insoluble fibrils. The amyloid form has been proposed as a generic structure that can be adopted by all proteins under conditions where the native protein is destabilized. This process is monitored using the amyloid dye ThT as indicator of the presence of amyloids. Because various intermediate forms of α-syn develop during the process of fibril formation, we decided to collect β-sheet-rich structures at different time points during the fibrillation assay: (i) at the early inflection of the sigmoid curve, obtaining the form that we define here "oligomers"; (ii) at the middle portion of the curve, acquiring the "short amyloid fibrils"; and (iii) at plateau, attaining the "long amyloid fibrils" of α-syn (collection times are highlighted by red arrows in **Figure 3.1.2**).

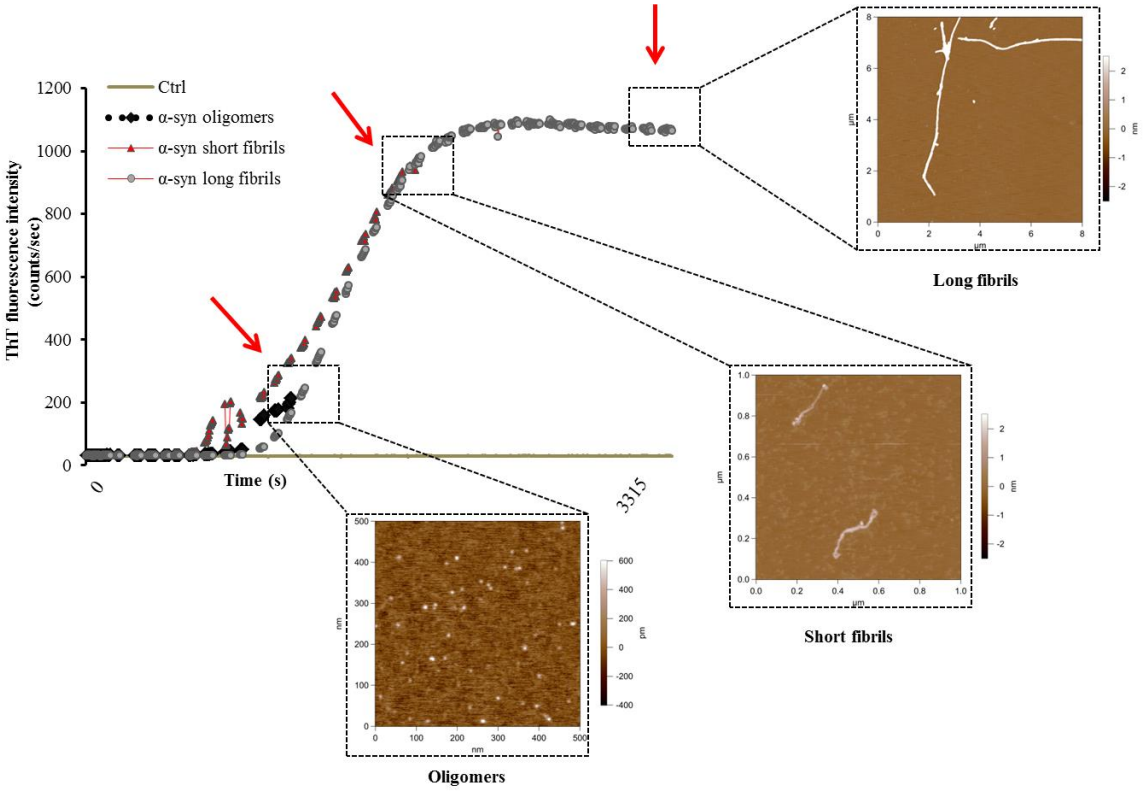

Figure 3.1.2 ***In vitro*** **conversion and AFM characterization of three different recombinant α-syn assemblies.** Kinetics for the formation of β-sheet-rich assemblies: human α-syn oligomer (dotted black line), human α-syn short fibrils (red triangle line) and human α-syn long fibrils (gray dotted line), and control (gray solid line). Red arrows indicate the collection time of the aggregates.

Afterwards, we checked their quaternary structures using the atomic force microscopy technique which is a great high-resolution tool for the investigation of 3D structures of aggregated forms. Indeed, from the statistical analysis of three different preparations **(Figure 3.1.2**) we identified three different assemblies enriched in: (i) oligomeric structure, indicating

round spherical, ring-like characteristics (ii) short fibrils, the protofibril-like structure, and (iii) long fibrils, with long straight branched amyloid features (**Table 3.1.1.** lists all height and length values observed).

Table 3.1.1. Height (nm) and length (μm) data of three α-syn amyloid preparations.

α-Syn preparations	Height (nm)	St. Dev (h)	Length (μm)	St. Dev (L)
Oligomers	0.654	0.113	0.006	0.00172
Short fibrils	2.794	1.204	1.283	0.95824
Long fibrils	6.080	1.376	5.053	1.99995

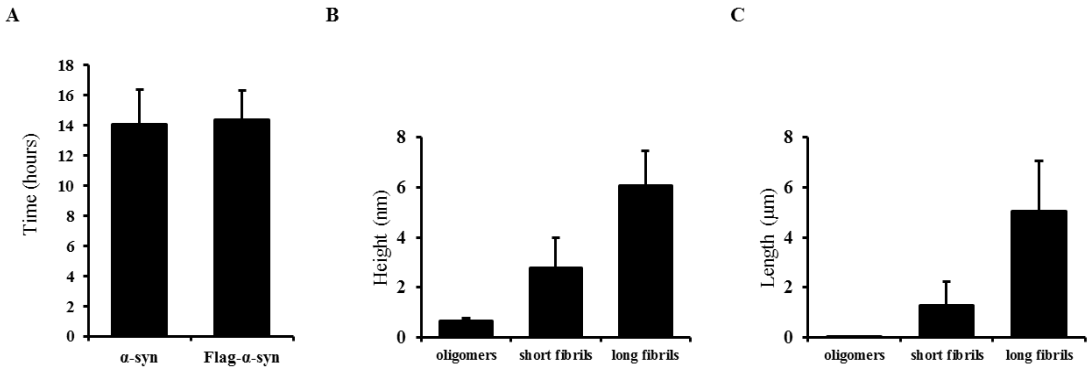

Figure 3.1.3. **(A) Lag phase, in hours, of all β-sheet structure preparations was measured using Thioflavin T assay.** The lag phase distribution of α-syn and FLAG-α-syn amyloid preparations showed no difference, indicating that the presence of FLAG-tag did not affect fibril formation. **(B)** AFM imaging analysis was performed at the end of the fibrillization reactions. AFM scan topographical images of α-syn deposited on mica surface. **(C)** The size of particles was measured: the typical height of α-syn oligomers was 0.65 ± 0.11 nm, the height of short and log fibrils was 2.79 ± 1.20 nm, and 6.08 ± 1.38 nm, respectively. The values are the average calculated on 20 fibrils. The error is the standard deviation.

3.1.2. Cell culture studies, from toxicity to accumulation of endogenous α-syn protein

Before applying these amyloidogenic species to cell cultures for transmissible studies we checked first what their toxicity was after 24 h of exposure. More precisely, we assessed the cytotoxicity of equal amounts of three different α-syn preparations on human neuroblastoma SH-SY5Y cells using the 3-(4,5-dimethylthiazol-2-yl)-2,5-diphenyltetrazolium bromide (MTT) assay. This assay is a quick and effective method for testing mitochondrial activity, which correlates quite well with cell proliferation. The results showed that there was no statistically significant difference in vitality among the various forms of α-syn preparations in

the cell line used (**Figure 3.1.4**), though the oligomeric species displayed eminent slightly lower vitality [372, 451, 452] (74.7% viable cells in SH-SY5Y cells), although not significant.

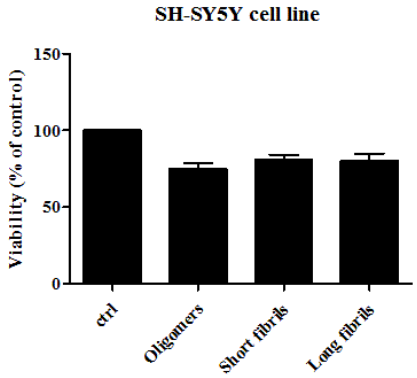

Figure 3.1.4. Toxicity of α-syn aggregates in SH-SY5Y cells. Cells were treated with 5 μg/mL α-syn oligomers, short, and long fibrils for 24 hours. Results are mean ± st. dev. of three independent experiments performed in six replicas.

Afterwards, we embraced two distinct approaches to confirm the internalization of exogenously added assemblies into cells. Both recombinant human nude α-syn fibrils and those tagged with the FLAG-tag were used. The employment of the FLAG-tagged protein permits the detection of exogenously added protein assemblies. Indeed, after seven days in culture short amyloid fibrils were able to enter the cells in a higher rate and promote the recruitment of endogenous α-syn into aggregates. Indubitably, these exogenously added assemblies must first enter the cytoplasm of the cells and persist for an adequate period in cellular compartments accessible to the native soluble α-syn protein in order to efficiently serve as a seed for aggregation process. A single exposure of β-sheet-rich short amyloid fibrils was sufficient to permit the recruitment of endogenous α-syn into PD-like inclusions in non-transfected SH-SY5Y cells. The SH-SY5Y cells exposed to FLAG-tagged short amyloid fibrils were double-stained with either an anti-human α-syn antibody or an anti-FLAG immunoglobulin (**Figure 3.1.5**). The immunoreactivity was mostly cytosolic, with co-localization of anti-FLAG and anti-human α-syn antibody.

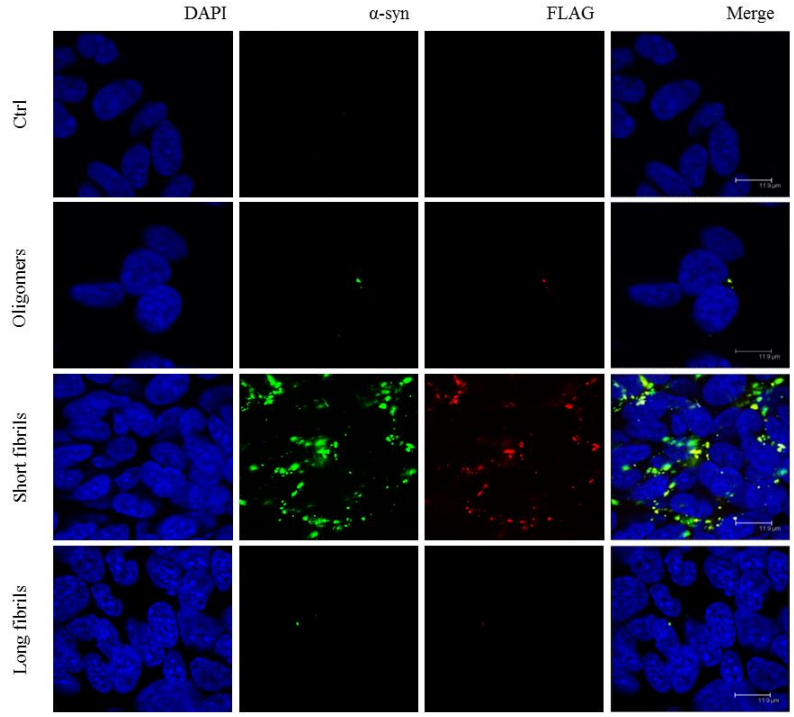

Figure 3.1.5. Internalization of FLAG-α-syn amyloids into neuroblastoma cells SH-SY5Y. α-Syn deposition (green) was detected by anti-human α-syn antibody. Immunofluorescence was performed on cells exposed to FLAG-α-syn amyloids (oligomers, short amyloid fibrils and long fibrils) for 7 days. Bars, 11.9 μm.

Subsequently, we analyzed the aggregation of the endogenous α-syn over multiple passages upon exposure to recombinant short amyloid fibrils. For this purpose we measured the levels of α-syn using immunofluorescence after one single exposure in the SH-SY5Y cells at passage 0 (p0, **Figure 3.1.6**). Only a residual staining of α-syn could be observed in the subsequent passage (p1) and no staining was detectable in the next two passages (p2 and p3). Surprisingly, punctate aggregates of endogenous α-syn appeared at passages four to six (p4-p6). At passage p4 we could detect many small, dispersed aggregates, whereas at the following passages p5 and p6 we began to observe larger aggregates and perinuclear inclusions in the cytoplasm of SH-SY5Y cells (**Figure 3.1.6**, white arrows). Cell sub-clones have been passaged up to passage 12 without apparent loss of aggregates, confirming a sustained aggregation of endogenous α-syn (data not shown). Therefore, the α-syn-short fibril treated SH-SY5Y cells are able to promote, upon sub-passaging, stable aggregation of endogenous α-syn.

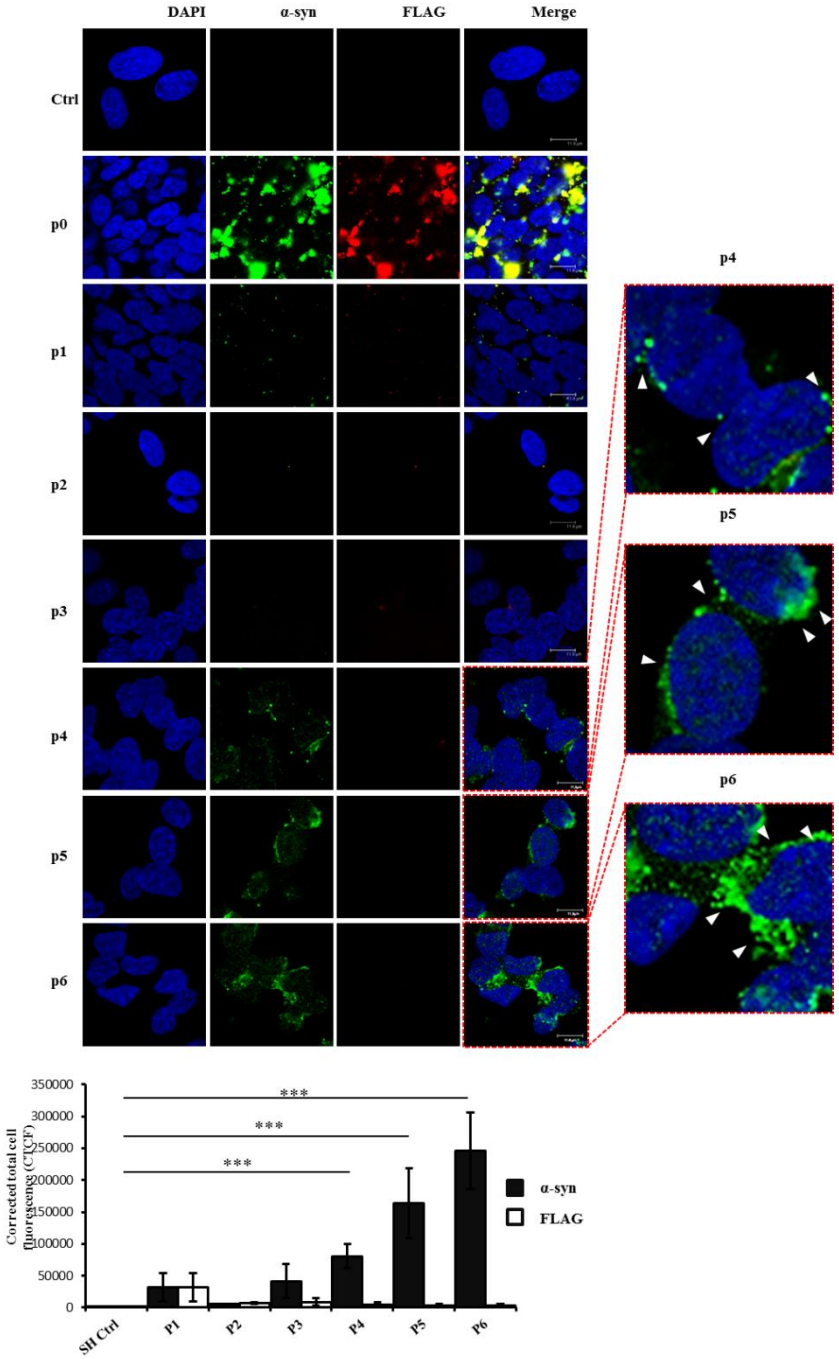

Figure 3.1.6. Infection of the non-transfected SH-SY5Y cells with α-syn short amyloid fibrils and sub-passing over time. (A) Cells were treated with recombinant human FLAG-α-syn short fibrils. Cells were cultured on coverslips for each passage (p0 to p6). The deposition of exogenous short amyloid fibrils FLAG-α-syn (red) was detected by anti-FLAG antibody. Human endogenous α-syn detected by anti-human α-syn (C-20)-R antibody (green). The nuclei were stained with DAPI (blue). Bar, 12 μm. On the right p4, p5, and p6 zoomed images. Lower graph of the corrected total cell fluorescence (CTCF) from immunofluorescence imaging shows the induction of endogenous α-syn in SH (neuroblastoma SH-SY5Y cell line) treated with human α-syn short amyloid fibrils during the passages (bottom panel). The analysis was performed on at least 150 cells, n = 3, ***p < 0.005. Values are mean ± SD.

The PCR analysis confirmed that the levels of α-syn transcripts were not altered after infection, suggesting that this increase of α-syn was occurring at the protein level (**Figure 3.1.7**).

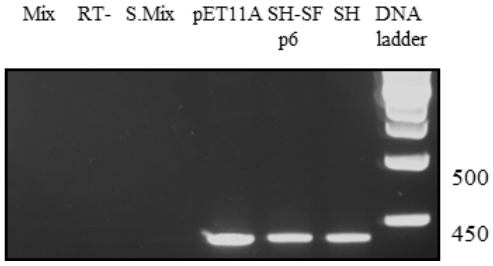

Figure 3.1.7. mRNA levels at p6 after α-syn short amyloid fibril treatment. PCR analyses directed to α-syn using the total RNA extracted from non-transfected SH-SY5Y cells. Mix, RT-, S. Mix: negative controls, pET11A: positive control, SH-SF p6: SH-SY5Y cells passaged six times after exposure to short amyloid fibrils, SH: SH-SY5Y cells not treated with short amyloid fibrils. α-Syn was detected after 25 cycles and the treatment with short amyloid fibrils did not change α-syn mRNA levels after six passages in cell culture.

As widely reported the α-syn aggregates in LBs are amyloids that are characterized by β-sheet structures [59, 69]. These structures can be selectively recognized by thiazole dyes, such as ThT and ThS. The latter are considered markers of amyloid-like conformation [453]. To implement the conformational information of aggregates that were accumulating in SH-SY5Y cells, we double-stained the cells with an anti-α-syn antibody and ThS. Interestingly, the endogenous inclusions induced at p6 were ThS-positive (**Figure 3.1.8**), confirming a significant content in β-sheets, comparable to LBs. Thus, the fact that these α-syn aggregates share hallmark features of PD-like LBs led us to conclude that α-syn short amyloid fibrils seed and recruit normal, endogenous α-syn to form pathologic aggregates in the SH-SY5Y cell line. In our analysis we did not include any other β-sheet rich amyloids, like β-galactose or others, since it has already been reported that use of these controls did not result in inclusion formation [75]. Furthermore, Sanders and collegues already reported that in their system the use of neurodegenerative-involved proteins as controls (Aβ, huntingtin, α-syn) did promote the seeding of endogenous tau protein, underlying the existence of so called "homotypic seeding" [31].

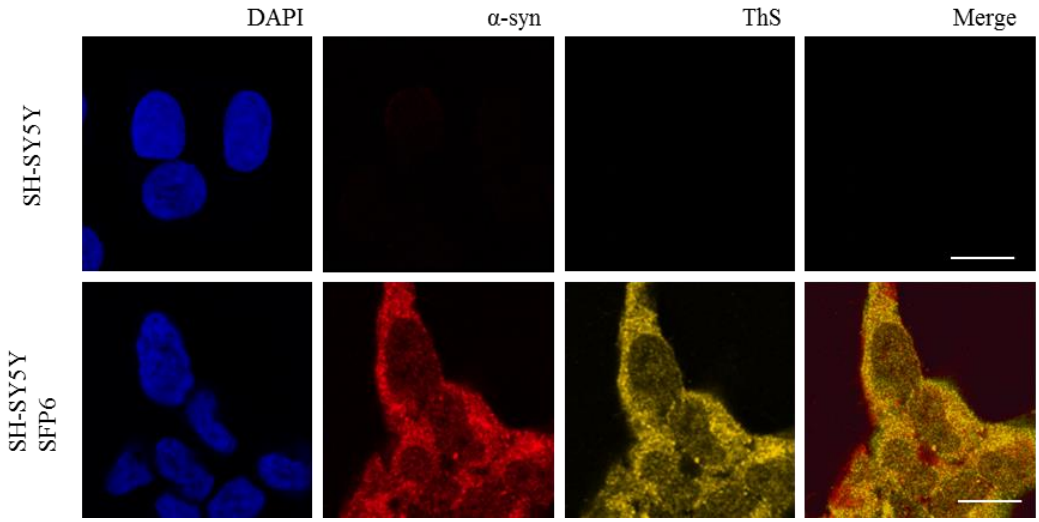

Figure 3.1.8. Thioflavin-S (ThS) positive staining of endogenous α-syn aggregates. SH-SY5Y cells were treated with recombinant human α-syn short amyloid fibrils (SF: short amyloid fibrils of α-syn) and sub-passed at sixth passage (p6). The deposition and level of α-syn (red) in α-syn-treated cell lines after six passages were detected by anti-α-syn antibody. The colocalization was observed between the ThS signal (yellow) and anti-human α-syn antibody (red). The nuclei (blue) were stained with DAPI. Scale bars, 12 μm.

3.1.3. Short amyloid fibrils of α-syn induce accumulation earlier in transfected SH-SY5Y cells

Since it has been reported that the addition of exogenous preformed fibrils of α-syn is able to induce LB-like inclusion formation in cells that overexpress the α-syn protein [75, 376], we wanted to examine whether our amyloid preparations were able to do so as well. In order to investigate this we used SH-SY5Y cells stably transfected with α-syn protein. First of all we applied three different preparations to cell culture and we could appreciate that also in these experimental conditions the short amyloid fibrils were internalized at a higher rate, if compared to the other two preparations (oligomers and long amyloid fibrils **Figure 3.1.9**).

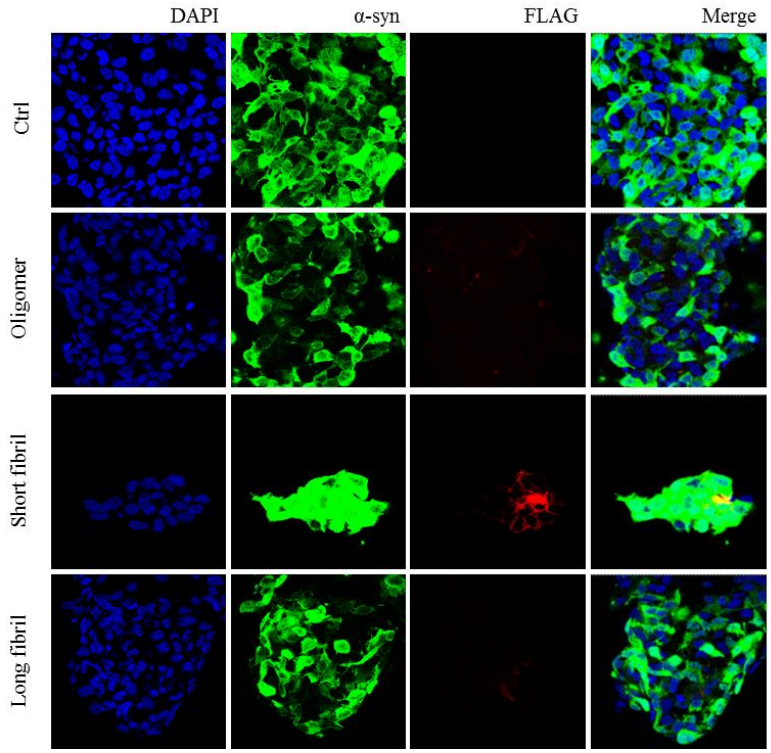

Figure 3.1.9. Internalization of FLAG-α-syn amyloids into neuroblastoma cells SH-SY5Y that overexpresses human α-syn protein. α-Syn deposition (green) was detected by anti-hu α-syn antibody. Immunofluorescence was performed on cells exposed to FLAG-α-syn amyloids (oligomers, short amyloid fibrils and long fibrils) for 7 days. Bar, 11.9 μm.

Next, we treated these cells with α-syn short amyloid fibrils and after passaging the cells, we observed stronger staining and, most importantly, the presence of several spots of α-syn throughout the cytosol. The accumulation of α-syn was confirmed using the Western blot technique at p5 in both SH-SY5Y that overexpress α-syn and the non-transfected cells (**Figure 3.1.15 B**). This suggests that α-syn short amyloid fibrils are able to seed aggregation of overexpressed α-syn in this cellular model. Due to the already high levels of α-syn in SH-SY5Y cells that overexpress human WT α-syn, the formation of endogenous α-syn aggregates upon infection with recombinant assemblies was evident earlier (p2) compared with non-transfected SH-SY5Y cells (p4) (**Figure 3.1.10**).

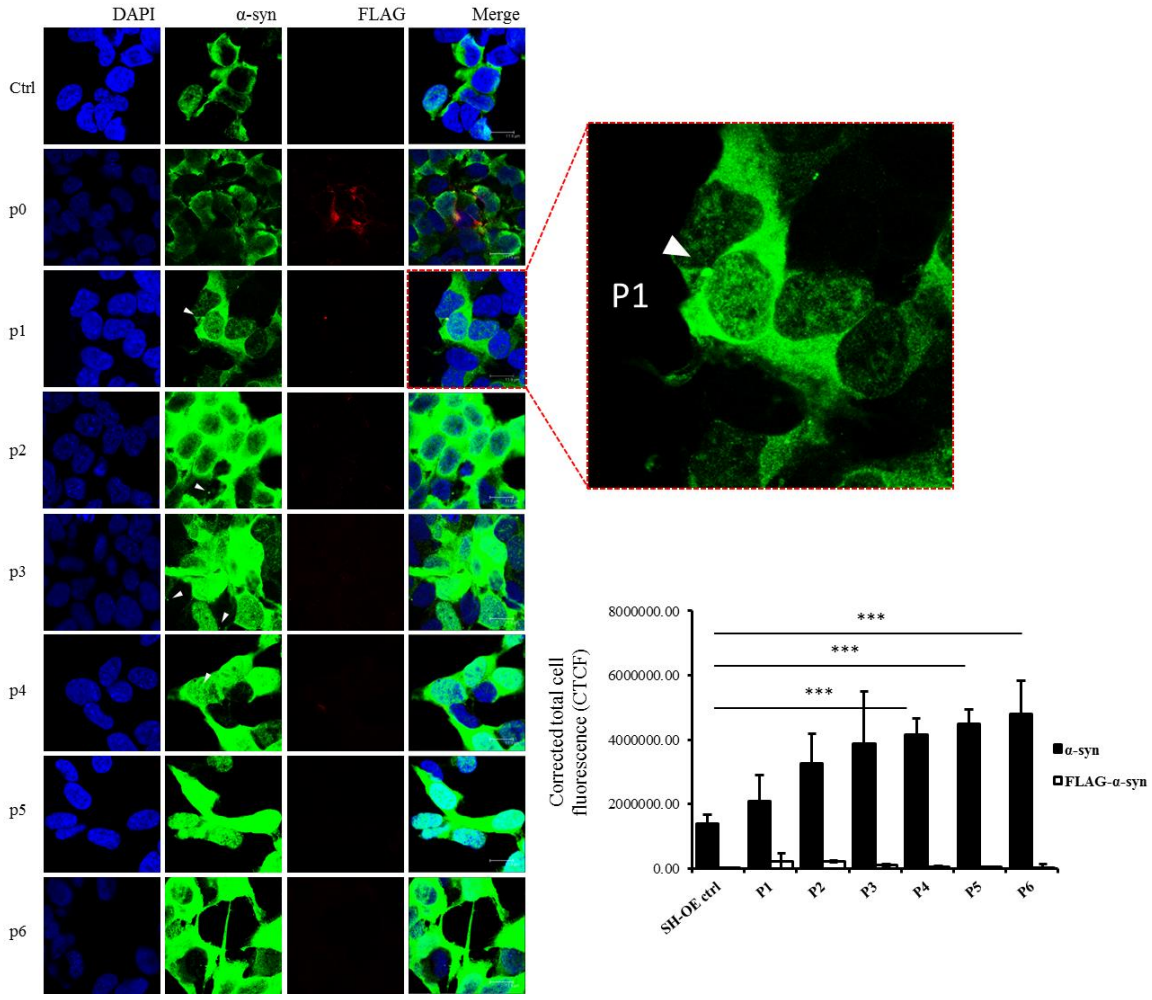

Figure 3.1.10. Infection of the transfected SH-SY5Y cells with α-syn short amyloid fibrils and sub-passing over time. The SH-SY5Y cells that stably overexpress human wild-type α-syn (SH-OE) were treated with recombinant human FLAG-α-syn short fibrils. Cells were cultured on coverslips for each passage (p0 to p6). The deposition of exogenous short amyloid fibrils FLAG-α-syn (red) was detected by anti-FLAG antibody. Human endogenous α-syn detected by anti-human α-syn (C-20)-R antibody (green). The nuclei were stained with DAPI (blue). Bar, 12 μm. The lower graph of corrected total cell fluorescence (CTCF) from immunofluorescence imaging shows the induction of endogenous α-syn in SH (neuroblastoma SH-SY5Y cell line) treated with human α-syn short amyloid fibrils during the passages (bottom panel). The analysis was performed on at least 150 cells, n = 3, ***$p < 0.005$. Values are mean ± SD.

Moreover, the aggregates in SH-SY5Y overexpressing α-syn at passage p6 were ThS-positive (**Figure 3.1.11**).

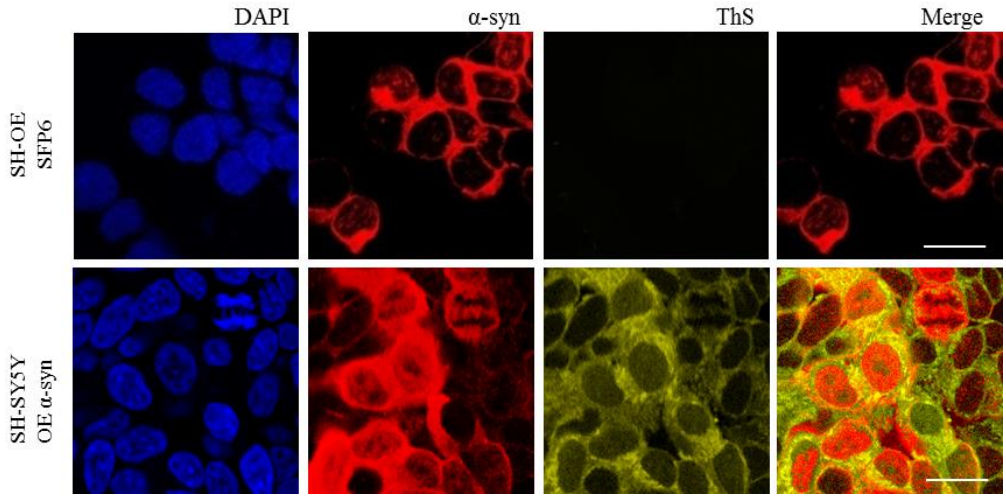

Figure 3.1.11. Thioflavin-S (ThS) positive staining of endogenous α-syn aggregates. SH-SY5Y cells were treated with recombinant human α-syn short amyloid fibrils (SF: short amyloid fibrils of α-syn) and sub-passed at sixth passage (p6). The deposition and level of α-syn (red) in α-syn-treated cell lines after six passages were detected by anti-α-syn antibody. The colocalization was observed between the ThS signal (yellow) and anti-human α-syn antibody (red). The nuclei (blue) were stained with DAPI. Scale bars, 12 μm.

To further characterize endogenous α-syn aggregates, the cell lines were probed with an antibody specific for α-syn phosphorylated at position 129 (p-Ser129). This post-translational modification of α-syn aggregates has been found in LBs of PD brains. Moreover, p-Ser129 α-syn has been reported to accumulate in the nuclei of α-syn transfected cells [454], and in Tg mice that express human α-syn [455]. A single-staining immunofluorescence confirmed higher levels of p-Ser129 α-syn within the nucleus after nine passages upon infection (SH-SFp9 and SH-OE SFp9, **Figure 3.1.12**) in both non-transfected and transfected SH-SY5Y cells, compared to control non-treated cells (Figure 3.1.13, lower panel). Since exogenous recombinant short amyloid fibrils are not phosphorylated *in vitro*, these modifications occur *de novo* within the cell after treatment and passaging. In addition, the cytoplasm of several α-syn treated SH-SY5Y cells contained α-syn aggregates (**Figure 3.1.12**, top panel).

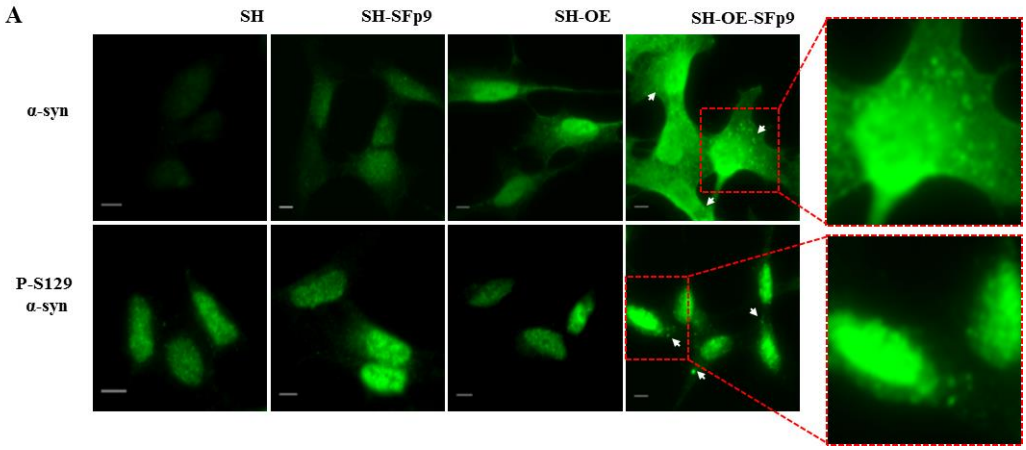

Figure 3.1.12. Short amyloid fibrils induce the formation of phosphorylated α-syn aggregates over passages. Presence of phosphorylated α-syn aggregates in SH-SY5Y overexpressing α-syn (SH-OE, top left panel). From left to right: neuroblastoma SH-SY5Y (SH), SH-SY5Y treated with human α-syn short amyloid fibrils at passage 9 (SH-SFp9), SH-SY5Y overexpressing α-syn (SH-OE) and SH-SY5Y overexpressing α-syn-treated with human α-syn short amylod fibrils at passage 9 (SH-OE-SFp9). Cells were immunolabeled with anti-α-syn antibody (green, upper panel) or anti-phospho S129 α-syn Ab59264 (green, lower panel). Scale bars, 5 μm. Arrows point at α-syn aggregates. Images are representative of at least three independent experiments.

Quantitative analysis showed that the number of cells with these cytoplasmic inclusions was remarkably higher in amyloid-treated cells compared to non-treated cells (54.8% vs. 7.7%, $p<0.001$) (**Figure 3.1.13**). Thus, we concluded that although overexpression of α-syn induces aggregation, this occurs to a much greater extent when combined with treatment. Interestingly, in amyloid-treated cells we found the same increase in phosphorylated aggregates compared to transfected cells (44.7% vs. 9.2%, $p < 0.001$) (**Figure 3.1.13**) indicating that most α-syn aggregates induced by short amyloid fibrils are phosphorylated. Together, these observations indicate that the endogenous α-syn aggregates in this cell culture model exhibit LB-like defining features.

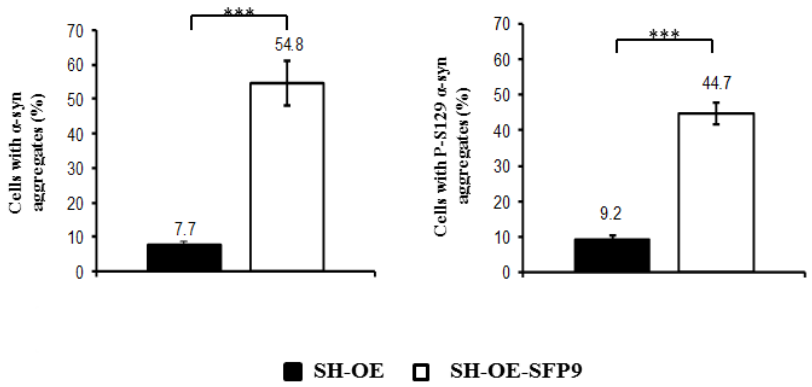

Figure 3.1.13. Quantification of phosphorylated α-syn aggregates in SH-SY5Y α-syn-treated cells. Bar diagram showing quantification of α-syn aggregates (left) and phospho S129 α-syn aggregates (right) in SH-SY5Y α-syn cells and SH-SY5Y α-syn-treated cells. ***p < 0.001 (Student t test, n > 150 cells counted for each condition per experiment). Error bars represent the SEM.

Furthermore, we were able to characterize biochemically these α-syn inclusions. More precisely, we used differential extraction methods (as schematically illustrated in **Figure 3.1.14**) to evaluate the presence of detergent-insoluble α-syn aggregates.

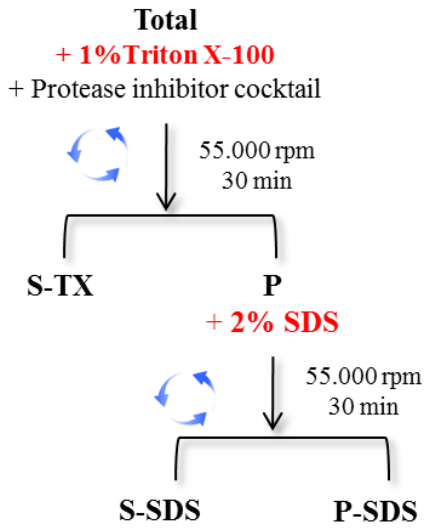

Figure 3.1.14. Scheme of serial extraction of detergent resistant α-syn amyloids. Cells were scraped into 1% TritonX-100 buffer containing phosphatase inhibitor cocktail. Following the 30min centrifugation two fractions were separated (S-TX) and the Pellet (P) was suspended in 2% SDS in TBS that was further centrifuged obtaining other two fractions, S-SDS and P-SDS. Samples were separated by SDS-PAGE and transferred onto nitrocellulose membrane that was immunoprobed with anti α-syn antibodies.

Unequivocally, the sequential extraction with 1% Triton X-100 followed by 2% SDS lysis buffer confirmed the insolubility of endogenous α-syn aggregates in these buffers. The

cells treated with short amyloid fibrils revealed formerly at p5 a substantial amount of Triton X-100 insoluble α-syn and high molecular weight species (HMW), which required SDS buffer for solubilization (**Figure 3.1.15 C**). Dissimilar to the weak signal observed in the SDS supernatant fraction (S), in the pellet fraction (P) we detected bands in the stacking part of the SDS-PAGE gel, which are comparable to those of short amyloid fibrils formed *in vitro* (**Figure 3.1.15 A**).

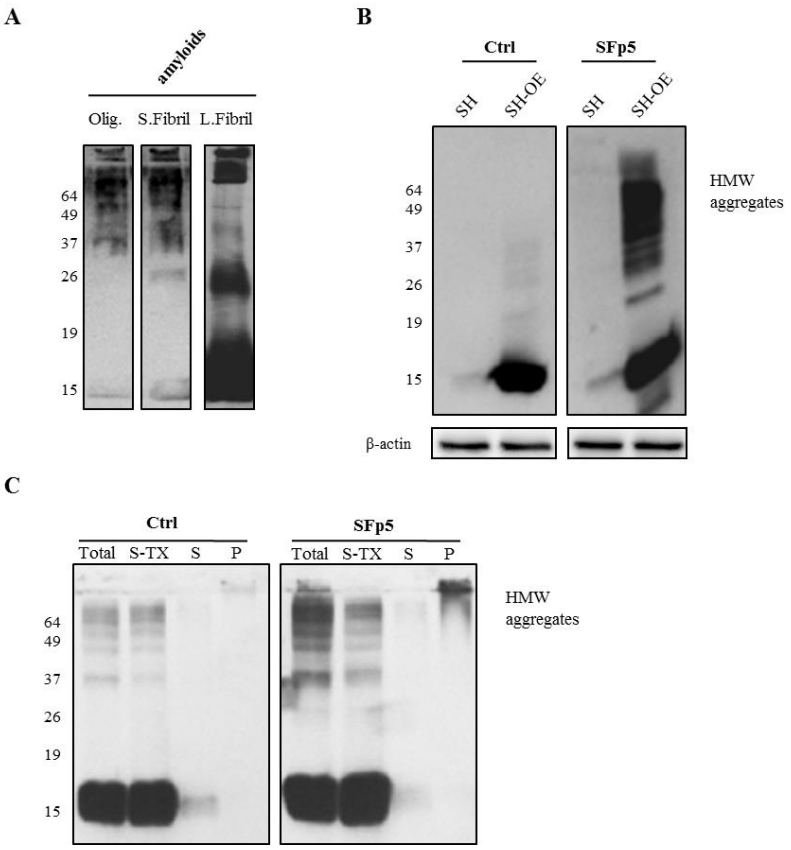

Figure 3.1.15. Aggregation of α-syn in dopaminergic human cell lines treated with recombinant human α-syn short amyloid fibrils and sub-passaged over five passages (p5). (A) Western blot of different assemblies formed *in vitro*. (B) Western blot of cell lysates (SH: SH-SY5Y cells; SH-OE SH-SY5Y overexpressing human α-syn); Ctrl: non-treated cells. SFp5: α-syn short amyloid fibril-treated cells at fifth passage. HMW: High molecular weight aggregates. (C) Western blot analysis of aggregated SH-OE cell lysates treated with α-syn short amyloid fibrils, and non-treated (Ctrl); Total: total cell lysates. Sequential extraction of α-syn aggregates in 1% Triton X-100 lysis buffer (S-TX), followed by 2% SDS lysis buffer (S). (P): a pellet fraction after the pellet was treated with 2% SDS. Anti-human α-syn (C-20)-R antibody was used.

3.1.4. Effect of the addition of human α-syn amyloids in murine GT-1 cell line

Having studied the aggregation properties of recombinant human FLAG-tagged α-syn and its ability to infect human neuroblastoma SH-SY5Y cell line *in vitro*, we questioned

whether this material would be suitable to induce aggregation of endogenous α-syn in murine cell lines. In particular, we treated with short amyloid fibrils mouse hypothalamic GT-1 cell lines. As shown in **Figure 3.1.16**, GT-1 cells were exposed to human α-syn short fibrils following the same procedure applied to SH-SY5Y cell line. In the GT-1 cell line, expression of endogenous mouse α-syn was low and, as expected, human α-syn was missing (**Figure 3.1.16**). A signal derived from immuno-positive human α-syn short fibrils was visible at early passages (p0 to p1, **Figure 3.1.16**, in red) but it was absent in subsequent passages (p2 to p4, **Figure 3.1.16**). At later passages, there was a marked increase in granular immuno-positive mouse α-syn signal (p3 to p4, **Figure 3.1.16**, in green). Again, the corrected total cell fluorescence measurements showed a steady increase in the signal of immuno-positive mouse α-syn, whereas the signal derived from FLAG-tagged recombinant human α-syn short fibrils abruptly decreased over the first two passages (**Figure 3.1.16**, graph).

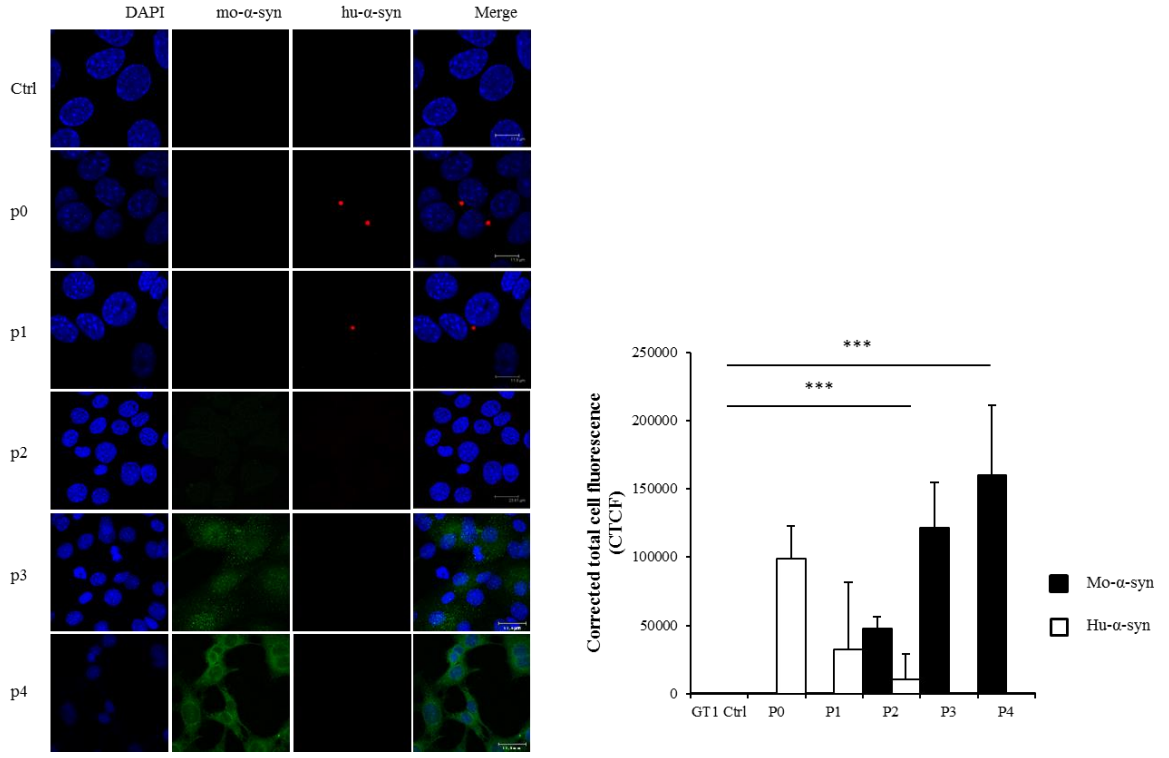

Figure 3.1.16. Treatment with short amyloid fibrils in another cell line (GT-1 cells) induces the same behavior. (A) Immunofluorescence images show the induction of endogenous mouse α-syn in GT1 cells after infection with human α-syn short amyloid fibrils over four passages. The detection of exogenously added short amyloid fibrils was performed using an anti-hu α-syn antibody [LB 509] (red). Mouse endogenous α-syn was detected by anti-mo α-syn antibody D37A6 (green). The nuclei were stained with DAPI (blue). Bars of Ctrl, p0 and p1 are 12 µm; bars of p2, p3, p4 are 24 µm. The graph shows the analysis of the relative corrected total cell fluorescence (CTCF) of endogenous α-syn in GT-1 cells treated with human α-syn short amyloid fibrils during the passages. The analysis was performed on at least 150 cells, n = 3, ***$p < 0.005$. Values are mean ± SD.

The presence of aggregated endogenous mouse α-syn in treated GT-1 cell line was evaluated using ThS to assess the extent of binding to β-sheet-rich structures such as amyloids (**Figure 3.1.17**).

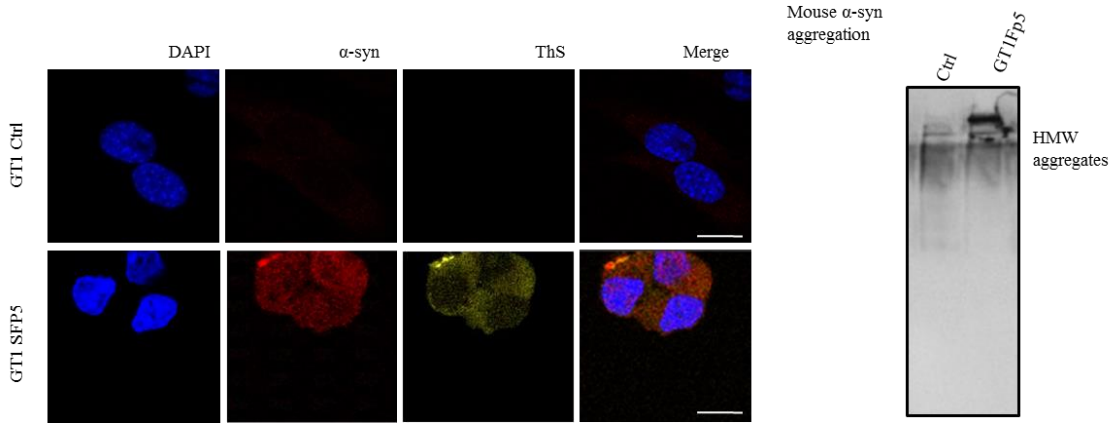

Figure 3.1.17. ThS staining of endogenous aggregated α-syn in GT-1- cells treated with short amyloid fibrils. The nuclei were stained with DAPI (blue). Bars are 12 μm; Western blot shows the presence of HMW aggregates in cell lysates exposed to short amyloid fibrils (immunoprobed with anti-α-syn antibody; SFp5: human α-syn short amyloid infected cells at fifth passage).

3.1.5. *In vivo* studies

Based on these findings, we performed *in vivo* stereotaxic injections of human α-syn short amyloid fibrils into SN of CD-1 WT mice. We chose this brain area as injection site because of its high susceptibility to accumulate α-syn pathology characteristic of PD. Even though none of the animals showed any significant behavioral changes, all mice were sacrificed and the brains were analyzed immunohistochemically (IHC). Implementing the α-syn IHC method we were able to detect LB-like pathology in neurons. More specifically, the α-syn intraneuronal aggregates detected were p-Ser129 positive. This staining pattern was detectible in neurons of specific brain regions, in particular in amygdala and cerebral cortex, areas far from the injection site (**Figure 3.1.18 A, B, C**). These pathological inclusions were localized both in the soma and in the neurites, whereas no staining for phosphorylated α-syn was detected in mice inoculated with monomers, oligomers, or long fibers of α-syn (**Figure 3.1.18 D, E, F**). Anatomically, the amygdala is connected with the SN, the site of stereotaxic injections. The striatum and the amygdala central nucleus have projections from SN, and the stria terminalis serves as a major output pathway of the amygdala. These findings strongly indicate that spreading of phosphorylated α-syn pathology does not occur by simple diffusion or non-specific transport. Thus, our results are in accordance with other reported works that

show that recombinant α-syn short fibrils are wholly sufficient to initiate PD-like LBs/LNs ant to transmit disease *in vivo* [76, 81].

To gain insights into a query whether synthetic α-syn amyloid fibrils could behave as infectious agents during passaging *in vivo* (as observed in cell culture *in vitro*), we performed the second passage of stereotaxic injections using BH derived from the first passage. Similar transmission studies are performed in prion field, assessing the transmissibility of scrapie forms. In the recent work reported by Masuda-Suzukake and colleagues [456] intracerebral injection with sarkosyl-insoluble fraction prepared from WT mice injected with synthetic α-syn fibrils can also induce phosphorylated α-syn pathology in WT mice. In our case the injection of the whole BH from the first passage show negative IHC for p-Ser129 α-syn, however it showed microglial activation in CNS (**Figure 3.1.18 G, H, I)**. Nevertheless, similar findings were observed when the extracts of brains with DLB showed lower propagation efficiency than recombinant α-syn fibrils [76]. However, in accordance with our results several reports show that sustained microglial activation is important contributors to the pathogenic processes in PD [85, 457]. The role of innate immune responses of microglia in neurodegenerative processes in many CNS diseases has become increasingly evident [458, 459].

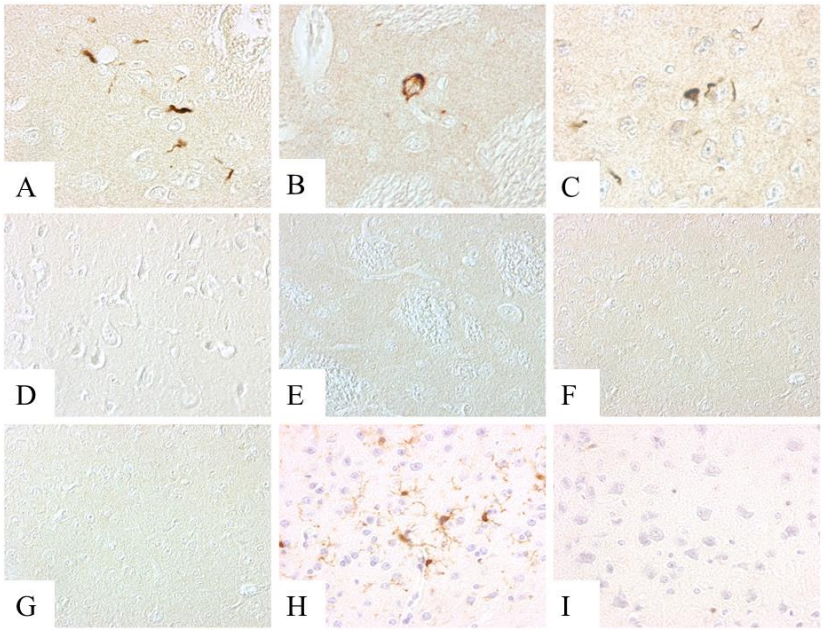

Figure 3.1.18. Immunohistochemical staining for p-Ser129 α-syn in CNS. The α-syn pathology cargo, consisting of LBs in cerebral cortex (A, D, G), striatum (B, E), and amygdala (C, F) stained with anti-p-Ser129 Ab. Iba1 was used as a marker of microglia activation (cerebral cortex: H, I). In the first passage (A-F), inclusions of phosphorylated α-syn are present in neuronal soma and neurites in the brain of mice inoculated with α-syn short fibrils (A-C), whereas they are absent in mice inoculated with other types of fibrils or PBS (the brain of a mouse injected with α-syn long fibers is shown in D-F). In the second passage (G-I), inclusions of p-Ser129 α-syn are not present in mice inoculated with the BH that received α-syn short fibrils (G) but marked and diffuse microglial activation was detected (H) whereas this was absent in the control mice (I). Magnification: 40x in all panels.

In conclusion, a single inoculation of recombinant human short α-syn amyloids in SN of WT mice can induce α-syn aggregation, accumulation and phosphorylation *in vivo*. It is well known that prion propagation can cross the species barrier [460] and the efficiency of propagation depends on the amino acid sequences of prion proteins. In the case of α-syn, mouse and human α-syn share 95% amino acid sequence homology, and this may be the reason why endogenous mouse α-syn is capable of aggregation by inoculation of human α-syn fibrils. Another factor may be that mouse α-syn protein has a threonine residue at amino acid position 53, which is known as an aggregation-prone mutation in familial PD [42].

On the other hand the second passage experiments did not induce the formation of α-syn pathology most probably due to the use of whole BH, and not isolated LBs fraction or sarkosyl-insoluble fraction. This relatively low efficiency may be explained by the lesser amount of abnormal α-syn contained in the brain extracts.

Part II: Cellular prion protein binds α-synuclein fibrils

While the function of the cellular form of the prion protein is still under debate, several reports attributed numerous roles to this GPI-anchored protein; such as involvement in regulation of the immune system and its responses, signal transduction, synaptic transmission, copper binding, etc. Moreover, recent findings describe PrP^{C} as being involved in binding and modulation of toxicity of amyloids involved in neurodegenerative disorders (such as Aβ oligomers in AD, and PrP^{Sc} in TSEs).

Certainly, the endogenous expression of PrP^{C} is essential for TSE pathogenesis and its transmission. Actually, the direct interaction of PrP^{C} with the pathogenic form, called PrP^{Sc}, has been validated. This interaction leads to the conformational change of the cellular form that subsequently gets converted into β-sheet rich PrP^{Sc} isoform. As mentioned in the introduction part of this PhD Thesis, three distinct regions have been recognized as essential for this binding: one localized in the C-terminal part, and the other two in the N-terminal part of the cellular prion protein. Interestingly, the same two amino-terminal regions have been found to interact with other amyloidogenic proteins, such as Aβ (for details see **CHAPTER I** *"Introduction"*).

In **Part II** of this thesis we focused on the investigation whether the cellular prion form is able to bind other amyloids involved in other neurodegenerative disorders, such as α-syn amyloids. In order to explore this, we used the same methodology employed to obtain synthetic mammalian prions, and formed recombinant mouse α-syn amyloids, which we applied in cell culture.

Results II

3.2.1. Preparation of mouse α-syn fibrils and structural characterization

Similarly to the preparation of synthetic human α-syn fibrils reported in Results I (**Part I**), here we performed the fibrillation assay using the mouse α-syn sequence. The latter contains in its sequence seven different amino acids, compared to human protein: A53T, S87N, L100M, N103G, A107Y, D121G, and N122S. Interestingly, among these seven residues mouse α-syn protein contains a Threonine at the position 53, similarly to a naturally occurring mutation in humans (A53T) that is found to be a cause of the familial form of PD. This substitution most probably influences time of fibril formation (called lag phase) [229]. When we compared the lag periods, we could observe different kinetics of fibril formation between human and mouse sequence (**Figure 3.2.1**): the human α-syn showed a longer lag phase of 13.3 ± 2.3 h, whereas the mouse α-syn fibril formation showed only 2.4 ± 0.23 h of lag phase.

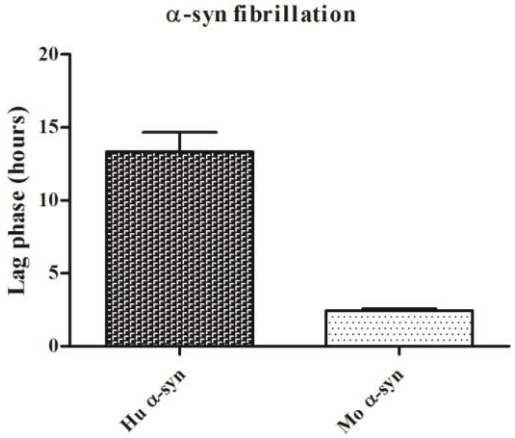

Figure 3.2.1. Lag phases of fibril formation for human and mouse α-syn protein. The mouse α-syn protein forms fibrils much faster compared to human protein (13.3 ± 2.3 h vs 2.4 ± 0.23 h).

Using the fibrillation method we obtained mouse α-syn fibrils. First, we performed the fibrillation in three days (**Figure 3.2.2 A** purple dashed square) in order to increase fibril concentration and to reach a phase where the most of soluble protein is converted into fibrils. Second, knowing the lag phase of mouse α-syn fibril formation, we also formed the short α-syn amyloids interrupting fibrillation reaction after six hours (forming α-syn amyloid preparation called F.NON). After 5 minutes of sonication the distribution of short fibrils was changed (from now defined as F.sonic). As shown in graphs in **Figure 3.2.2 B** number of

counts bellow 20 nm increased after 5 minutes sonication, confirming that the sonication process breaks fibrils into smaller species. Indeed, in AFM images we could observe the presence of fractionate fibril polymers and multiple seeds deposited on the mica surface (**Figure 3.2.2 B**). High molecular weight species including dimers, and monomers were detected by Western blot (**Figure 3.2.2 C**).

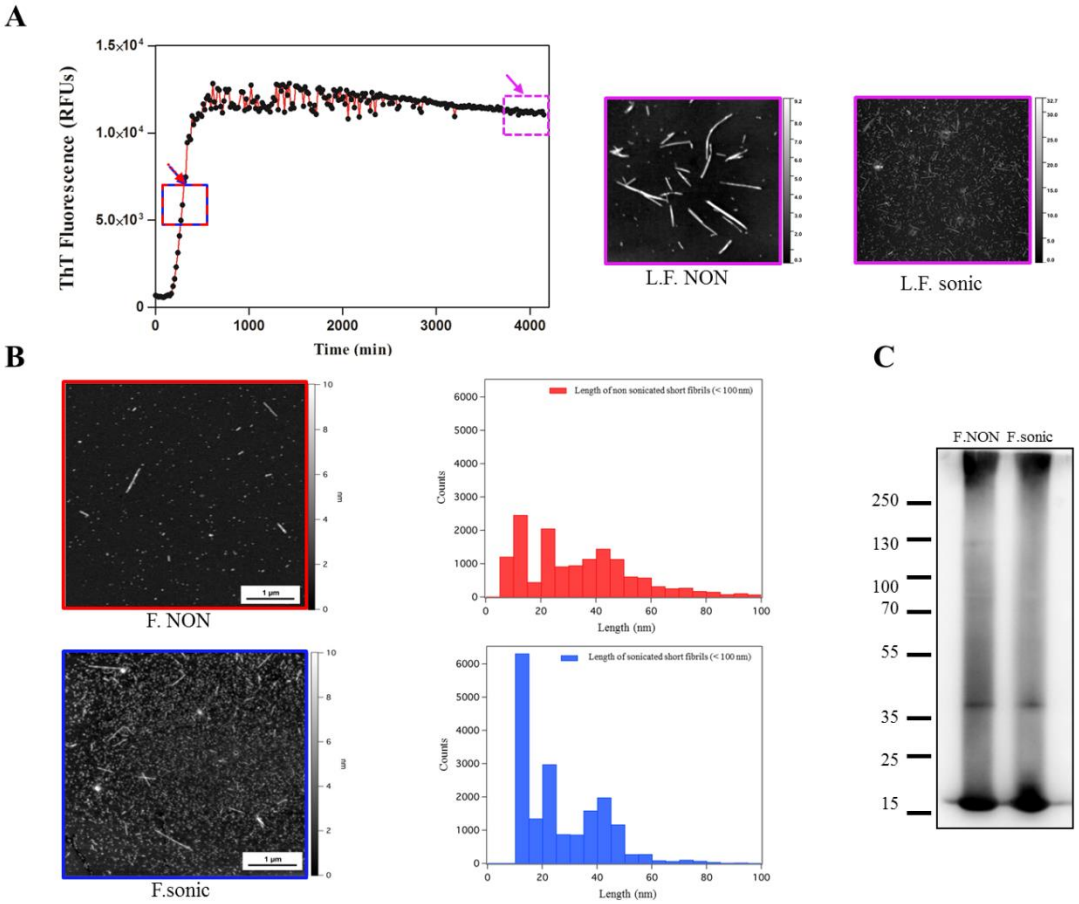

Figure 3.2.2. Characterization of mouse α-syn fibrils. Fibrillation curves (**A**) of recombinant mouse α-syn protein with respective AFM images of long fibrils before and after sonication (L.F. NON and L.F. sonic, respectively). (**B**) A more detailed AFM analysis has been performed on short amyloid fibrils before and after sonication (F.NON and F.sonic) with corresponding counts for sample. (**C**) The WB depicts the biochemical profile of short amyloid fibrils before and after 5 min of sonication.

After morphological characterization we moved on to cell culture studies. First, we checked the toxicity of these preparations using the aforementioned viability assay. This is an important step in toxicity studies required to determine the cellular response to exogenously added agents. Notably, using the MTT assay we did not detect any significant reduction in cell viability after 24 h exposure to different α-syn amyloid preparations (F. sonic and F.

NON, **Figure 3.2.3**). Four different neuroblastoma (N2a) cell lines were exposed to the same concentrations of sonicated and non-sonicated α-syn fibrils. Here we used the murine neuroblastoma N2a cell line that endogenously expresses the cellular form of PrP (N2a). This cell line is frequently used in studies on the PrP protein [437, 461, 462]. The N2a KO is the cell line where the PrP^{C} protein has been ablated using the new CRISPR-Cas9-Based Knockout system [293], while N2a PrPFL is the same cell line were the expression of the full-length PrP protein has been re-introduced using the transfection procedure. Finally, the cells that are chronically infected with RML prion strain and replicate prions (ScN2a) were also used [437]. This cell line is a valid tool for studying prion replication.

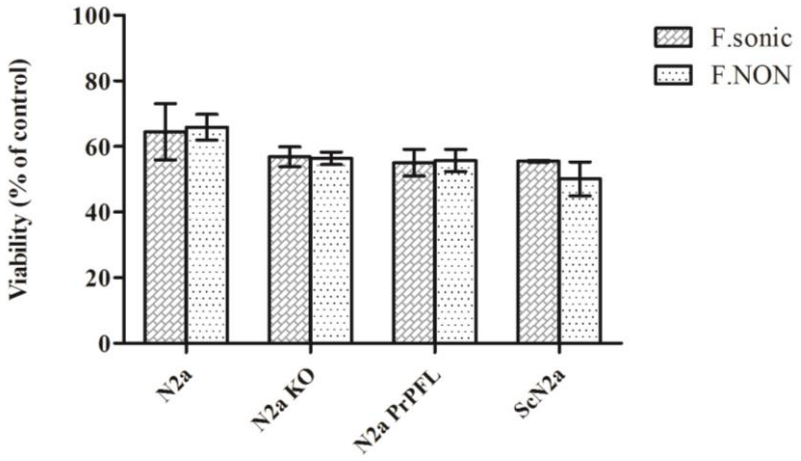

Figure 3.2.3. Cell viability of cells treated with sonicated and non-sonicated α-syn fibrils. Cell viability of N2a cells that express endogenously the PrP^{C} protein (N2a), PrP^{C} knockout cells (N2a KO), in cells in which the cellular prion protein expression was re-introduced (N2a PrPFL), and in scrapie infected cells (ScN2a).

3.2.2. Cells expressing cellular prion protein take-up α-syn fibrils to a major extent

Several previous works report that PrP^{C} binds disease-associated aggregates, such as PrP^{Sc} and Aβ oligomers. This observation led us to hypothesize that PrP^{C} may bind, in general, a variety of β-sheet enriched forms. In order to verify this, we quantified the uptake of mouse α-syn fibrils in the cell lines mentioned above. More precisely, to determine the uptake of exogenously added α-syn fibrils, N2a cells were treated with 2μM (30μg/ml) of α-syn fibrils for 24 h. In parallel, also N2a KO cells were treated with the same concentration of α-syn amyloid preparations. After 24 h of incubation 81.2 ± 3.1% of N2a cells that endogenously express PrP^{C} protein were able to take-up the α-syn fibrils, while the N2a KO cells had significantly fewer α-syn fibrils within the cytoplasm (30.7 ± 4.4 %). Moreover, we compared whether sonication implies any different uptake profile in these cells, and the

difference was not significant among the two cell lines (**Table 3.2.1**)**.** When we re-introduced the PrP^C protein in N2a KO cells (N2a PrPFL) the uptake was comparable to N2a cells that endogenously express the cellular prion protein (**Table 3.2.1**)**.**

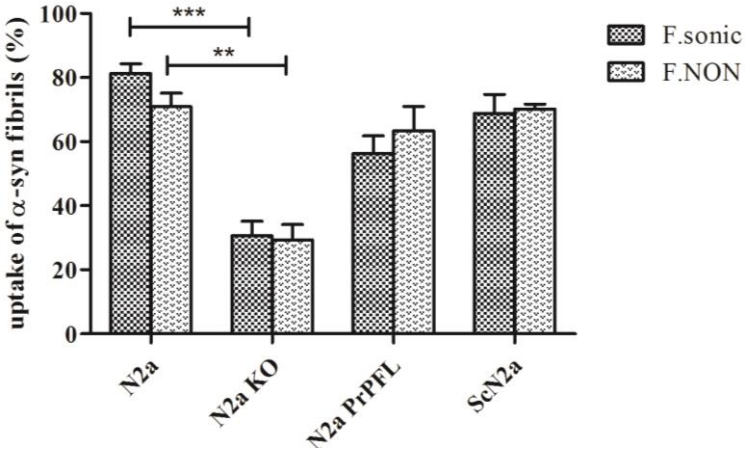

Figure 3.2.3. Uptake of mo α-syn fibrils in neuroblastoma cells. The analysis was performed following the immunofluorescence protocol described in Material and Methods. A total of four hundred cells were counted in blind in three independent experiments. Data are represented as mean±SD. Data were evaluated by unpaired T-test. Statistical analysis is indicated as: * = $p < 0.05$, ** = $p < 0.01$, *** = $p < 0.001$.

Table 3.2.1. Uptake of mo α-syn fibrils in different neuroblastoma cells

Cell line: α-syn fibrils	N2a	N2a PrPFL	N2a KO	ScN2a
F. sonic	81.2 ± 3.1	56.3 ± 5.5	30.7 ± 4.4	68.8 ± 5.9
F. NON	70.5 ± 6.0	63.3 ± 7.6	29.4 ± 4.7	70.1 ± 1.6

In this part of the work we have highlighted the potential ability of PrP^C expressing cells to uptake α-syn amyloids in a higher rate compared to those that do not express the cellular prion protein.

3.2.3 Exogenously added α-syn fibrils induce an increase of endogenous prion protein

From the immunoblotting analysis we have found that treatment with α-syn fibrils induces an increase of PrP^C protein levels in N2a cells after 4 days of treatment (**Figure 3.2.4** compare line ctrl and p0). After subsequent culturing in α-syn fibrils-free medium the protein

levels of cellular prion protein were higher, although this increase was not significant over multiple passages (only at passage p2).

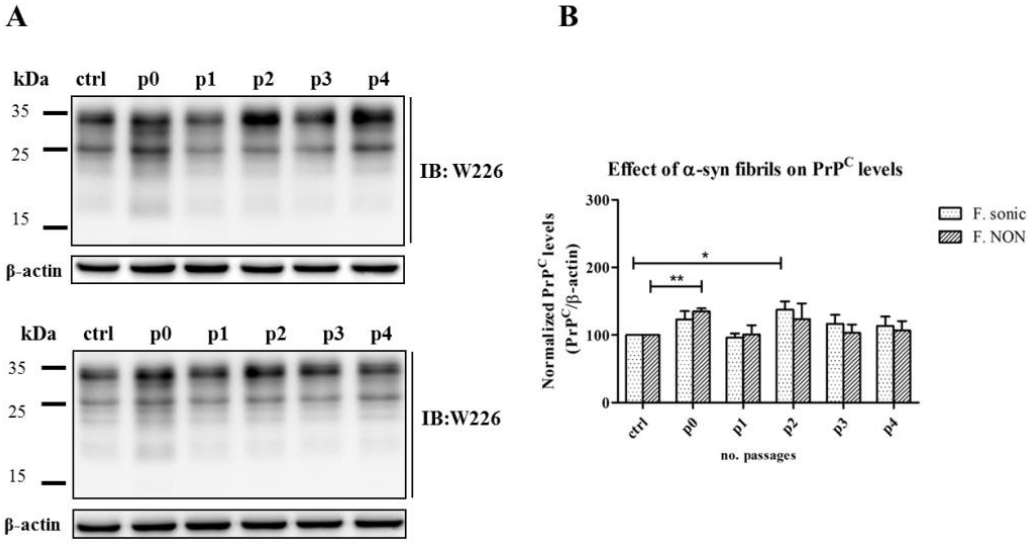

Figure 3.2.4. Effect of α-syn preparations on PrP protein levels in N2a cells. A) The cell lysates were prepared as described in Materials and Methods and analyzed by SDS-PAGE and WB, using W226 anti-PrP antibody. Each line was loaded with 30 μg of total protein. **B)** The quantification of three independent experiments is shown in the graph. The values are shown as a percentage of total PrP relative to β-actin (that is a loading control). Data are represented as mean±SD. Data were evaluated by unpaired T-test. Statistical analysis is indicated as: * = $p < 0.05$, ** = $p < 0.01$, *** = $p < 0.001$.

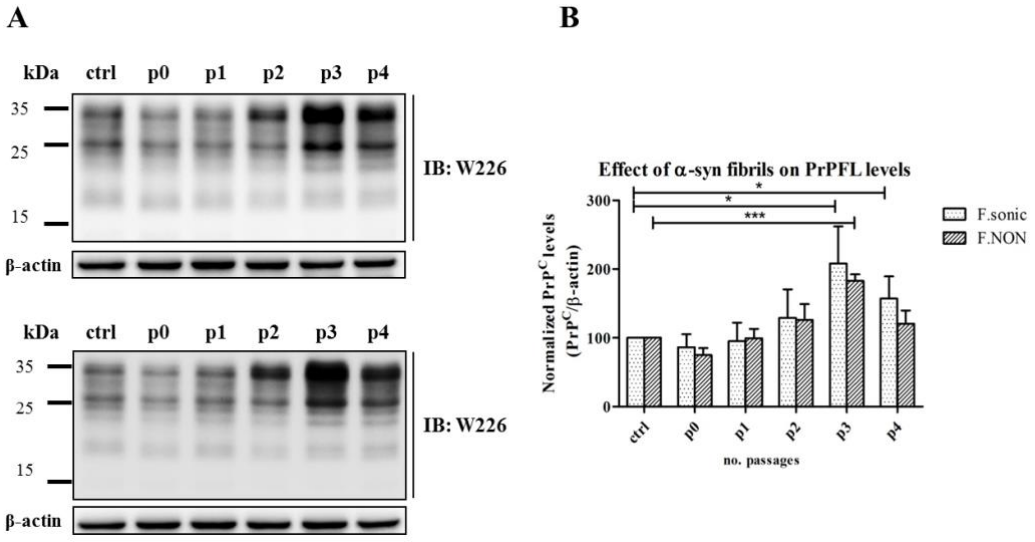

Figure 3.2.5. Effect of α-syn preparations on PrPFL levels in N2a PrPFL cells. A) The cell lysates were prepared as described in Materials and Methods and analyzed by SDS-PAGE and WB, using W226 anti-PrP antibody. Each line was loaded with 30 μg of total protein. **B)** The quantification of three independent experiments is shown in the graph. The values are shown as a percentage of total PrP relative to β-actin (that is a

loading control). Data are represented as mean±SD. Data were evaluated by unpaired T-test. Statistical analysis is indicated as: * = p < 0.05, ** = p < 0.01, *** = p < 0.001.

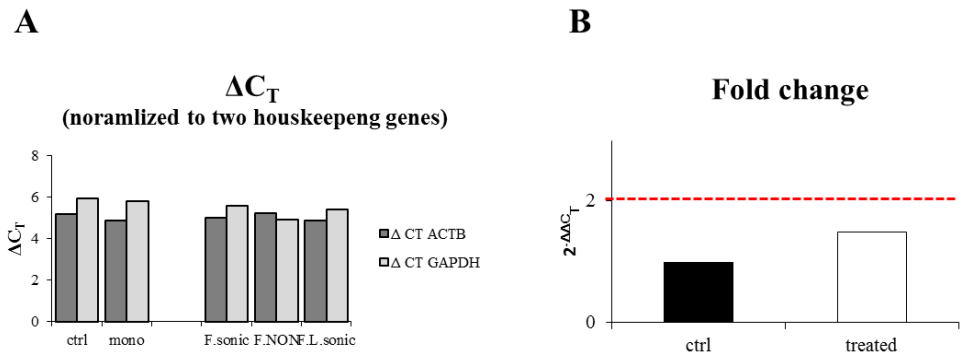

Figure 3.2.6. RT-PCR analysis of N2a non treated and treated samples. A) ΔC_T values for *Prnp* gene shows no variability among control and α-syn treated samples. Normalization of RT-qPCR data was performed on two housekeeping genes, ACTB (dark grey) and GAPDH (light grey). **B)** $\Delta\Delta C_T$ values in control and treated samples. The relative expression ratio was calculated using the $\Delta\Delta C_T$ method. Although positive fold change is observed the threshold is not reached indicating that the increase was not significant.

To verify at what level this increase was occurring we isolated total RNA from N2a treated cells and controls and PrP mRNA was quantified by real-time PCR (RT-PCR). The results showed that high protein levels of PrP were not correlated with high mRNA levels (**Figure 3.2.6**), indicating that treatment with fibrils increases PrP protein levels at a post-transcriptional level.

Table 3.2.2. Data analyzed by Fisher's test (F test) and Student's t-tests (T-test). According to two tests no significant difference was observed between the two groups using two reference genes.

Reference gene	F test	T test
ACTB	0.727	0.988
GAPDH	0.408	0.112

PrP^C is subjected to proteolytic processing that produce biologically active fragments. The processing of the prion protein is thought to influence not only the course of the prion diseases but also other neurodegenerative diseases [463]. Indeed, as initially reported for chicken PrP and later extended for mammalian PrP^C, a released soluble fragment of approximately 11kD (termed N1) and a N-terminally truncated membrane-attached counterpart of approximately 18 kD (termed C1, which after deglycosylation runs at approximately 16 kD [464]) were found in transfected cell lines and, more importantly, under

physiological conditions in brain homogenates and cerebrospinal fluid [295, 464, 465]. The corresponding cleavage was termed α-cleavage (discriminating it from another upstream β-cleavage site) and was identified by sequencing and epitope mapping at positions K110/H111 or H111/M112 (human sequence) located directly upstream of the hydrophobic core domain [296]. In fact, α-cleavage is the main proteolytic processing event yielding C1 fragments [465]. When N2a cells treated with α-syn fibrils were deglycosylated with PNGase to remove N-linked oligosaccharides, we could observe that the lower bands (called C1 fragment,) were more intense in α-syn treated cell lysates. To confirm that the lower bands were C1 fragment membranes were probed with two different antibodies, recognizing the C-terminal (mouse mAb W226), and N-terminal part (mouse mAb SAF34) of PrP. When the membrane was probed with C-terminal Ab the full length and 16kDa bad were present, while probing the membrane with N-terminal Ab the lower band could not be detected (**Figure 3.2.7**) confirming the presence of C1 fragment.

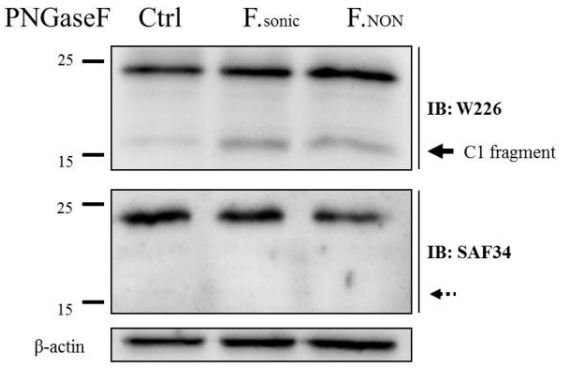

Figure 3.2.7. Electrophoretic pattern of PNGase F digested PrP^C in cells treated with α-syn fibrils. After PNGase F deglycosylation cell lysates were separated by SDS-PAGE and PrP was immunoblotted with two Abs that recognize C-terminal part (W226 upper membrane), and N-terminal of the prion protein (SAF34 lower membrane). β-actin is a loading control.

3.2.4 Exogenously added α-syn fibrils rapidly diminish the PrP^{Sc} levels in scrapie infected ScN2a cells

The same concentrations of α-syn fibrils (F.sonic and F.NON) were added to scrapie-infected N2a cells (ScN2a) and maintained in incubation for 4 days. Cells were then collected and PrP^{Sc} levels were analyzed by immunoblotting before and after proteolysis (proteinase K digestion, 20μg/ml, 37°C for 1h). To our surprise the levels of PrP^{Sc} in cells treated with

F.sonic α-syn fibrils were undetectable, while the treatment with F.NON α-syn fibrils dramatically reduced PrP^{Sc} (although a faint signal was present **Figure 3.2.8**). In control samples treated with PBS buffer, after PK digestion, the characteristic pattern of N-terminally truncated fragments of di-, mono- and non-glycosylated PrP was observed, with a predominance of mono-glycosylated PrP.

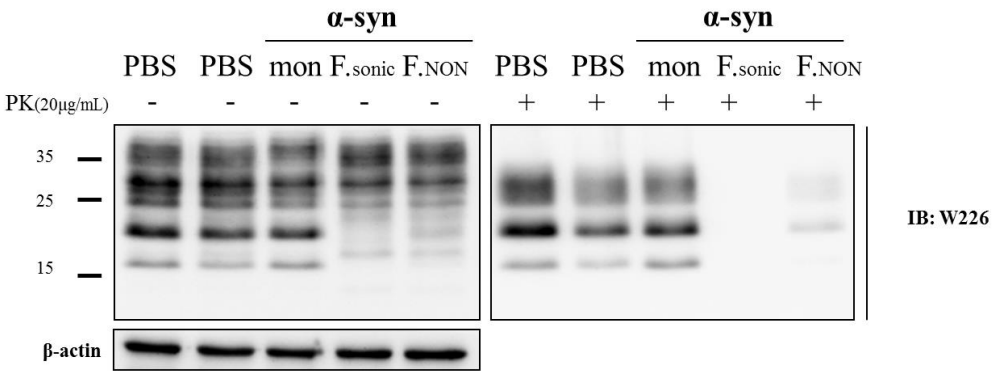

Figure 3.2.8. Western blot analysis of PrP^{Sc} in ScN2a cell lysates after treatment with α-syn fibrils. Following the treatment with different α-syn preparations, total PrP and PK-resistant PrP^{Sc} proteins were separated by SDS-PAGE and detected with anti-PrP Ab (W226). β-actin is a loading control.

This effect of α-syn on PrP^{Sc} levels was observable only when α-syn was in its fibrillary form, considering that the same concentration of monomeric α-syn did not have any effect on PrP^{Sc} amount (**Figure 3.2.8**, line *"mon"* stands for monomeric α-syn). Moreover, even if the time of fibrillation was longer (3 days), maintaining the same time of sonication (5 min), the effect on PrP^{Sc} was the total abolishment of PK-resistant form (**Figure 3.2.9**).

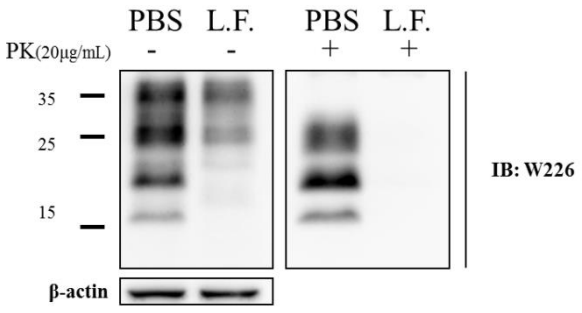

Figure 3.2.9. Western blot analysis of PK-resistant PrP^{Sc} in ScN2a cell lysates after treatment with sonicated long fibrils of α-syn (L.F. sonic). Following the treatment with sonicated long fibrils of α-syn (L.F.), total PrP and PK-resistant PrP^{Sc} proteins were separated by SDS-PAGE and detected with anti-PrP Ab (W226). β-actin is a loading control.

Furthermore, this effect on PrP^{Sc} was investigated also by immunofluorescence analysis. Here, we can note that, in control condition, after denaturation with 6M Gnd·HCl a PK-resistant PrP was present within the ScN2a cells (**Figure 3.2.10**). The control cells showed a typical punctate and aggregate-like pattern after the denaturation step (indicated by white arrows), while the treated cells presented a diffuse cytoplasmic staining with anti-PrP antibody (green staining). Consistent with the Western blot analysis, the immunofluorescence experiments showed lower signal relative to PrP^{Sc} deposits, after exposure to exogenous α-syn preparations.

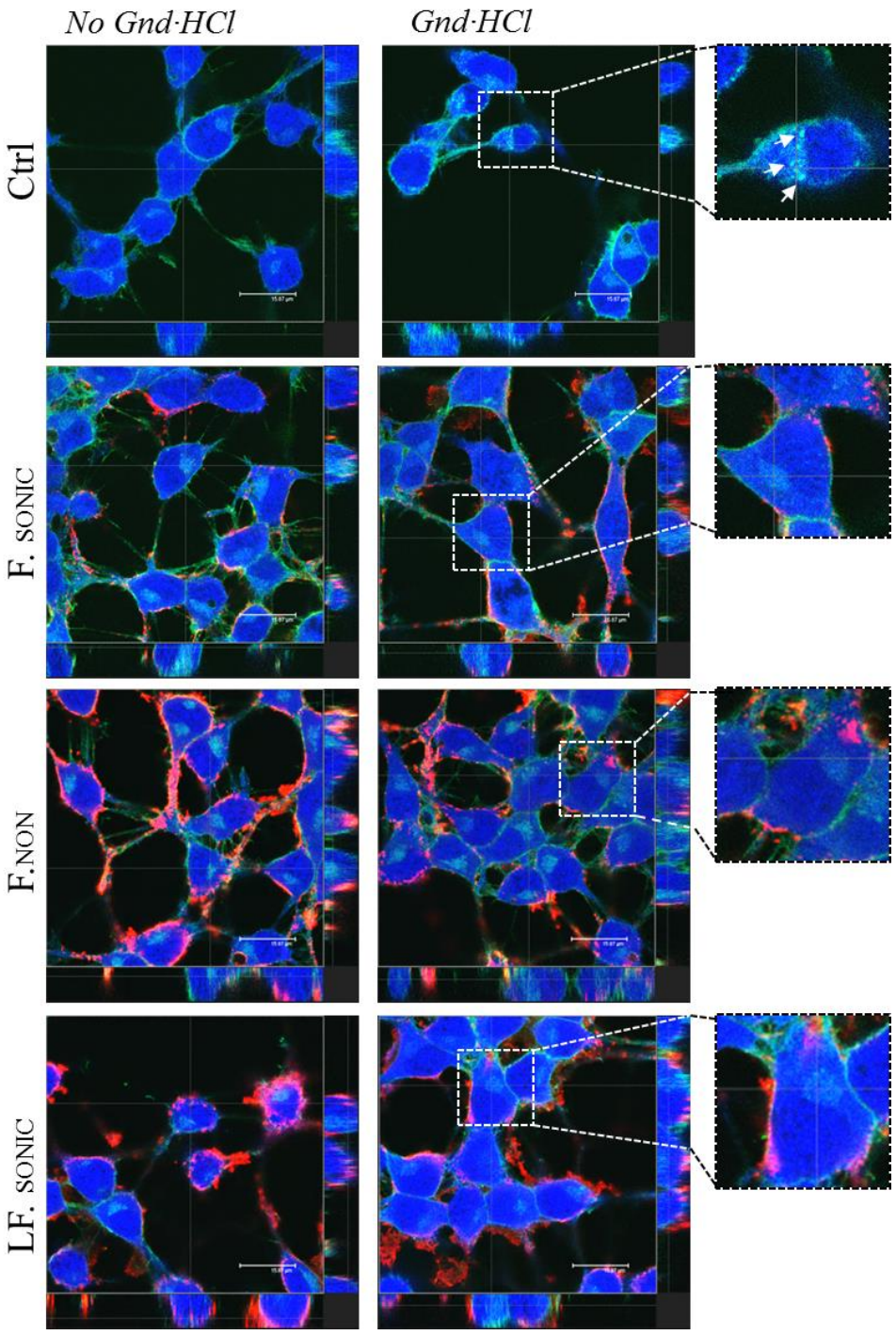

Figure 3.2.10. Detection of PrP^{Sc} in ScN2a cells before and after treatment (4 days) with different α-syn preparations by immunofluorescence technique [440, 441]. Denaturation with 6M Gnd·HCl expose the epitopes that normally are buried within the aggregates, allowing to visualization of the PrP^{Sc} form in ScN2a cells. After 4 days of incubation with different α-syn preparations (F.sonic, F.NON. LF.sonic) the cells were fixed, permeabilised, and then denatured with 6M Gnd·HCl or not treated with Gdn·HCl. Cells were stained with anti-PrP Ab (W226, in green) and anti-α-syn Ab ((C-20)-R, in red). The whole cell cytoplasm, including nuclei, was stained with CellMask (in blue). Composite Z-stack image of ScN2a cell line treated with α-syn amyloid preparations. One of 20 z-stacks (0.22μm) of confocal image is shown in the panel. Bars: 15.87 μm.

As mentioned above the processing of the prion protein might influence the course of the prion diseases. The PrP109-122 region is one of the α-helical regions that were postulated to acquire a β-sheet structure in PrP^{Sc} and it plays a critical role in the conformational changes underlyin the conversion of PrP^{C} to PrP^{Sc} [261, 466]. PrP106-126 peptide is prone to form fibrils similar to those present in the PrP amyloid plaques of prion diseases [467], and it is cytotoxic [264]. The α-cleavage between PrP amino acid residues 110-110 or 111-112 disrupts the PrP106-126 region that is critical for both prion replication and PrP toxicity and generates the bioactive N1 and C1 fragments [468]. In our case, when ScN2a cells were treated with α-syn fibrils and when the cell lysates were enzymatically deglycosylated with PNGase F we could observe that the 19kDa proteinase-resistant core disappears after α-syn fibril treatment, compared to controls (first three lines), which is in agreement with the PK digested WB profile (**Figure 3.2.8**). In case of F.NON treatment the PK-resistant band was faint, which confirms also the fact that not all PrP^{Sc} was cleared. Following the deglycosylation we have the formation of another band bellow 15 kDa (C1 fragment), which was more intense in α-syn fibrils treated cells (**Figure 3.2.11 A**, indicated by arrow). As for N2a cells, we confirmed that the lower bands correspond to C1 fragment by probing the membranes with two different antibodies that recognize C- or N-terminal part, W226 and SAF34 respectively. As observed in **Figure 3.2.11 B** when the membrane was probed with N-terminal Ab the lower band could not be detected.

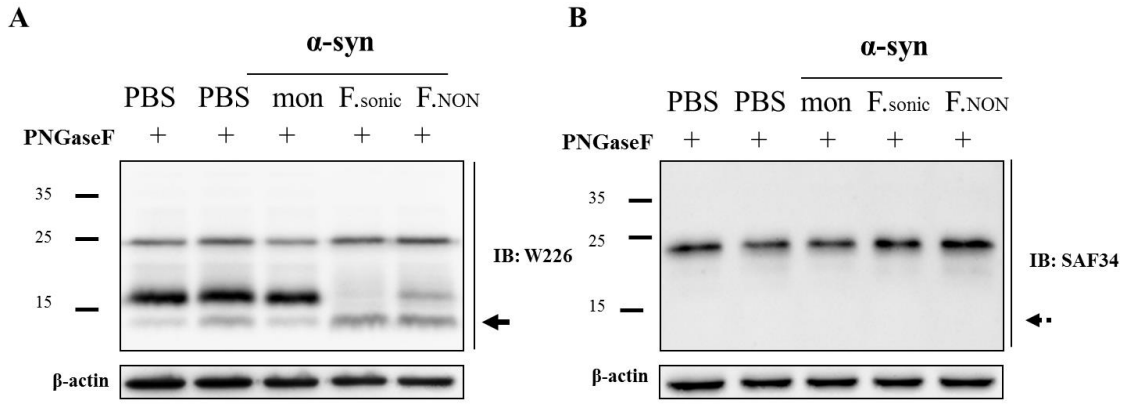

Figure 3.2.11. Electrophoretic pattern of PNGase F digested PrP in ScN2a cells treated with different α-syn forms. After PNGase F deglycosylation cell lysates were separated by SDS-PAGE and PrP was immunoblotted with two Abs that recognize **A)** C-terminal (W226), and **B)** N-terminal of the prion protein (SAF34). Solid black arrow shows the presence of C1 fragment recognized with C-terminal Ab, while the broken black arrow indicates the absence of the bands when the membrane was probed with N-terminal Ab. β-actin is a loading control.

Next, in order to determine whether PrP^{Sc} re-accumulates after removal of α-syn fibrils, the scrapie-infected cells were maintained in culture over multiple passages in α-syn fibril-

free medium. After 4 serial passages (p) in α-syn fibril-free medium very low PrP^{Sc} levels could be detected in cells treated with sonicated α-syn fibrils (F.sonic, **Figure 3.2.12** from p0 to p4 PrP^{Sc} recovered up to ~6%). On the contrary, the absence of sonication (F.NON) returned the PrP^{Sc} levels to about 80% of the level of untreated controls, after serial passages (**Figure 3.2.13** p0 to p4). This observation was predictable since the reduction of PrP^{Sc} levels upon treatment with F.NON was lower compared to F.sonic treatment, allowing the residual PrP^{Sc} to drive generation of new scrapie molecules faster over passages then F.sonic treatment. This analysis led us to conclude that the reversibility effect on PrP^{Sc} was different between the sonicated and non-sonicated preparations. Thus, we hypothesized that the sonicated fibrils, which are smaller in dimensions, bind to cellular prion protein in a way that the substrate necessary for prion replication is subtracted for further replication process of the PrP^{Sc} isoform. Indeed, it is reported that PrP^{Sc} directly binds to PrP^{C} and triggers its conformational misfolding into new PrP^{Sc} molecules. Here, we hypothesize that the inhibitory effect of α-syn fibrils is due to the specific binding to PrP^{C} molecules on the cell surface, which in this way blocks the docking of PrP^{Sc} template for further replication.

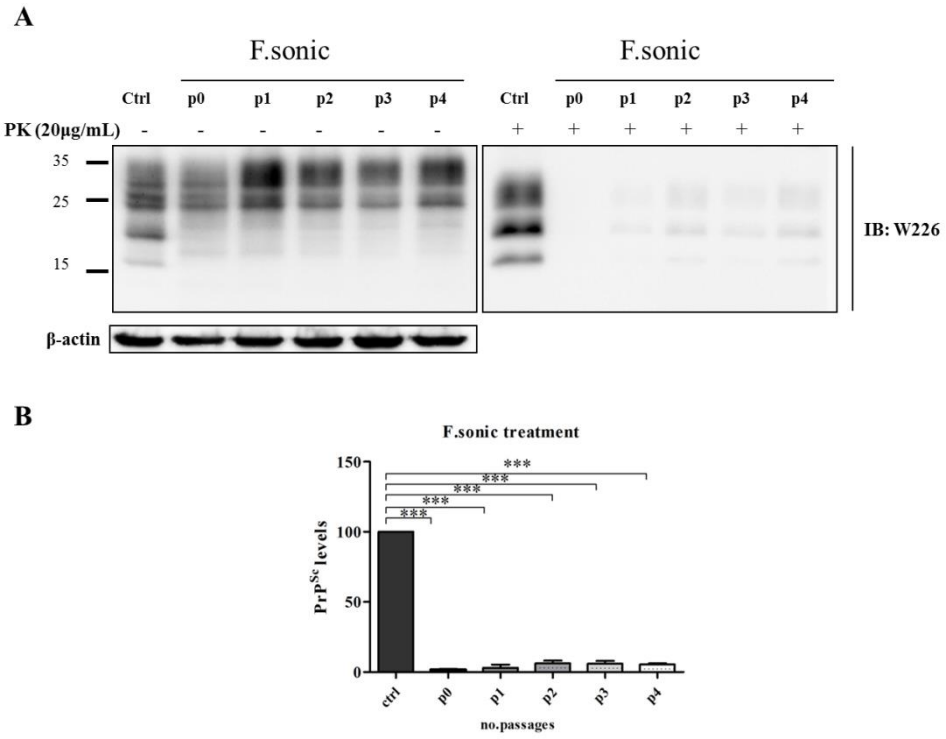

Figure 3.2.12. Western blot analysis of PK-resistant PrP^{Sc} in ScN2a cell lysates after treatment with sonicated α-syn fibrils (F.sonic) over serial passages. A) The cell lysates were prepared as described in Materials and Methods and analyzed by SDS-PAGE and WB, using W226 anti-PrP antibody. Each line was loaded with 30 µg of total protein for total PrP, whereas for the PK-resistant form analysis 500µg/ml was

digested. **B)** The quantification of three independent experiments is shown in the lower graph. The values are shown as a percentage of PK-resistant form relative to total PrP/actin. β-actin is a loading control. Data are represented as mean±SD. Data were evaluated by unpaired T-test. Statistical analysis is indicated as: * = p < 0.05, ** = p < 0.01, *** = p < 0.001.

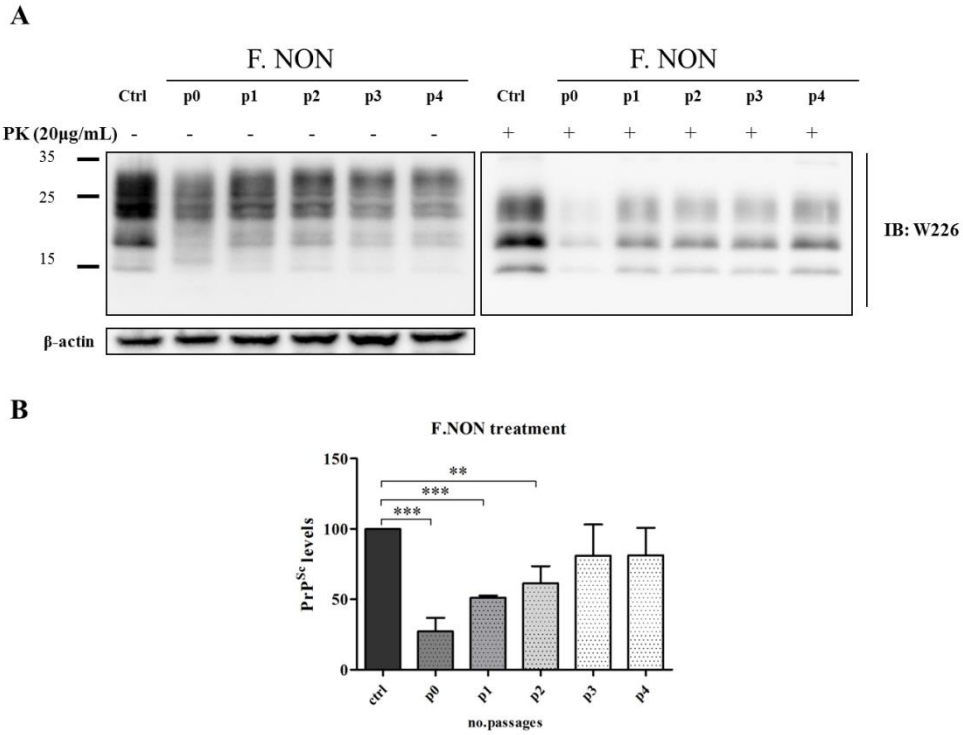

Figure 3.2.13. Western blot analysis of PK-resistant PrP^{Sc} in ScN2a cell lysates after treatment with non-sonicated α-syn fibrils (F.NON) over serial passages. A) The cell lysates were prepared as described in Materials and Methods and analyzed by SDS-PAGE and WB, using W226 anti-PrP antibody. Each line was loaded with 30 µg for total PrP, whereas for the PK-resistant form analysis 500µg/ml was digested. **B)** The quantification of three independent experiments is shown in the lower graph. The values are shown as a percentage of PK-resistant form relative to total PrP/actin. β-actin is a loading control. Data are represented as mean±SD. Data were evaluated by unpaired T-test. Statistical analysis is indicated as: * = p < 0.05, ** = p < 0.01, *** = p < 0.001.

3.2.5 Assessment of different α-syn preparations efficiency to inhibit RML amplification by means of PMCA

In an attempt to analyze whether α-syn preparations were able to inhibit the prion conversion we used the PMCA, an *in vitro* technique that mimics PrP^{C} → PrP^{Sc} conversion process (**Figure 3.2.14 A**). It has been shown that this method features *in vivo* prion replication. Briefly, we performed the experiment using three different ratios of α-syn fibrils and PrP^{C} (1:1, 3:1, and 10:1) and confirmed that the α-syn fibrils inhibit prion conversion at

the first round of cyclic amplification (**Figure 3.2.14. B** upper panel). Control experiments were carried out using a monomeric α-syn or only a PBS buffer (**Figure 3.2.14 C**). At the second round of PMCA the higher concentrations (Ratio 10:1) were still able to inhibit the PrP^{Sc} conversion if compared to both, monomeric α-syn and buffer only (**Figure 3.2.14 B** and **C** lower panel).

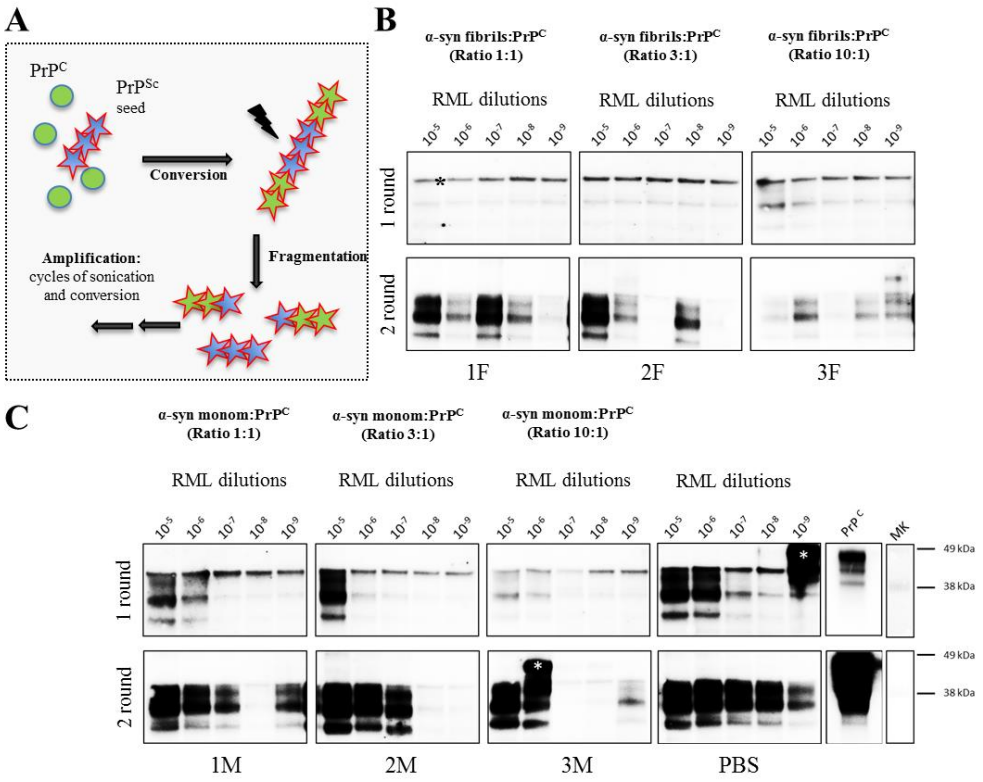

Figure 3.2.14. Effects of α-syn fibrils and monomeric α-syn on cyclic amplification of PrP^{Sc}. A) Schematic illustration of the PMCA method. **B)** The effect of α-syn fibrils on conversion of PrP^{Sc} in two rounds of PMCA show the inhibition effect compared to control conditions where the monomeric α-syn was used or only a buffer **(C)**. The number of cycles of incubation-sonication and the ratios α-syn fibrils : PrP^{C} are indicated. F= α-syn fibrils; M= α-syn monomers; * = unspecific binding (white asterisk: uncomplete PK digestion), MK= marker.

Furthermore, the cell lysates of ScN2a cells treated with α-syn fibrils and sub-cultured four times in α-syn-free medium were used to seed the reaction. Importantly, the membranes were probed with another Ab that recognizes N-terminal part of the prion protein, the 6d11 Ab (epitope aa. 97–100). As indicated in **Figure 3.2.15** the lysates before PMCA amplification presented low signal (upper panel, NO PMCA) indicating that possibly α-syn fibrils could bind the protein in the epitope of W226 Ab (aa. 144-152) as we observed lower signal when the membrane was probed with that Ab. Nevertheless, the lysates over serial

passages were able to amplify in PMCA harboring a PK-resistant signal after the first round of amplification, although, intensity of the bands were lower if compared to control samples (compare upper and lower panels not lanes P0-P4).

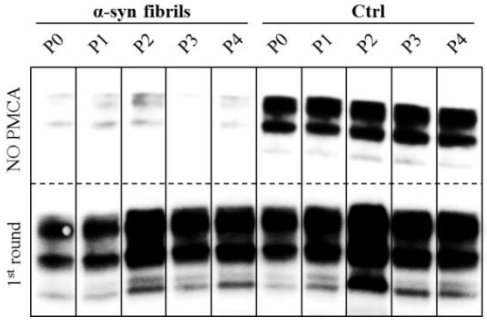

Figure 3.2.15. PMCA analysis of cell lysates from ScN2a cell line treated with α-syn fibrils. Upper panel shows the cell lysates of ScN2a cells treated with F.sonic probed with 6d11 Ab, whereas the lower panel shows that the PrP^{Sc} is still present and is able to catalyze further converion of PK-resistant scrapie form. However, the intensity of bands is lower compared to control lysates indicating lower amount.

3.2.6 Cross-linking experiments

To confirm the effective interaction of PrP^{C} and exogenously added α-syn fibrils in cell culture we pursued to apply *in situ* cross-linking. Previous study identified PrP^{C} in high molecular mass (HMM) complexes together with N-CAM protein, showing the interaction of the two proteins [462] in N2a cells that were cross-linked with formaldehyde (FA). We performed the cross-linking using 1% FA on α-syn treated N2a cells. This mild *in situ* cross-linking revealed the presence of PrP^{C} in HMM complexes (**Figure 3.2.16 A**) as well as α-syn, which was observed when the membrane was probed with an anti-α-syn Ab (**Figure 3.2.16 B**).

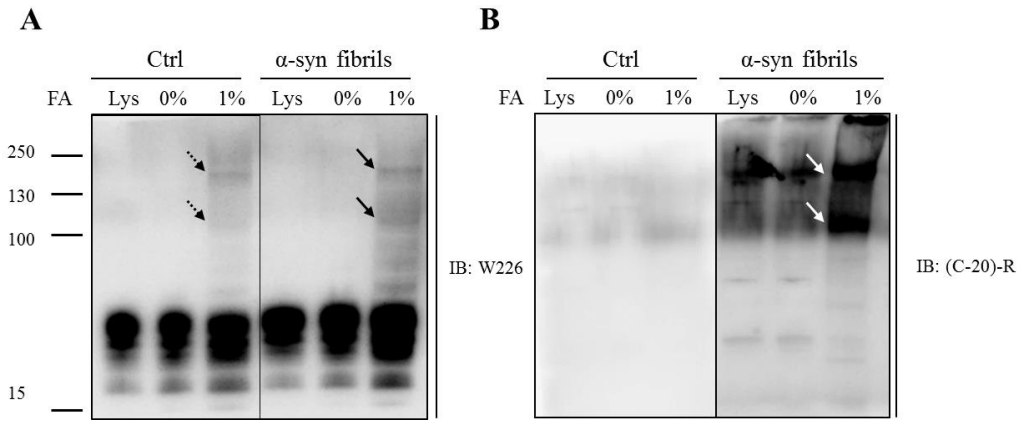

Figure 3.2.16. *In situ* cross-linking of N2a cells treated with α-syn fibrils, using 1% of formaldehyde cross-linker. A) Dashed black arrows indicate the presence of the PrP protein in HMM complexes after *in situ* cross-linking in non-treated N2a cells (Ctrl), whereas the solid black arrow shows the more intense bands in α-syn

treated N2a cells (α-syn fibrils). **B)** When the membrane was probed with the anti-α-syn Ab (C-20)-R bands were co-localizing (solid white arrows) with those probed with anti-PrP Ab W226 (solid black arrows).

To corroborate these data we used a bi-functional protein-protein cross-linking reagent, disuccinimidyl glutarate (DSG). The protocol used for this purpose is described in Material and Methods [443, 444]. This compound is better for cross-linking protein complexes and it forms covalent non reducible amine bonds between lysine residues (note that α-syn contains 15 lysine residues). Similarly to above reported results, after DGS cross-linking the cells that were treated with α-syn fibrils presented HMM complexes when the membranes were immunoblotted with both anti-PrP and anti-α-syn antibodies (**Figure 3.2.17 A, B**). Important of note is that in both, FA and DSG cross-linked samples, bands were present at ~100kDa and above 130 kDa (~180 kDa). Most interestingly in DSG cross-linked samples the F.sonic band (immunoblotted with C-20-R) was more intense if compared to all other bands, indicating that probably the sonicated short amyloid fibrils bind to PrP^C protein a more efficient manner.

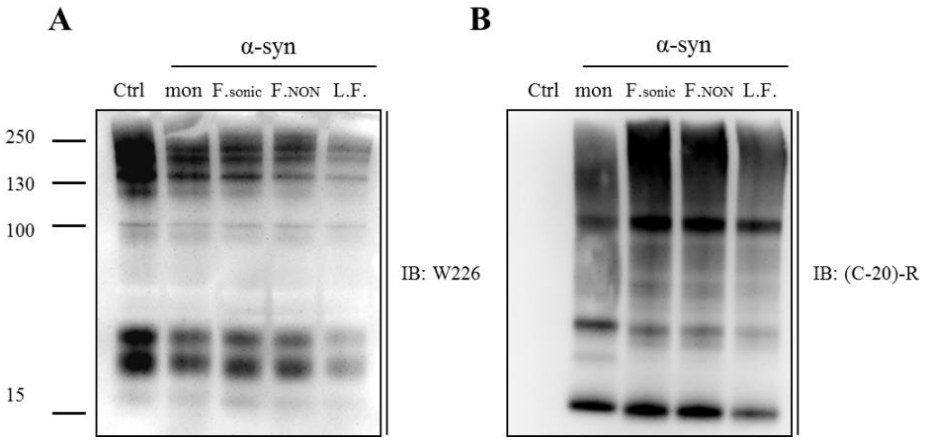

Figure 3.2.17. *In situ* cross-linking of N2a cells treated with α-syn fibrils, using 1mM disuccinimidyl glutarate cross-linker. A) Immunodetection of cross-linked samples that were treated with diverse α-syn preparations (mon=monomeric α-syn, F.sonic=sonicated α-syn fibrils, F.NON=non sonicated α-syn fibrils, and L.F.=long α-syn fibrils that were sonicated) with anti-PrP Ab W226; **B)** immunoblotting of DSG cross-linked samples with anti-α-syn Ab (C-20)-R.

3.2.7. *In vivo* experiments

To investigate whether these *in vitro* findings are evident *in vivo* we performed unilateral inoculation of α-syn fibrils into the SN of female FVB *Prnp* $^{+/+}$ (WT mice) and FVB *Prnp*$^{0/0}$ mice (KO mice).

Luk et al. reported DA neuronal loss and motor dysfunction (by Rotarod test and wire hang test) in WT mice injected with mouse α-syn fibrils at 6 months after inoculation into

striatum [78]. In contrast, our fibril-injected mice did not show motor or cognitive dysfunctions compared to control mice at different time points after injection (3 and 15 mpi). The different phenotypes of these mice might be explained by differences in the injection sites [striatum in Luk et al. and SN in our study]. However our data are in accordance with findings reported by Masuda-Suzukake and co-workers [76].

The induction and spreading of α-syn inclusions were examined with immunohistochemistry at 9 months after α-syn fibril inoculation within SN. Preliminary IHC analysis of two randomly chosen mice revealed that PK-resistant α-syn inclusions were present in higher amount in WT mice injected with α-syn fibrils, whereas the KO injected mice had lower number of aggregates after PK-digestion (**Figure 3.2.18**). However, in KO mice injection into SN induced α-syn pathology mainly in SN, hippocampus and amygdala, while WT mice accumulated high quantities of α-syn inclusions in wide range of cortex, striatum and thalamus.

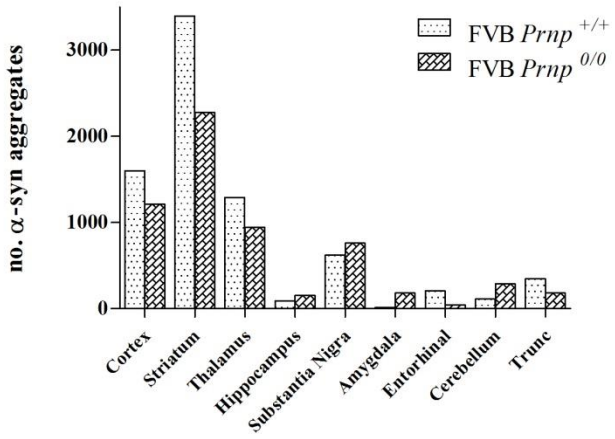

Figure 3.2.18. Accumulation of PK-resistant α-syn pathology in the brain of mice injected with α-syn fibrils. Quantification analysis of PK-resistant α-syn deposits, nine months after injection of mouse α-syn fibrils in mice, showed major accumulation of PK-resistant mouse α-syn in WT mice compared to KO injected mice. The distribution of aggregates was significantly different among PrP expressing mice and those where the expression of PrP protein was abolished.

The main characteristic of the LBs in α-synucleinopathies is the presence of α-syn that is phosphorylated at Serine 129 (p-Ser129). To investigate whether the α-syn aggregates that we observed in FVB-injected mice had LB/LN-like characteristics we performed staining with anti p-Ser129 Ab. Indeed, immunofluorescence analysis revealed that in WT α-syn injected

mice hyperphosphorylated α-syn lesions were detected throughout the CNS in neurites and in soma (**Figure 3.2.19**).

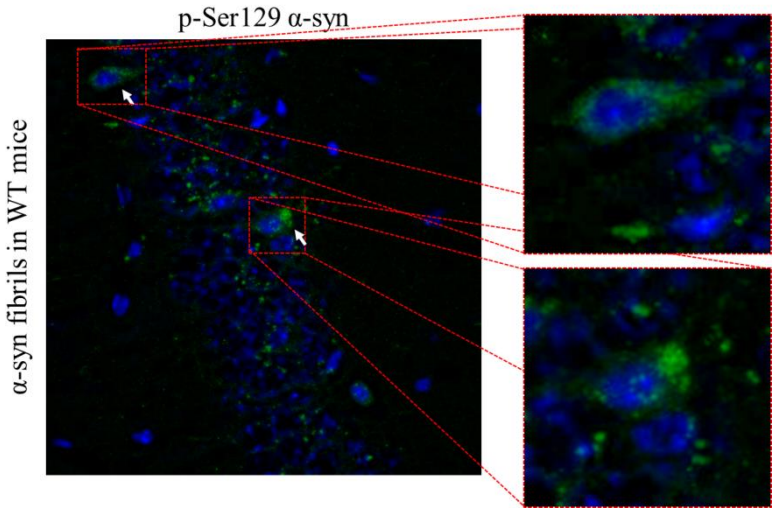

Figure 3.2.19. Immunofluorescence analysis of α-syn fibrils injected WT mice. The immunofluorescence with an anti-phospho-Ser129 α-syn Ab confirmed the presence of hyperphosphorylated α-syn inclusions (in green) in WT brains. Blue is the DAPI.

In conclusion, our preliminary *in vivo* data show that a single inoculation of recombinant α-syn fibrils (F.sonic) is sufficient to induce widespread CNS α-syn pathology in WT mice and in lesser extent in KO FVB mice. Despite the unilateral injection of α-syn fibrils, PK-resistant α-syn pathology appeared bilaterally, though it was more abundant on the injection side. These results suggest that PK-resistant α-syn does not spread by simple diffusion and the propensity to accumulate α-syn seems to differ among brain regions (most probably dependent on the expression levels of both, α-syn and PrP^{C}). As Masuda-Suzukake et al. reported induction of α-syn pathology in WT mice is time and brain region-dependent [76]. Although the mechanism remains to be clarified, exogenous α-syn fibrils may enter cells through a selective mechanism(s), i.e. mediated by PrP^{C}. Alternatively, differences in expression levels of endogenous α-syn or cellular environments (expression of the PrP^{C}) may also be important for formation of the pathology.

CHAPTER IV

Discussion and conclusion

In the first part of this Thesis we discussed whether the α-syn protein had analogous characteristics to the prion protein. Indeed, we showed that also α-syn, a small cytosolic protein, is able to behave as a prion-like protein when is in its β-sheet enriched conformation. On a molecular level, a prion-like protein is often defined as a pathologically misfolded protein that can impart its misfold onto a neighboring native protein through physical interaction, thus providing more template for subsequent conversion. In accordance with this definition we showed here that, when neuroblastoma SH-SY5Y cells are exposed to short α-syn amyloid preparation, accumulation of endogenous α-syn protein is observed. Moreover, overexpression of soluble protein is not necessary to obtain this effect (aggregates appear at p4 in WT SH-SY5Y cells) although the effect is observed earlier when the protein is overexpressed (accumulation appears already at p1 in SH-SY5Y overexpressing soluble α-syn).

Furthermore, in CD-1 WT mice intracerebral injections of recombinant human α-syn amyloids triggered accumulation of phosphorylated α-syn, a hallmark of PD. Pathological α-syn spread occur along major CNS pathways to regions, such as amygdala, striatum, cerebral cortex, far from injection site (SN), showing that spreading process was not casual but it followed a prion-like propagation.

In conclusion, in the **Part I** we show that recombinant human α-syn can adopt a conformation that is able to recruit soluble native α-syn in WT cell lines and convert it, regardless of the species, into molecular assemblies that replicate and accumulate *in vitro*. This event is paralleled by the introduction of post-translational modifications such as phosphorylation at Ser129, a hallmark of pathological α-syn.

Several evidence reported in **Part II** led us speculate that the cellular prion protein might mediate the uptake of α-syn fibrils leading to the major pathology expansion. As proteomic and genome-wide association studies are making unexpected links between different neurodegenerative disorders, suggesting that the pathological process underlying these diseases may join on a few molecular hubs, emerging evidence indicate that PrP^{C} might be one of such hubs. PrP^{C} might act as a transducer of neurotoxicity of various pathogenic protein aggregates. As Iraci and colleagues [420] reported that understanding the physiological role of PrP^{C} protein, the molecular interaction of different PrP^{C} domains with pathogenic aggregates might shed light on the neurotoxic processes that are involved in different neurodegeneration disorders.

In this study the role of the cellular prion protein in binding α-syn amyloids was examined as a possible novel function for PrP^{C}. The obtained results suggest that the cellular prion protein might bind α-syn amyloids (typical of PD). Indeed, our strategy to use cell culture that express cellular prion protein (N2a cells) and those that do not (N2a KO cells) suggested that PrP^{C} might mediate the uptake of α-syn amyloids.

On the other hand, treatment of scrapie infected cells (ScN2a) revealed a complete abolishment of PrP^{Sc} levels. Similar experiments were performed by Peretz et al. using recombinant antibody antigen-binding fragments (Fabs) to prevent PrP^{C} conversion in the same cell line that we used in our study (ScN2a). They observed a direct relationship between the Ab binding to surface PrP^{C} and the inhibition of PrP^{Sc} formation. The authors suggested that Ab acted by promoting binding of PrP^{C} to remove the substrate required for PrP^{Sc} production. Thus, they propose that the presence of Abs or other agents might reduce the formation of nascent PrP^{Sc} molecules, and that at each round of cell division the effective PrP^{Sc} concentration gets diluted.

We observed similar findings with sonicated α-syn preparations, where the treatment for four days lowered the PrP^{Sc} level in cell culture, while the α-syn fibrils that were not sonicated (F.NON) did so, but to a lesser extent. Most importantly this effect was perceived after a removal of α-syn preparation from cell culture and cells were cultured in α-syn-free medium for subsequent four passages. We speculate here that the sonicated α-syn fibrils bind to surface PrP^{C} abolishing the substrate required for PrP^{Sc} production. Most probably the fragmentation induced by sonication led to the formation of smaller α-syn particles that were able to interact with the cellular prion protein.

Following *in vivo* inoculations in FVB WT and KO mice support what we observed *in vitro*, in N2a and N2a KO cell lines. We showed that the intracerebral injection of synthetic α-syn fibrils induce α-syn pathology within the brain much efficiently in animals that express cellular prion protein, like observed *in vitro* in N2a cell lines. Several independent studies showed the accumulation of α-syn pathology after intracerebral inoculation of synthetic α-syn fibrils in WT mice [76, 78], and in transgenic mice [81, 82, 89]. However, the mechanisms through which exogenously injected fibrils enter within the cells and through which insoluble α-syn is transported to other neurons remain unknown. In this study we showed that the spreading of pathology to more distal brain regions occurs less efficiently in mice that do not express cellular prion protein compared to WT animals. On the contrary, the lack of PrP^C expression implies major pathology in site of injection (SN) and closer areas such as hippocampus and amygdala.

Therefore, the potential function of PrP^C in binding and mediating cell-to-cell spread of α-syn amyloids offers an intriguing new function of PrP^C and opens a very interesting field of research. Apart from opening new avenues in PD and prion research, identification of such a receptor provides a potentially valuable target for pharmacological intervention.

References

1. Jucker, M. and L.C. Walker, *Self-propagation of pathogenic protein aggregates in neurodegenerative diseases.* Nature, 2013. **501**(7465): p. 45-51.
2. Guo, J.L. and V.M. Lee, *Cell-to-cell transmission of pathogenic proteins in neurodegenerative diseases.* Nat Med, 2014. **20**(2): p. 130-8.
3. Holtzman, D.M., J.C. Morris, and A.M. Goate, *Alzheimer's disease: the challenge of the second century.* Sci Transl Med, 2011. **3**(77): p. 77sr1.
4. Nelson, P.T., et al., *Correlation of Alzheimer disease neuropathologic changes with cognitive status: a review of the literature.* J Neuropathol Exp Neurol, 2012. **71**(5): p. 362-81.
5. Serpell, L.C. and J.M. Smith, *Direct visualisation of the beta-sheet structure of synthetic Alzheimer's amyloid.* J Mol Biol, 2000. **299**(1): p. 225-31.
6. Rossor, M.N., et al., *Alzheimer's disease families with amyloid precursor protein mutations.* Ann N Y Acad Sci, 1993. **695**: p. 198-202.
7. Zhang, S., et al., *Association between variant amyloid deposits and motor deficits in FAD-associated presenilin-1 mutations: A systematic review.* Neurosci Biobehav Rev, 2015.
8. Baker, H.F., et al., *Evidence for the experimental transmission of cerebral beta-amyloidosis to primates.* Int J Exp Pathol, 1993. **74**(5): p. 441-54.
9. Fritschi, S.K., et al., *Abeta seeds resist inactivation by formaldehyde.* Acta Neuropathol, 2014. **128**(4): p. 477-84.
10. Stohr, J., et al., *Purified and synthetic Alzheimer's amyloid beta (Abeta) prions.* Proc Natl Acad Sci U S A, 2012. **109**(27): p. 11025-30.
11. Stohr, J., et al., *Distinct synthetic Abeta prion strains producing different amyloid deposits in bigenic mice.* Proc Natl Acad Sci U S A, 2014.
12. Mehta, A.K., et al., *Context dependence of protein misfolding and structural strains in neurodegenerative diseases.* Biopolymers, 2013. **100**(6): p. 722-30.
13. Meinhardt, J., et al., *Abeta(1-40) fibril polymorphism implies diverse interaction patterns in amyloid fibrils.* J Mol Biol, 2009. **386**(3): p. 869-77.
14. Nilsson, K.P., et al., *Imaging distinct conformational states of amyloid-beta fibrils in Alzheimer's disease using novel luminescent probes.* ACS Chem Biol, 2007. **2**(8): p. 553-60.
15. Paravastu, A.K., et al., *Molecular structural basis for polymorphism in Alzheimer's beta-amyloid fibrils.* Proc Natl Acad Sci U S A, 2008. **105**(47): p. 18349-54.
16. Paravastu, A.K., et al., *Seeded growth of beta-amyloid fibrils from Alzheimer's brain-derived fibrils produces a distinct fibril structure.* Proc Natl Acad Sci U S A, 2009. **106**(18): p. 7443-8.
17. Petkova, A.T., et al., *Self-propagating, molecular-level polymorphism in Alzheimer's beta-amyloid fibrils.* Science, 2005. **307**(5707): p. 262-5.
18. Heilbronner, G., et al., *Seeded strain-like transmission of beta-amyloid morphotypes in APP transgenic mice.* EMBO Rep, 2013. **14**(11): p. 1017-22.
19. Lu, J.X., et al., *Molecular structure of beta-amyloid fibrils in Alzheimer's disease brain tissue.* Cell, 2013. **154**(6): p. 1257-68.
20. Meyer-Luehmann, M., et al., *Exogenous induction of cerebral beta-amyloidogenesis is governed by agent and host.* Science, 2006. **313**(5794): p. 1781-4.
21. Rosen, R.F., et al., *Deficient high-affinity binding of Pittsburgh compound B in a case of Alzheimer's disease.* Acta Neuropathol, 2010. **119**(2): p. 221-33.
22. Rosen, R.F., L.C. Walker, and H. Levine, 3rd, *PIB binding in aged primate brain: enrichment of high-affinity sites in humans with Alzheimer's disease.* Neurobiol Aging, 2011. **32**(2): p. 223-34.
23. Goedert, M., et al., *Tau proteins of Alzheimer paired helical filaments: abnormal phosphorylation of all six brain isoforms.* Neuron, 1992. **8**(1): p. 159-68.
24. Goedert, M., et al., *Multiple isoforms of human microtubule-associated protein tau: sequences and localization in neurofibrillary tangles of Alzheimer's disease.* Neuron, 1989. **3**(4): p. 519-26.

25. Gomez-Isla, T., et al., *Profound loss of layer II entorhinal cortex neurons occurs in very mild Alzheimer's disease.* J Neurosci, 1996. **16**(14): p. 4491-500.
26. Braak, H. and E. Braak, *Neuropathological stageing of Alzheimer-related changes.* Acta Neuropathol, 1991. **82**(4): p. 239-59.
27. Hyman, B.T., et al., *Alzheimer's disease: cell-specific pathology isolates the hippocampal formation.* Science, 1984. **225**(4667): p. 1168-70.
28. de Calignon, A., et al., *Propagation of tau pathology in a model of early Alzheimer's disease.* Neuron, 2012. **73**(4): p. 685-97.
29. Liu, L., et al., *Trans-synaptic spread of tau pathology in vivo.* PLoS One, 2012. **7**(2): p. e31302.
30. Lee, V.M., M. Goedert, and J.Q. Trojanowski, *Neurodegenerative tauopathies.* Annu Rev Neurosci, 2001. **24**: p. 1121-59.
31. Sanders, D.W., et al., *Distinct tau prion strains propagate in cells and mice and define different tauopathies.* Neuron, 2014. **82**(6): p. 1271-88.
32. Boluda, S., et al., *Differential induction and spread of tau pathology in young PS19 tau transgenic mice following intracerebral injections of pathological tau from Alzheimer's disease or corticobasal degeneration brains.* Acta Neuropathol, 2015. **129**(2): p. 221-37.
33. Clavaguera, F., et al., *Brain homogenates from human tauopathies induce tau inclusions in mouse brain.* Proc Natl Acad Sci U S A, 2013. **110**(23): p. 9535-40.
34. Cleveland, D.W., S.Y. Hwo, and M.W. Kirschner, *Physical and chemical properties of purified tau factor and the role of tau in microtubule assembly.* J Mol Biol, 1977. **116**(2): p. 227-47.
35. Frost, B., R.L. Jacks, and M.I. Diamond, *Propagation of tau misfolding from the outside to the inside of a cell.* J Biol Chem, 2009. **284**(19): p. 12845-52.
36. Nonaka, T., et al., *Seeded aggregation and toxicity of {alpha}-synuclein and tau: cellular models of neurodegenerative diseases.* J Biol Chem, 2010. **285**(45): p. 34885-98.
37. Guo, J.L. and V.M. Lee, *Seeding of normal Tau by pathological Tau conformers drives pathogenesis of Alzheimer-like tangles.* J Biol Chem, 2011. **286**(17): p. 15317-31.
38. Iba, M., et al., *Synthetic tau fibrils mediate transmission of neurofibrillary tangles in a transgenic mouse model of Alzheimer's-like tauopathy.* J Neurosci, 2013. **33**(3): p. 1024-37.
39. Guo, J.L. and V.M. Lee, *Neurofibrillary tangle-like tau pathology induced by synthetic tau fibrils in primary neurons over-expressing mutant tau.* FEBS Lett, 2013. **587**(6): p. 717-23.
40. Falcon, B., et al., *Conformation determines the seeding potencies of native and recombinant Tau aggregates.* J Biol Chem, 2015. **290**(2): p. 1049-65.
41. Recchia, A., et al., *Alpha-synuclein and Parkinson's disease.* FASEB J, 2004. **18**(6): p. 617-26.
42. Polymeropoulos, M.H., et al., *Mutation in the alpha-synuclein gene identified in families with Parkinson's disease.* Science, 1997. **276**(5321): p. 2045-7.
43. Kruger, R., et al., *Ala30Pro mutation in the gene encoding alpha-synuclein in Parkinson's disease.* Nat Genet, 1998. **18**(2): p. 106-8.
44. Zarranz, J.J., et al., *The new mutation, E46K, of alpha-synuclein causes Parkinson and Lewy body dementia.* Ann Neurol, 2004. **55**(2): p. 164-73.
45. Appel-Cresswell, S., et al., *Alpha-synuclein p.H50Q, a novel pathogenic mutation for Parkinson's disease.* Mov Disord, 2013. **28**(6): p. 811-3.
46. Olanow, C.W. and W.G. Tatton, *Etiology and pathogenesis of Parkinson's disease.* Annu Rev Neurosci, 1999. **22**: p. 123-44.
47. Langston, J.W. and P.A. Ballard, Jr., *Parkinson's disease in a chemist working with 1-methyl-4-phenyl-1,2,5,6-tetrahydropyridine.* N Engl J Med, 1983. **309**(5): p. 310.
48. Spillantini, M.G., et al., *Alpha-synuclein in Lewy bodies.* Nature, 1997. **388**(6645): p. 839-40.
49. Spillantini, M.G., et al., *alpha-Synuclein in filamentous inclusions of Lewy bodies from Parkinson's disease and dementia with lewy bodies.* Proc Natl Acad Sci U S A, 1998. **95**(11): p. 6469-73.
50. Braak, H., et al., *Staging of brain pathology related to sporadic Parkinson's disease.* Neurobiol Aging, 2003. **24**(2): p. 197-211.

51. Braak, H., et al., *Idiopathic Parkinson's disease: possible routes by which vulnerable neuronal types may be subject to neuroinvasion by an unknown pathogen.* J Neural Transm, 2003. **110**(5): p. 517-36.
52. Braak, H., et al., *Cognitive status correlates with neuropathologic stage in Parkinson disease.* Neurology, 2005. **64**(8): p. 1404-10.
53. O'Sullivan, S.S., et al., *Nonmotor symptoms as presenting complaints in Parkinson's disease: a clinicopathological study.* Mov Disord, 2008. **23**(1): p. 101-6.
54. Li, J.Y., et al., *Lewy bodies in grafted neurons in subjects with Parkinson's disease suggest host-to-graft disease propagation.* Nat Med, 2008. **14**(5): p. 501-3.
55. Kordower, J.H., et al., *Lewy body-like pathology in long-term embryonic nigral transplants in Parkinson's disease.* Nat Med, 2008. **14**(5): p. 504-6.
56. Kordower, J.H., et al., *Transplanted dopaminergic neurons develop PD pathologic changes: a second case report.* Mov Disord, 2008. **23**(16): p. 2303-6.
57. Lennox, G., et al., *Diffuse Lewy body disease: correlative neuropathology using anti-ubiquitin immunocytochemistry.* J Neurol Neurosurg Psychiatry, 1989. **52**(11): p. 1236-47.
58. Fujiwara, H., et al., *alpha-Synuclein is phosphorylated in synucleinopathy lesions.* Nat Cell Biol, 2002. **4**(2): p. 160-4.
59. Serpell, L.C., et al., *Fiber diffraction of synthetic alpha-synuclein filaments shows amyloid-like cross-beta conformation.* Proc Natl Acad Sci U S A, 2000. **97**(9): p. 4897-902.
60. Crowther, R.A., S.E. Daniel, and M. Goedert, *Characterisation of isolated alpha-synuclein filaments from substantia nigra of Parkinson's disease brain.* Neurosci Lett, 2000. **292**(2): p. 128-30.
61. Biere, A.L., et al., *Parkinson's disease-associated alpha-synuclein is more fibrillogenic than beta- and gamma-synuclein and cannot cross-seed its homologs.* J Biol Chem, 2000. **275**(44): p. 34574-9.
62. Conway, K.A., J.D. Harper, and P.T. Lansbury, *Accelerated in vitro fibril formation by a mutant alpha-synuclein linked to early-onset Parkinson disease.* Nat Med, 1998. **4**(11): p. 1318-20.
63. Uversky, V.N., J. Li, and A.L. Fink, *Evidence for a partially folded intermediate in alpha-synuclein fibril formation.* J Biol Chem, 2001. **276**(14): p. 10737-44.
64. Munishkina, L.A., et al., *Conformational behavior and aggregation of alpha-synuclein in organic solvents: modeling the effects of membranes.* Biochemistry, 2003. **42**(9): p. 2720-30.
65. Munishkina, L.A., et al., *The effect of macromolecular crowding on protein aggregation and amyloid fibril formation.* J Mol Recognit, 2004. **17**(5): p. 456-64.
66. Li, J., V.N. Uversky, and A.L. Fink, *Effect of familial Parkinson's disease point mutations A30P and A53T on the structural properties, aggregation, and fibrillation of human alpha-synuclein.* Biochemistry, 2001. **40**(38): p. 11604-13.
67. Ghosh, D., et al., *The Parkinson's disease-associated H50Q mutation accelerates alpha-Synuclein aggregation in vitro.* Biochemistry, 2013. **52**(40): p. 6925-7.
68. Greenbaum, E.A., et al., *The E46K mutation in alpha-synuclein increases amyloid fibril formation.* J Biol Chem, 2005. **280**(9): p. 7800-7.
69. Conway, K.A., J.D. Harper, and P.T. Lansbury, Jr., *Fibrils formed in vitro from alpha-synuclein and two mutant forms linked to Parkinson's disease are typical amyloid.* Biochemistry, 2000. **39**(10): p. 2552-63.
70. Volles, M.J. and P.T. Lansbury, Jr., *Vesicle permeabilization by protofibrillar alpha-synuclein is sensitive to Parkinson's disease-linked mutations and occurs by a pore-like mechanism.* Biochemistry, 2002. **41**(14): p. 4595-602.
71. Fredenburg, R.A., et al., *The impact of the E46K mutation on the properties of alpha-synuclein in its monomeric and oligomeric states.* Biochemistry, 2007. **46**(24): p. 7107-18.
72. Narhi, L., et al., *Both familial Parkinson's disease mutations accelerate alpha-synuclein aggregation.* J Biol Chem, 1999. **274**(14): p. 9843-6.
73. Yonetani, M., et al., *Conversion of wild-type alpha-synuclein into mutant-type fibrils and its propagation in the presence of A30P mutant.* J Biol Chem, 2009. **284**(12): p. 7940-50.

74. Choi, W., et al., *Mutation E46K increases phospholipid binding and assembly into filaments of human alpha-synuclein.* FEBS Lett, 2004. **576**(3): p. 363-8.
75. Luk, K.C., et al., *Exogenous alpha-synuclein fibrils seed the formation of Lewy body-like intracellular inclusions in cultured cells.* Proc Natl Acad Sci U S A, 2009. **106**(47): p. 20051-6.
76. Masuda-Suzukake, M., et al., *Prion-like spreading of pathological alpha-synuclein in brain.* Brain, 2013. **136**(Pt 4): p. 1128-38.
77. Desplats, P., et al., *Inclusion formation and neuronal cell death through neuron-to-neuron transmission of alpha-synuclein.* Proc Natl Acad Sci U S A, 2009. **106**(31): p. 13010-5.
78. Luk, K.C., et al., *Pathological alpha-synuclein transmission initiates Parkinson-like neurodegeneration in nontransgenic mice.* Science, 2012. **338**(6109): p. 949-53.
79. Volpicelli-Daley, L.A., et al., *Exogenous alpha-synuclein fibrils induce Lewy body pathology leading to synaptic dysfunction and neuron death.* Neuron, 2011. **72**(1): p. 57-71.
80. Sacino, A.N., et al., *Induction of CNS alpha-synuclein pathology by fibrillar and non-amyloidogenic recombinant alpha-synuclein.* Acta Neuropathol Commun, 2013. **1**(1): p. 38.
81. Luk, K.C., et al., *Intracerebral inoculation of pathological alpha-synuclein initiates a rapidly progressive neurodegenerative alpha-synucleinopathy in mice.* J Exp Med, 2012. **209**(5): p. 975-86.
82. Mougenot, A.L., et al., *Prion-like acceleration of a synucleinopathy in a transgenic mouse model.* Neurobiol Aging, 2012. **33**(9): p. 2225-8.
83. Rockenstein, E., et al., *Differential neuropathological alterations in transgenic mice expressing alpha-synuclein from the platelet-derived growth factor and Thy-1 promoters.* J Neurosci Res, 2002. **68**(5): p. 568-78.
84. Chesselet, M.F., et al., *A progressive mouse model of Parkinson's disease: the Thy1-aSyn ("Line 61") mice.* Neurotherapeutics, 2012. **9**(2): p. 297-314.
85. Sacino, A.N., et al., *Brain injection of alpha-synuclein induces multiple proteinopathies, gliosis, and a neuronal injury marker.* J Neurosci, 2014. **34**(37): p. 12368-78.
86. Peelaerts, W., et al., *alpha-Synuclein strains cause distinct synucleinopathies after local and systemic administration.* Nature, 2015. **522**(7556): p. 340-4.
87. Bousset, L., et al., *Structural and functional characterization of two alpha-synuclein strains.* Nat Commun, 2013. **4**: p. 2575.
88. Recasens, A., et al., *Lewy body extracts from Parkinson disease brains trigger alpha-synuclein pathology and neurodegeneration in mice and monkeys.* Ann Neurol, 2014. **75**(3): p. 351-62.
89. Watts, J.C., et al., *Transmission of multiple system atrophy prions to transgenic mice.* Proc Natl Acad Sci U S A, 2013. **110**(48): p. 19555-60.
90. Guo, J.L., et al., *Distinct alpha-synuclein strains differentially promote tau inclusions in neurons.* Cell, 2013. **154**(1): p. 103-17.
91. Haik, S., et al., *Alpha-synuclein-immunoreactive deposits in human and animal prion diseases.* Acta Neuropathol, 2002. **103**(5): p. 516-20.
92. Kovacs, G.G., et al., *Genetic Creutzfeldt-Jakob disease associated with the E200K mutation: characterization of a complex proteinopathy.* Acta Neuropathol, 2011. **121**(1): p. 39-57.
93. Spillantini, M.G., et al., *Filamentous alpha-synuclein inclusions link multiple system atrophy with Parkinson's disease and dementia with Lewy bodies.* Neurosci Lett, 1998. **251**(3): p. 205-8.
94. Cleveland, D.W. and J.D. Rothstein, *From Charcot to Lou Gehrig: deciphering selective motor neuron death in ALS.* Nat Rev Neurosci, 2001. **2**(11): p. 806-19.
95. Elden, A.C., et al., *Ataxin-2 intermediate-length polyglutamine expansions are associated with increased risk for ALS.* Nature, 2010. **466**(7310): p. 1069-75.
96. Deng, H.X., et al., *Mutations in UBQLN2 cause dominant X-linked juvenile and adult-onset ALS and ALS/dementia.* Nature, 2011. **477**(7363): p. 211-5.
97. Wu, C.H., et al., *Mutations in the profilin 1 gene cause familial amyotrophic lateral sclerosis.* Nature, 2012. **488**(7412): p. 499-503.

98. Rakhit, R., et al., *Monomeric Cu,Zn-superoxide dismutase is a common misfolding intermediate in the oxidation models of sporadic and familial amyotrophic lateral sclerosis.* J Biol Chem, 2004. **279**(15): p. 15499-504.
99. Rakhit, R., et al., *Oxidation-induced misfolding and aggregation of superoxide dismutase and its implications for amyotrophic lateral sclerosis.* J Biol Chem, 2002. **277**(49): p. 47551-6.
100. Furukawa, Y., et al., *Complete loss of post-translational modifications triggers fibrillar aggregation of SOD1 in the familial form of amyotrophic lateral sclerosis.* J Biol Chem, 2008. **283**(35): p. 24167-76.
101. Bruijn, L.I., et al., *ALS-linked SOD1 mutant G85R mediates damage to astrocytes and promotes rapidly progressive disease with SOD1-containing inclusions.* Neuron, 1997. **18**(2): p. 327-38.
102. Cleveland, D.W., *From Charcot to SOD1: mechanisms of selective motor neuron death in ALS.* Neuron, 1999. **24**(3): p. 515-20.
103. Chia, R., et al., *Superoxide dismutase 1 and tgSOD1 mouse spinal cord seed fibrils, suggesting a propagative cell death mechanism in amyotrophic lateral sclerosis.* PLoS One, 2010. **5**(5): p. e10627.
104. Prudencio, M., et al., *Variation in aggregation propensities among ALS-associated variants of SOD1: correlation to human disease.* Hum Mol Genet, 2009. **18**(17): p. 3217-26.
105. Wang, J., et al., *Fibrillar inclusions and motor neuron degeneration in transgenic mice expressing superoxide dismutase 1 with a disrupted copper-binding site.* Neurobiol Dis, 2002. **10**(2): p. 128-38.
106. Schwab, C., et al., *Colocalization of transactivation-responsive DNA-binding protein 43 and huntingtin in inclusions of Huntington disease.* J Neuropathol Exp Neurol, 2008. **67**(12): p. 1159-65.
107. Nakashima-Yasuda, H., et al., *Co-morbidity of TDP-43 proteinopathy in Lewy body related diseases.* Acta Neuropathol, 2007. **114**(3): p. 221-9.
108. Amador-Ortiz, C., et al., *TDP-43 immunoreactivity in hippocampal sclerosis and Alzheimer's disease.* Ann Neurol, 2007. **61**(5): p. 435-45.
109. Polymenidou, M., et al., *Long pre-mRNA depletion and RNA missplicing contribute to neuronal vulnerability from loss of TDP-43.* Nat Neurosci, 2011. **14**(4): p. 459-68.
110. Furukawa, Y., et al., *A seeding reaction recapitulates intracellular formation of Sarkosyl-insoluble transactivation response element (TAR) DNA-binding protein-43 inclusions.* J Biol Chem, 2011. **286**(21): p. 18664-72.
111. Guo, W., et al., *An ALS-associated mutation affecting TDP-43 enhances protein aggregation, fibril formation and neurotoxicity.* Nat Struct Mol Biol, 2011. **18**(7): p. 822-30.
112. Johnson, B.S., et al., *TDP-43 is intrinsically aggregation-prone, and amyotrophic lateral sclerosis-linked mutations accelerate aggregation and increase toxicity.* J Biol Chem, 2009. **284**(30): p. 20329-39.
113. Nonaka, T., et al., *Prion-like properties of pathological TDP-43 aggregates from diseased brains.* Cell Rep, 2013. **4**(1): p. 124-34.
114. Aguzzi, A. and L. Rajendran, *The transcellular spread of cytosolic amyloids, prions, and prionoids.* Neuron, 2009. **64**(6): p. 783-90.
115. Hardy, J. and D.J. Selkoe, *The amyloid hypothesis of Alzheimer's disease: progress and problems on the road to therapeutics.* Science, 2002. **297**(5580): p. 353-6.
116. Collins, S.J., V.A. Lawson, and C.L. Masters, *Transmissible spongiform encephalopathies.* Lancet, 2004. **363**(9402): p. 51-61.
117. Budka, H., *Neuropathology of prion diseases.* Br Med Bull, 2003. **66**: p. 121-30.
118. Brown, P., *Reflections on a half-century in the field of transmissible spongiform encephalopathy.* Folia Neuropathol, 2009. **47**(2): p. 95-103.
119. Griffith, J.S., *Self-replication and scrapie.* Nature, 1967. **215**(5105): p. 1043-4.
120. Prusiner, S.B., *Novel proteinaceous infectious particles cause scrapie.* Science, 1982. **216**(4542): p. 136-44.

121. Prusiner, S.B., *Prions.* Proc Natl Acad Sci U S A, 1998. **95**(23): p. 13363-83.
122. Aguzzi, A. and C.J. Sigurdson, *Antiprion immunotherapy: to suppress or to stimulate?* Nat Rev Immunol, 2004. **4**(9): p. 725-36.
123. Legname, G., et al., *Synthetic mammalian prions.* Science, 2004. **305**(5684): p. 673-6.
124. Castilla, J., et al., *In vitro generation of infectious scrapie prions.* Cell, 2005. **121**(2): p. 195-206.
125. Deleault, N.R., et al., *Formation of native prions from minimal components in vitro.* Proc Natl Acad Sci U S A, 2007. **104**(23): p. 9741-6.
126. Wang, F., et al., *Generating a prion with bacterially expressed recombinant prion protein.* Science, 2010. **327**(5969): p. 1132-5.
127. Zhou, Z., et al., *Crowded cell-like environment accelerates the nucleation step of amyloidogenic protein misfolding.* J Biol Chem, 2009. **284**(44): p. 30148-58.
128. Prusiner, S.B., *Molecular biology of prion diseases.* Science, 1991. **252**(5012): p. 1515-22.
129. Jarrett, J.T. and P.T. Lansbury, Jr., *Seeding "one-dimensional crystallization" of amyloid: a pathogenic mechanism in Alzheimer's disease and scrapie?* Cell, 1993. **73**(6): p. 1055-8.
130. Govaerts, C., et al., *Evidence for assembly of prions with left-handed beta-helices into trimers.* Proc Natl Acad Sci U S A, 2004. **101**(22): p. 8342-7.
131. DeMarco, M.L., et al., *Structural properties of prion protein protofibrils and fibrils: an experimental assessment of atomic models.* Biochemistry, 2006. **45**(51): p. 15573-82.
132. DeMarco, M.L. and V. Daggett, *From conversion to aggregation: protofibril formation of the prion protein.* Proc Natl Acad Sci U S A, 2004. **101**(8): p. 2293-8.
133. Colby, D.W. and S.B. Prusiner, *Prions.* Cold Spring Harb Perspect Biol, 2011. **3**(1): p. a006833.
134. Parchi, P., et al., *Molecular basis of phenotypic variability in sporadic Creutzfeldt-Jakob disease.* Ann Neurol, 1996. **39**(6): p. 767-78.
135. Piccardo, P., et al., *Phenotypic variability of Gerstmann-Straussler-Scheinker disease is associated with prion protein heterogeneity.* J Neuropathol Exp Neurol, 1998. **57**(10): p. 979-88.
136. Zhang, L., et al., *Semi-quantitative analysis of alpha-synuclein in subcellular pools of rat brain neurons: an immunogold electron microscopic study using a C-terminal specific monoclonal antibody.* Brain Res, 2008. **1244**: p. 40-52.
137. Maroteaux, L. and R.H. Scheller, *The rat brain synucleins; family of proteins transiently associated with neuronal membrane.* Brain Res Mol Brain Res, 1991. **11**(3-4): p. 335-43.
138. Iwai, A., et al., *The precursor protein of non-A beta component of Alzheimer's disease amyloid is a presynaptic protein of the central nervous system.* Neuron, 1995. **14**(2): p. 467-75.
139. Dickson, D.W., et al., *Widespread alterations of alpha-synuclein in multiple system atrophy.* Am J Pathol, 1999. **155**(4): p. 1241-51.
140. Iwatsubo, T., *Pathological biochemistry of alpha-synucleinopathy.* Neuropathology, 2007. **27**(5): p. 474-8.
141. Jo, E., et al., *alpha-Synuclein membrane interactions and lipid specificity.* J Biol Chem, 2000. **275**(44): p. 34328-34.
142. Zhu, M. and A.L. Fink, *Lipid binding inhibits alpha-synuclein fibril formation.* J Biol Chem, 2003. **278**(19): p. 16873-7.
143. Bisaglia, M., et al., *The 11-mer repeats of human alpha-synuclein in vesicle interactions and lipid composition discrimination: a cooperative role.* Biopolymers, 2006. **84**(3): p. 310-6.
144. Davidson, W.S., et al., *Stabilization of alpha-synuclein secondary structure upon binding to synthetic membranes.* J Biol Chem, 1998. **273**(16): p. 9443-9.
145. Jao, C.C., et al., *Structure of membrane-bound alpha-synuclein studied by site-directed spin labeling.* Proc Natl Acad Sci U S A, 2004. **101**(22): p. 8331-6.
146. Goedert, M., *Filamentous nerve cell inclusions in neurodegenerative diseases: tauopathies and alpha-synucleinopathies.* Philos Trans R Soc Lond B Biol Sci, 1999. **354**(1386): p. 1101-18.
147. Dufty, B.M., et al., *Calpain-cleavage of alpha-synuclein: connecting proteolytic processing to disease-linked aggregation.* Am J Pathol, 2007. **170**(5): p. 1725-38.

148. Chen, L. and M.B. Feany, *Alpha-synuclein phosphorylation controls neurotoxicity and inclusion formation in a Drosophila model of Parkinson disease.* Nat Neurosci, 2005. **8**(5): p. 657-63.
149. Nishie, M., et al., *Accumulation of phosphorylated alpha-synuclein in the brain and peripheral ganglia of patients with multiple system atrophy.* Acta Neuropathol, 2004. **107**(4): p. 292-8.
150. Bartels, T., J.G. Choi, and D.J. Selkoe, *alpha-Synuclein occurs physiologically as a helically folded tetramer that resists aggregation.* Nature, 2011. **477**(7362): p. 107-10.
151. Burre, J., et al., *Properties of native brain alpha-synuclein.* Nature, 2013. **498**(7453): p. E4-6; discussion E6-7.
152. Goncalves, S. and T.F. Outeiro, *Assessing the subcellular dynamics of alpha-synuclein using photoactivation microscopy.* Mol Neurobiol, 2013. **47**(3): p. 1081-92.
153. McLean, P.J., S. Ribich, and B.T. Hyman, *Subcellular localization of alpha-synuclein in primary neuronal cultures: effect of missense mutations.* J Neural Transm Suppl, 2000(58): p. 53-63.
154. Mori, F., et al., *Immunohistochemical comparison of alpha- and beta-synuclein in adult rat central nervous system.* Brain Res, 2002. **941**(1-2): p. 118-26.
155. Greten-Harrison, B., et al., *alphabetagamma-Synuclein triple knockout mice reveal age-dependent neuronal dysfunction.* Proc Natl Acad Sci U S A, 2010. **107**(45): p. 19573-8.
156. Uversky, V.N., et al., *Biophysical properties of the synucleins and their propensities to fibrillate: inhibition of alpha-synuclein assembly by beta- and gamma-synucleins.* J Biol Chem, 2002. **277**(14): p. 11970-8.
157. Park, J.Y. and P.T. Lansbury, Jr., *Beta-synuclein inhibits formation of alpha-synuclein protofibrils: a possible therapeutic strategy against Parkinson's disease.* Biochemistry, 2003. **42**(13): p. 3696-700.
158. Ji, H., et al., *Identification of a breast cancer-specific gene, BCSG1, by direct differential cDNA sequencing.* Cancer Res, 1997. **57**(4): p. 759-64.
159. Lavedan, C., et al., *Identification, localization and characterization of the human gamma-synuclein gene.* Hum Genet, 1998. **103**(1): p. 106-12.
160. Duda, J.E., et al., *The expression of alpha-, beta-, and gamma-synucleins in olfactory mucosa from patients with and without neurodegenerative diseases.* Exp Neurol, 1999. **160**(2): p. 515-22.
161. Buchman, V.L., et al., *Persyn, a member of the synuclein family, has a distinct pattern of expression in the developing nervous system.* J Neurosci, 1998. **18**(22): p. 9335-41.
162. Withers, G.S., et al., *Delayed localization of synelfin (synuclein, NACP) to presynaptic terminals in cultured rat hippocampal neurons.* Brain Res Dev Brain Res, 1997. **99**(1): p. 87-94.
163. Jakes, R., M.G. Spillantini, and M. Goedert, *Identification of two distinct synucleins from human brain.* FEBS Lett, 1994. **345**(1): p. 27-32.
164. Nemani, V.M., et al., *Increased expression of alpha-synuclein reduces neurotransmitter release by inhibiting synaptic vesicle reclustering after endocytosis.* Neuron, 2010. **65**(1): p. 66-79.
165. Fleming, S.M., et al., *Olfactory deficits in mice overexpressing human wildtype alpha-synuclein.* Eur J Neurosci, 2008. **28**(2): p. 247-56.
166. Kuo, Y.M., et al., *Extensive enteric nervous system abnormalities in mice transgenic for artificial chromosomes containing Parkinson disease-associated alpha-synuclein gene mutations precede central nervous system changes.* Hum Mol Genet, 2010. **19**(9): p. 1633-50.
167. Noorian, A.R., et al., *Alpha-synuclein transgenic mice display age-related slowing of gastrointestinal motility associated with transgene expression in the vagal system.* Neurobiol Dis, 2012. **48**(1): p. 9-19.
168. Wang, L., et al., *Abnormal colonic motility in mice overexpressing human wild-type alpha-synuclein.* Neuroreport, 2008. **19**(8): p. 873-6.
169. Lundblad, M., et al., *Impaired neurotransmission caused by overexpression of alpha-synuclein in nigral dopamine neurons.* Proc Natl Acad Sci U S A, 2012. **109**(9): p. 3213-9.

170. Scott, D. and S. Roy, *alpha-Synuclein inhibits intersynaptic vesicle mobility and maintains recycling-pool homeostasis.* J Neurosci, 2012. **32**(30): p. 10129-35.
171. Chandra, S., et al., *Alpha-synuclein cooperates with CSPalpha in preventing neurodegeneration.* Cell, 2005. **123**(3): p. 383-96.
172. Burre, J., et al., *Alpha-synuclein promotes SNARE-complex assembly in vivo and in vitro.* Science, 2010. **329**(5999): p. 1663-7.
173. Payton, J.E., et al., *Protein-protein interactions of alpha-synuclein in brain homogenates and transfected cells.* Brain Res Mol Brain Res, 2001. **95**(1-2): p. 138-45.
174. Dev, K.K., et al., *Part II: alpha-synuclein and its molecular pathophysiological role in neurodegenerative disease.* Neuropharmacology, 2003. **45**(1): p. 14-44.
175. Uversky, V.N., *Alpha-synuclein misfolding and neurodegenerative diseases.* Curr Protein Pept Sci, 2008. **9**(5): p. 507-40.
176. Chen, R.H., et al., *alpha-Synuclein membrane association is regulated by the Rab3a recycling machinery and presynaptic activity.* J Biol Chem, 2013. **288**(11): p. 7438-49.
177. Lee, H.J., et al., *Impairment of microtubule-dependent trafficking by overexpression of alpha-synuclein.* Eur J Neurosci, 2006. **24**(11): p. 3153-62.
178. Okochi, M., et al., *Constitutive phosphorylation of the Parkinson's disease associated alpha-synuclein.* J Biol Chem, 2000. **275**(1): p. 390-7.
179. Bennett, M.K., K.G. Miller, and R.H. Scheller, *Casein kinase II phosphorylates the synaptic vesicle protein p65.* J Neurosci, 1993. **13**(4): p. 1701-7.
180. Gross, S.D., et al., *A phosphatidylinositol 4,5-bisphosphate-sensitive casein kinase I alpha associates with synaptic vesicles and phosphorylates a subset of vesicle proteins.* J Cell Biol, 1995. **130**(3): p. 711-24.
181. Jensen, P.H., et al., *Binding of alpha-synuclein to brain vesicles is abolished by familial Parkinson's disease mutation.* J Biol Chem, 1998. **273**(41): p. 26292-4.
182. Chung, K.K., et al., *Parkin ubiquitinates the alpha-synuclein-interacting protein, synphilin-1: implications for Lewy-body formation in Parkinson disease.* Nat Med, 2001. **7**(10): p. 1144-50.
183. Smith, W.W., et al., *Alpha-synuclein phosphorylation enhances eosinophilic cytoplasmic inclusion formation in SH-SY5Y cells.* J Neurosci, 2005. **25**(23): p. 5544-52.
184. Azeredo da Silveira, S., et al., *Phosphorylation does not prompt, nor prevent, the formation of alpha-synuclein toxic species in a rat model of Parkinson's disease.* Hum Mol Genet, 2009. **18**(5): p. 872-87.
185. Nakamura, T., et al., *Activation of Pyk2/RAFTK induces tyrosine phosphorylation of alpha-synuclein via Src-family kinases.* FEBS Lett, 2002. **521**(1-3): p. 190-4.
186. Chen, L., et al., *Tyrosine and serine phosphorylation of alpha-synuclein have opposing effects on neurotoxicity and soluble oligomer formation.* J Clin Invest, 2009. **119**(11): p. 3257-65.
187. Rott, R., et al., *Monoubiquitylation of alpha-synuclein by seven in absentia homolog (SIAH) promotes its aggregation in dopaminergic cells.* J Biol Chem, 2008. **283**(6): p. 3316-28.
188. Tofaris, G.K., et al., *Ubiquitination of alpha-synuclein in Lewy bodies is a pathological event not associated with impairment of proteasome function.* J Biol Chem, 2003. **278**(45): p. 44405-11.
189. Sakamoto, M., et al., *Progressive accumulation of ubiquitin and disappearance of alpha-synuclein epitope in multiple system atrophy-associated glial cytoplasmic inclusions: triple fluorescence study combined with Gallyas-Braak method.* Acta Neuropathol, 2005. **110**(4): p. 417-25.
190. Hejjaoui, M., et al., *Towards elucidation of the role of ubiquitination in the pathogenesis of Parkinson's disease with semisynthetic ubiquitinated alpha-synuclein.* Angew Chem Int Ed Engl, 2011. **50**(2): p. 405-9.
191. Pountney, D.L., et al., *SUMO-1 marks the nuclear inclusions in familial neuronal intranuclear inclusion disease.* Exp Neurol, 2003. **184**(1): p. 436-46.
192. Pountney, D.L., et al., *SUMO-1 marks subdomains within glial cytoplasmic inclusions of multiple system atrophy.* Neurosci Lett, 2005. **381**(1-2): p. 74-9.

193. Riley, B.E., H.Y. Zoghbi, and H.T. Orr, *SUMOylation of the polyglutamine repeat protein, ataxin-1, is dependent on a functional nuclear localization signal.* J Biol Chem, 2005. **280**(23): p. 21942-8.
194. Shinbo, Y., et al., *Proper SUMO-1 conjugation is essential to DJ-1 to exert its full activities.* Cell Death Differ, 2006. **13**(1): p. 96-108.
195. Steffan, J.S., et al., *SUMO modification of Huntingtin and Huntington's disease pathology.* Science, 2004. **304**(5667): p. 100-4.
196. Ueda, H., et al., *Enhanced SUMOylation in polyglutamine diseases.* Biochem Biophys Res Commun, 2002. **293**(1): p. 307-13.
197. Kataoka, M., et al., *Structural characterization of the molten globule of alpha-lactalbumin by solution X-ray scattering.* Protein Sci, 1997. **6**(2): p. 422-30.
198. Oh, Y., et al., *Human Polycomb protein 2 promotes alpha-synuclein aggregate formation through covalent SUMOylation.* Brain Res, 2011. **1381**: p. 78-89.
199. Herrera, F.E., et al., *Inhibition of alpha-synuclein fibrillization by dopamine is mediated by interactions with five C-terminal residues and with E83 in the NAC region.* PLoS One, 2008. **3**(10): p. e3394.
200. Rekas, A., et al., *The structure of dopamine induced alpha-synuclein oligomers.* Eur Biophys J, 2010. **39**(10): p. 1407-19.
201. Bisaglia, M., et al., *Dopamine quinones interact with alpha-synuclein to form unstructured adducts.* Biochem Biophys Res Commun, 2010. **394**(2): p. 424-8.
202. Giasson, B.I., et al., *Oxidative damage linked to neurodegeneration by selective alpha-synuclein nitration in synucleinopathy lesions.* Science, 2000. **290**(5493): p. 985-9.
203. Norris, E.H., et al., *Effects of oxidative and nitrative challenges on alpha-synuclein fibrillogenesis involve distinct mechanisms of protein modifications.* J Biol Chem, 2003. **278**(29): p. 27230-40.
204. Paxinou, E., et al., *Induction of alpha-synuclein aggregation by intracellular nitrative insult.* J Neurosci, 2001. **21**(20): p. 8053-61.
205. Hodara, R., et al., *Functional consequences of alpha-synuclein tyrosine nitration: diminished binding to lipid vesicles and increased fibril formation.* J Biol Chem, 2004. **279**(46): p. 47746-53.
206. Yamin, G., V.N. Uversky, and A.L. Fink, *Nitration inhibits fibrillation of human alpha-synuclein in vitro by formation of soluble oligomers.* FEBS Lett, 2003. **542**(1-3): p. 147-52.
207. Souza, J.M., et al., *Dityrosine cross-linking promotes formation of stable alpha -synuclein polymers. Implication of nitrative and oxidative stress in the pathogenesis of neurodegenerative synucleinopathies.* J Biol Chem, 2000. **275**(24): p. 18344-9.
208. Conway, K.A., et al., *Kinetic stabilization of the alpha-synuclein protofibril by a dopamine-alpha-synuclein adduct.* Science, 2001. **294**(5545): p. 1346-9.
209. Glaser, C.B., et al., *Methionine oxidation, alpha-synuclein and Parkinson's disease.* Biochim Biophys Acta, 2005. **1703**(2): p. 157-69.
210. Hokenson, M.J., et al., *Role of individual methionines in the fibrillation of methionine-oxidized alpha-synuclein.* Biochemistry, 2004. **43**(15): p. 4621-33.
211. Uversky, V.N., et al., *Methionine oxidation inhibits fibrillation of human alpha-synuclein in vitro.* FEBS Lett, 2002. **517**(1-3): p. 239-44.
212. Yamin, G., et al., *Certain metals trigger fibrillation of methionine-oxidized alpha-synuclein.* J Biol Chem, 2003. **278**(30): p. 27630-5.
213. Zhou, W., et al., *Methionine oxidation stabilizes non-toxic oligomers of alpha-synuclein through strengthening the auto-inhibitory intra-molecular long-range interactions.* Biochim Biophys Acta, 2010. **1802**(3): p. 322-30.
214. Chen, L., et al., *Ribosylation rapidly induces alpha-synuclein to form highly cytotoxic molten globules of advanced glycation end products.* PLoS One, 2010. **5**(2): p. e9052.
215. Padmaraju, V., et al., *Role of advanced glycation on aggregation and DNA binding properties of alpha-synuclein.* J Alzheimers Dis, 2011. **24 Suppl 2**: p. 211-21.

216. Nasstrom, T., et al., *The lipid peroxidation metabolite 4-oxo-2-nonenal cross-links alpha-synuclein causing rapid formation of stable oligomers.* Biochem Biophys Res Commun, 2009. **378**(4): p. 872-6.
217. Esterbauer, H., R.J. Schaur, and H. Zollner, *Chemistry and biochemistry of 4-hydroxynonenal, malonaldehyde and related aldehydes.* Free Radic Biol Med, 1991. **11**(1): p. 81-128.
218. Nasstrom, T., et al., *The lipid peroxidation products 4-oxo-2-nonenal and 4-hydroxy-2-nonenal promote the formation of alpha-synuclein oligomers with distinct biochemical, morphological, and functional properties.* Free Radic Biol Med, 2011. **50**(3): p. 428-37.
219. Qin, Z., et al., *Effect of 4-hydroxy-2-nonenal modification on alpha-synuclein aggregation.* J Biol Chem, 2007. **282**(8): p. 5862-70.
220. Dudek, S.M. and G.V. Johnson, *Transglutaminase catalyzes the formation of sodium dodecyl sulfate-insoluble, Alz-50-reactive polymers of tau.* J Neurochem, 1993. **61**(3): p. 1159-62.
221. Schmid, A.W., et al., *Dissecting the mechanisms of tissue transglutaminase-induced cross-linking of alpha-synuclein: implications for the pathogenesis of Parkinson disease.* J Biol Chem, 2009. **284**(19): p. 13128-42.
222. Segers-Nolten, I.M., et al., *Tissue transglutaminase modulates alpha-synuclein oligomerization.* Protein Sci, 2008. **17**(8): p. 1395-402.
223. Li, J., V.N. Uversky, and A.L. Fink, *Conformational behavior of human alpha-synuclein is modulated by familial Parkinson's disease point mutations A30P and A53T.* Neurotoxicology, 2002. **23**(4-5): p. 553-67.
224. Bussell, R., Jr. and D. Eliezer, *Residual structure and dynamics in Parkinson's disease-associated mutants of alpha-synuclein.* J Biol Chem, 2001. **276**(49): p. 45996-6003.
225. Rospigliosi, C.C., et al., *E46K Parkinson's-linked mutation enhances C-terminal-to-N-terminal contacts in alpha-synuclein.* J Mol Biol, 2009. **388**(5): p. 1022-32.
226. Bertoncini, C.W., et al., *Familial mutants of alpha-synuclein with increased neurotoxicity have a destabilized conformation.* J Biol Chem, 2005. **280**(35): p. 30649-52.
227. Sung, Y.H. and D. Eliezer, *Residual structure, backbone dynamics, and interactions within the synuclein family.* J Mol Biol, 2007. **372**(3): p. 689-707.
228. Conway, K.A., et al., *Acceleration of oligomerization, not fibrillization, is a shared property of both alpha-synuclein mutations linked to early-onset Parkinson's disease: implications for pathogenesis and therapy.* Proc Natl Acad Sci U S A, 2000. **97**(2): p. 571-6.
229. Conway, K.A., et al., *Accelerated oligomerization by Parkinson's disease linked alpha-synuclein mutants.* Ann N Y Acad Sci, 2000. **920**: p. 42-5.
230. Giasson, B.I., et al., *Mutant and wild type human alpha-synucleins assemble into elongated filaments with distinct morphologies in vitro.* J Biol Chem, 1999. **274**(12): p. 7619-22.
231. Lawson, V.A., et al., *Prion protein glycosylation.* J Neurochem, 2005. **93**(4): p. 793-801.
232. Hegde, R.S., et al., *A transmembrane form of the prion protein in neurodegenerative disease.* Science, 1998. **279**(5352): p. 827-34.
233. Stewart, R.S., B. Drisaldi, and D.A. Harris, *A transmembrane form of the prion protein contains an uncleaved signal peptide and is retained in the endoplasmic Reticulum.* Mol Biol Cell, 2001. **12**(4): p. 881-9.
234. Vey, M., et al., *Subcellular colocalization of the cellular and scrapie prion proteins in caveolae-like membranous domains.* Proc Natl Acad Sci U S A, 1996. **93**(25): p. 14945-9.
235. Pan, T., et al., *Cell-surface prion protein interacts with glycosaminoglycans.* Biochem J, 2002. **368**(Pt 1): p. 81-90.
236. Rudd, P.M., et al., *Glycosylation differences between the normal and pathogenic prion protein isoforms.* Proc Natl Acad Sci U S A, 1999. **96**(23): p. 13044-9.
237. DeMarco, M.L. and V. Daggett, *Local environmental effects on the structure of the prion protein.* C R Biol, 2005. **328**(10-11): p. 847-62.
238. Ermonval, M., *Evolving views in prion glycosylation: functional and pathological implications.* Biochimie, 2003. **85**(1-2): p. 33-45.

239. Zuegg, J. and J.E. Gready, *Molecular dynamics simulation of human prion protein including both N-linked oligosaccharides and the GPI anchor.* Glycobiology, 2000. **10**(10): p. 959-74.
240. Hornemann, S., C. Schorn, and K. Wuthrich, *NMR structure of the bovine prion protein isolated from healthy calf brains.* EMBO Rep, 2004. **5**(12): p. 1159-64.
241. Wen, Y., et al., *Unique structural characteristics of the rabbit prion protein.* J Biol Chem, 2010. **285**(41): p. 31682-93.
242. Perez, D.R., F.F. Damberger, and K. Wuthrich, *Horse prion protein NMR structure and comparisons with related variants of the mouse prion protein.* J Mol Biol, 2010. **400**(2): p. 121-8.
243. Christen, B., et al., *NMR structure of the bank vole prion protein at 20 degrees C contains a structured loop of residues 165-171.* J Mol Biol, 2008. **383**(2): p. 306-12.
244. Gossert, A.D., et al., *Prion protein NMR structures of elk and of mouse/elk hybrids.* Proc Natl Acad Sci U S A, 2005. **102**(3): p. 646-50.
245. Calzolai, L., et al., *Prion protein NMR structures of chickens, turtles, and frogs.* Proc Natl Acad Sci U S A, 2005. **102**(3): p. 651-5.
246. Zahn, R., et al., *NMR solution structure of the human prion protein.* Proc Natl Acad Sci U S A, 2000. **97**(1): p. 145-50.
247. Lopez Garcia, F., et al., *NMR structure of the bovine prion protein.* Proc Natl Acad Sci U S A, 2000. **97**(15): p. 8334-9.
248. Calzolai, L., et al., *NMR structures of three single-residue variants of the human prion protein.* Proc Natl Acad Sci U S A, 2000. **97**(15): p. 8340-5.
249. James, T.L., et al., *Solution structure of a 142-residue recombinant prion protein corresponding to the infectious fragment of the scrapie isoform.* Proc Natl Acad Sci U S A, 1997. **94**(19): p. 10086-91.
250. Donne, D.G., et al., *Structure of the recombinant full-length hamster prion protein PrP(29-231): the N terminus is highly flexible.* Proc Natl Acad Sci U S A, 1997. **94**(25): p. 13452-7.
251. Antonyuk, S.V., et al., *Crystal structure of human prion protein bound to a therapeutic antibody.* Proc Natl Acad Sci U S A, 2009. **106**(8): p. 2554-8.
252. Eghiaian, F., et al., *Insight into the PrPC-->PrPSc conversion from the structures of antibody-bound ovine prion scrapie-susceptibility variants.* Proc Natl Acad Sci U S A, 2004. **101**(28): p. 10254-9.
253. Nicolas, O., R. Gavin, and J.A. del Rio, *New insights into cellular prion protein (PrPc) functions: the "ying and yang" of a relevant protein.* Brain Res Rev, 2009. **61**(2): p. 170-84.
254. Prusiner, S.B., et al., *Purification and structural studies of a major scrapie prion protein.* Cell, 1984. **38**(1): p. 127-34.
255. Laplanche, J.L., et al., *Prominent psychiatric features and early onset in an inherited prion disease with a new insertional mutation in the prion protein gene.* Brain, 1999. **122 (Pt 12)**: p. 2375-86.
256. Mead, S., et al., *Inherited prion disease with six octapeptide repeat insertional mutation--molecular analysis of phenotypic heterogeneity.* Brain, 2006. **129**(Pt 9): p. 2297-317.
257. Viles, J.H., M. Klewpatinond, and R.C. Nadal, *Copper and the structural biology of the prion protein.* Biochem Soc Trans, 2008. **36**(Pt 6): p. 1288-92.
258. Jones, C.E., et al., *Preferential Cu2+ coordination by His96 and His111 induces beta-sheet formation in the unstructured amyloidogenic region of the prion protein.* J Biol Chem, 2004. **279**(31): p. 32018-27.
259. Hijazi, N., et al., *Copper binding to PrPC may inhibit prion disease propagation.* Brain Res, 2003. **993**(1-2): p. 192-200.
260. Sigurdsson, E.M., et al., *Copper chelation delays the onset of prion disease.* J Biol Chem, 2003. **278**(47): p. 46199-202.
261. Caughey, B.W., et al., *Secondary structure analysis of the scrapie-associated protein PrP 27-30 in water by infrared spectroscopy.* Biochemistry, 1991. **30**(31): p. 7672-80.

262. Gasset, M., et al., *Perturbation of the secondary structure of the scrapie prion protein under conditions that alter infectivity.* Proc Natl Acad Sci U S A, 1993. **90**(1): p. 1-5.
263. Knaus, K.J., et al., *Crystal structure of the human prion protein reveals a mechanism for oligomerization.* Nat Struct Biol, 2001. **8**(9): p. 770-4.
264. Forloni, G., et al., *Neurotoxicity of a prion protein fragment.* Nature, 1993. **362**(6420): p. 543-6.
265. Norstrom, E.M. and J.A. Mastrianni, *The AGAAAAGA palindrome in PrP is required to generate a productive PrPSc-PrPC complex that leads to prion propagation.* J Biol Chem, 2005. **280**(29): p. 27236-43.
266. Holscher, C., H. Delius, and A. Burkle, *Overexpression of nonconvertible PrPc delta114-121 in scrapie-infected mouse neuroblastoma cells leads to trans-dominant inhibition of wild-type PrP(Sc) accumulation.* J Virol, 1998. **72**(2): p. 1153-9.
267. Chabry, J., B. Caughey, and B. Chesebro, *Specific inhibition of in vitro formation of protease-resistant prion protein by synthetic peptides.* J Biol Chem, 1998. **273**(21): p. 13203-7.
268. Barmada, S., et al., *GFP-tagged prion protein is correctly localized and functionally active in the brains of transgenic mice.* Neurobiol Dis, 2004. **16**(3): p. 527-37.
269. Sales, N., et al., *Cellular prion protein localization in rodent and primate brain.* Eur J Neurosci, 1998. **10**(7): p. 2464-71.
270. Moya, K.L., et al., *Immunolocalization of the cellular prion protein in normal brain.* Microsc Res Tech, 2000. **50**(1): p. 58-65.
271. Herms, J., et al., *Evidence of presynaptic location and function of the prion protein.* J Neurosci, 1999. **19**(20): p. 8866-75.
272. Mironov, A., Jr., et al., *Cytosolic prion protein in neurons.* J Neurosci, 2003. **23**(18): p. 7183-93.
273. Kanaani, J., et al., *Recombinant prion protein induces rapid polarization and development of synapses in embryonic rat hippocampal neurons in vitro.* J Neurochem, 2005. **95**(5): p. 1373-86.
274. Linden, R., et al., *Physiology of the prion protein.* Physiol Rev, 2008. **88**(2): p. 673-728.
275. Ford, M.J., et al., *A marked disparity between the expression of prion protein and its message by neurones of the CNS.* Neuroscience, 2002. **111**(3): p. 533-51.
276. Brown, D.R., et al., *Prion protein expression in muscle cells and toxicity of a prion protein fragment.* Eur J Cell Biol, 1998. **75**(1): p. 29-37.
277. Cashman, N.R., et al., *Cellular isoform of the scrapie agent protein participates in lymphocyte activation.* Cell, 1990. **61**(1): p. 185-92.
278. Dodelet, V.C. and N.R. Cashman, *Prion protein expression in human leukocyte differentiation.* Blood, 1998. **91**(5): p. 1556-61.
279. Durig, J., et al., *Differential constitutive and activation-dependent expression of prion protein in human peripheral blood leucocytes.* Br J Haematol, 2000. **108**(3): p. 488-95.
280. Li, R., et al., *The expression and potential function of cellular prion protein in human lymphocytes.* Cell Immunol, 2001. **207**(1): p. 49-58.
281. Manson, J., et al., *The prion protein gene: a role in mouse embryogenesis?* Development, 1992. **115**(1): p. 117-22.
282. Martinez del Hoyo, G., et al., *Prion protein expression by mouse dendritic cells is restricted to the nonplasmacytoid subsets and correlates with the maturation state.* J Immunol, 2006. **177**(9): p. 6137-42.
283. Rial, D., et al., *Cellular prion protein is present in dopaminergic neurons and modulates the dopaminergic system.* Eur J Neurosci, 2014. **40**(3): p. 2479-86.
284. Weissmann, C. and H. Bueler, *A mouse to remember.* Cell, 2004. **116**(2 Suppl): p. S111-3, 2 p following S113.
285. Bueler, H., et al., *Normal development and behaviour of mice lacking the neuronal cell-surface PrP protein.* Nature, 1992. **356**(6370): p. 577-82.

286. Manson, J.C., et al., *129/Ola mice carrying a null mutation in PrP that abolishes mRNA production are developmentally normal.* Mol Neurobiol, 1994. **8**(2-3): p. 121-7.
287. Sakaguchi, S., et al., *Loss of cerebellar Purkinje cells in aged mice homozygous for a disrupted PrP gene.* Nature, 1996. **380**(6574): p. 528-31.
288. Nishida, N., et al., *A mouse prion protein transgene rescues mice deficient for the prion protein gene from purkinje cell degeneration and demyelination.* Lab Invest, 1999. **79**(6): p. 689-97.
289. Moore, R.C., et al., *Ataxia in prion protein (PrP)-deficient mice is associated with upregulation of the novel PrP-like protein doppel.* J Mol Biol, 1999. **292**(4): p. 797-817.
290. Li, A., et al., *Identification of a novel gene encoding a PrP-like protein expressed as chimeric transcripts fused to PrP exon 1/2 in ataxic mouse line with a disrupted PrP gene.* Cell Mol Neurobiol, 2000. **20**(5): p. 553-67.
291. Hetz, C., K. Maundrell, and C. Soto, *Is loss of function of the prion protein the cause of prion disorders?* Trends Mol Med, 2003. **9**(6): p. 237-43.
292. Roucou, X., M. Gains, and A.C. LeBlanc, *Neuroprotective functions of prion protein.* J Neurosci Res, 2004. **75**(2): p. 153-61.
293. Mehrabian, M., et al., *CRISPR-Cas9-based knockout of the prion protein and its effect on the proteome.* PLoS One, 2014. **9**(12): p. e114594.
294. Dear, D.V., et al., *Effects of post-translational modifications on prion protein aggregation and the propagation of scrapie-like characteristics in vitro.* Biochim Biophys Acta, 2007. **1774**(7): p. 792-802.
295. Chen, S.G., et al., *Truncated forms of the human prion protein in normal brain and in prion diseases.* J Biol Chem, 1995. **270**(32): p. 19173-80.
296. Mange, A., et al., *Alpha- and beta- cleavages of the amino-terminus of the cellular prion protein.* Biol Cell, 2004. **96**(2): p. 125-32.
297. van der Kamp, M.W. and V. Daggett, *The consequences of pathogenic mutations to the human prion protein.* Protein Engineering, Design and Selection, 2009. **22**(8): p. 461-468.
298. Palmer, M.S., et al., *Homozygous prion protein genotype predisposes to sporadic Creutzfeldt-Jakob disease.* Nature, 1991. **352**(6333): p. 340-2.
299. Collinge, J., M.S. Palmer, and A.J. Dryden, *Genetic predisposition to iatrogenic Creutzfeldt-Jakob disease.* Lancet, 1991. **337**(8755): p. 1441-2.
300. Mastrianni, J.A., *The genetics of prion diseases.* Genet Med, 2010. **12**(4): p. 187-95.
301. Apetri, A.C., D.L. Vanik, and W.K. Surewicz, *Polymorphism at residue 129 modulates the conformational conversion of the D178N variant of human prion protein 90-231.* Biochemistry, 2005. **44**(48): p. 15880-8.
302. Swietnicki, W., et al., *Familial mutations and the thermodynamic stability of the recombinant human prion protein.* J Biol Chem, 1998. **273**(47): p. 31048-52.
303. Liemann, S. and R. Glockshuber, *Influence of amino acid substitutions related to inherited human prion diseases on the thermodynamic stability of the cellular prion protein.* Biochemistry, 1999. **38**(11): p. 3258-67.
304. Apetri, A.C., K. Surewicz, and W.K. Surewicz, *The effect of disease-associated mutations on the folding pathway of human prion protein.* J Biol Chem, 2004. **279**(17): p. 18008-14.
305. Parkin, E.T., et al., *Cellular prion protein regulates beta-secretase cleavage of the Alzheimer's amyloid precursor protein.* Proc Natl Acad Sci U S A, 2007. **104**(26): p. 11062-7.
306. Lauren, J., et al., *Cellular prion protein mediates impairment of synaptic plasticity by amyloid-beta oligomers.* Nature, 2009. **457**(7233): p. 1128-32.
307. Kostylev, M.A., et al., *Prion-Protein-interacting Amyloid-beta Oligomers of High Molecular Weight Are Tightly Correlated with Memory Impairment in Multiple Alzheimer Mouse Models.* J Biol Chem, 2015. **290**(28): p. 17415-38.
308. Colby, D.W., et al., *Protease-sensitive synthetic prions.* PLoS Pathog, 2010. **6**(1): p. e1000736.
309. Colby, D.W., et al., *Prion detection by an amyloid seeding assay.* Proc Natl Acad Sci U S A, 2007. **104**(52): p. 20914-9.

310. Baskakov, I.V., et al., *Pathway complexity of prion protein assembly into amyloid.* J Biol Chem, 2002. **277**(24): p. 21140-8.
311. Legname, G., et al., *Continuum of prion protein structures enciphers a multitude of prion isolate-specified phenotypes.* Proc Natl Acad Sci U S A, 2006. **103**(50): p. 19105-10.
312. Barria, M.A., et al., *De novo generation of infectious prions in vitro produces a new disease phenotype.* PLoS Pathog, 2009. **5**(5): p. e1000421.
313. Saa, P., J. Castilla, and C. Soto, *Ultra-efficient replication of infectious prions by automated protein misfolding cyclic amplification.* J Biol Chem, 2006. **281**(46): p. 35245-52.
314. Chen, B., et al., *Estimating prion concentration in fluids and tissues by quantitative PMCA.* Nat Methods, 2010. **7**(7): p. 519-20.
315. Castilla, J., et al., *Protein misfolding cyclic amplification for diagnosis and prion propagation studies.* Methods Enzymol, 2006. **412**: p. 3-21.
316. Herva, M.E., et al., *Anti-amyloid compounds inhibit alpha-synuclein aggregation induced by protein misfolding cyclic amplification (PMCA).* J Biol Chem, 2014. **289**(17): p. 11897-905.
317. Roostaee, A., et al., *Aggregation and neurotoxicity of recombinant alpha-synuclein aggregates initiated by dimerization.* Mol Neurodegener, 2013. **8**: p. 5.
318. Kim, H.J., et al., *Seed-dependent accelerated fibrillation of alpha-synuclein induced by periodic ultrasonication treatment.* J Microbiol Biotechnol, 2007. **17**(12): p. 2027-32.
319. Wilham, J.M., et al., *Rapid end-point quantitation of prion seeding activity with sensitivity comparable to bioassays.* PLoS Pathog, 2010. **6**(12): p. e1001217.
320. Atarashi, R., et al., *Simplified ultrasensitive prion detection by recombinant PrP conversion with shaking.* Nat Methods, 2008. **5**(3): p. 211-2.
321. Orru, C.D., et al., *Human variant Creutzfeldt-Jakob disease and sheep scrapie PrP(res) detection using seeded conversion of recombinant prion protein.* Protein Eng Des Sel, 2009. **22**(8): p. 515-21.
322. Bessen, R.A., et al., *Prion shedding from olfactory neurons into nasal secretions.* PLoS Pathog, 2010. **6**(4): p. e1000837.
323. Nonno, R., et al., *Efficient transmission and characterization of Creutzfeldt-Jakob disease strains in bank voles.* PLoS Pathog, 2006. **2**(2): p. e12.
324. Watts, J.C., et al., *Evidence that bank vole PrP is a universal acceptor for prions.* PLoS Pathog, 2014. **10**(4): p. e1003990.
325. Orru, C.D., et al., *Bank Vole Prion Protein As an Apparently Universal Substrate for RT-QuIC-Based Detection and Discrimination of Prion Strains.* PLoS Pathog, 2015. **11**(6): p. e1004983.
326. Safar, J., et al., *Eight prion strains have PrP(Sc) molecules with different conformations.* Nat Med, 1998. **4**(10): p. 1157-65.
327. Caughey, B., G.J. Raymond, and R.A. Bessen, *Strain-dependent differences in beta-sheet conformations of abnormal prion protein.* J Biol Chem, 1998. **273**(48): p. 32230-5.
328. Aucouturier, P., et al., *Biochemical and conformational variability of human prion strains in sporadic Creutzfeldt-Jakob disease.* Neurosci Lett, 1999. **274**(1): p. 33-6.
329. Bellon, A., et al., *Improved conformation-dependent immunoassay: suitability for human prion detection with enhanced sensitivity.* J Gen Virol, 2003. **84**(Pt 7): p. 1921-5.
330. Jones, E.M. and W.K. Surewicz, *Fibril conformation as the basis of species- and strain-dependent seeding specificity of mammalian prion amyloids.* Cell, 2005. **121**(1): p. 63-72.
331. Telling, G.C., et al., *Evidence for the conformation of the pathologic isoform of the prion protein enciphering and propagating prion diversity.* Science, 1996. **274**(5295): p. 2079-82.
332. Thomzig, A., et al., *Discriminating scrapie and bovine spongiform encephalopathy isolates by infrared spectroscopy of pathological prion protein.* J Biol Chem, 2004. **279**(32): p. 33847-54.
333. Pattison, I.H. and G.C. Millson, *Scrapie produced experimentally in goats with special reference to the clinical syndrome.* J Comp Pathol, 1961. **71**: p. 101-9.
334. Bessen, R.A. and R.F. Marsh, *Identification of two biologically distinct strains of transmissible mink encephalopathy in hamsters.* J Gen Virol, 1992. **73 (Pt 2)**: p. 329-34.
335. Bruce, M.E., *Scrapie strain variation and mutation.* Br Med Bull, 1993. **49**(4): p. 822-38.

336. Fraser, H., *Diversity in the neuropathology of scrapie-like diseases in animals.* Br Med Bull, 1993. **49**(4): p. 792-809.
337. Westaway, D., et al., *Distinct prion proteins in short and long scrapie incubation period mice.* Cell, 1987. **51**(4): p. 651-62.
338. Fraser, H. and A.G. Dickinson, *Scrapie in mice. Agent-strain differences in the distribution and intensity of grey matter vacuolation.* J Comp Pathol, 1973. **83**(1): p. 29-40.
339. Budka, H., et al., *Neuropathological diagnostic criteria for Creutzfeldt-Jakob disease (CJD) and other human spongiform encephalopathies (prion diseases).* Brain Pathol, 1995. **5**(4): p. 459-66.
340. Bessen, R.A. and R.F. Marsh, *Biochemical and physical properties of the prion protein from two strains of the transmissible mink encephalopathy agent.* J Virol, 1992. **66**(4): p. 2096-101.
341. Collinge, J., et al., *Molecular analysis of prion strain variation and the aetiology of 'new variant' CJD.* Nature, 1996. **383**(6602): p. 685-90.
342. Khalili-Shirazi, A., et al., *PrP glycoforms are associated in a strain-specific ratio in native PrPSc.* J Gen Virol, 2005. **86**(Pt 9): p. 2635-44.
343. Kascsak, R.J., et al., *Biochemical differences among scrapie-associated fibrils support the biological diversity of scrapie agents.* J Gen Virol, 1985. **66 (Pt 8)**: p. 1715-22.
344. Chianini, F., et al., *Rabbits are not resistant to prion infection.* Proc Natl Acad Sci U S A, 2012. **109**(13): p. 5080-5.
345. Morales, R., K. Abid, and C. Soto, *The prion strain phenomenon: molecular basis and unprecedented features.* Biochim Biophys Acta, 2007. **1772**(6): p. 681-91.
346. Smith, P.G. and R. Bradley, *Bovine spongiform encephalopathy (BSE) and its epidemiology.* Br Med Bull, 2003. **66**: p. 185-98.
347. Collee, J.G. and R. Bradley, *BSE: a decade on--Part I.* Lancet, 1997. **349**(9052): p. 636-41.
348. Collee, J.G. and R. Bradley, *BSE: a decade on--Part 2.* Lancet, 1997. **349**(9053): p. 715-21.
349. Collinge, J., *Variant Creutzfeldt-Jakob disease.* Lancet, 1999. **354**(9175): p. 317-23.
350. Polymenidou, M., et al., *Coexistence of multiple PrPSc types in individuals with Creutzfeldt-Jakob disease.* Lancet Neurol, 2005. **4**(12): p. 805-14.
351. Yull, H.M., et al., *Detection of type 1 prion protein in variant Creutzfeldt-Jakob disease.* Am J Pathol, 2006. **168**(1): p. 151-7.
352. Casalone, C., et al., *Identification of a second bovine amyloidotic spongiform encephalopathy: molecular similarities with sporadic Creutzfeldt-Jakob disease.* Proc Natl Acad Sci U S A, 2004. **101**(9): p. 3065-70.
353. Legname, G., et al., *Strain-specified characteristics of mouse synthetic prions.* Proc Natl Acad Sci U S A, 2005. **102**(6): p. 2168-73.
354. Ghaemmaghami, S., et al., *Convergent replication of mouse synthetic prion strains.* Am J Pathol, 2013. **182**(3): p. 866-74.
355. Duda, J.E., et al., *Concurrence of alpha-synuclein and tau brain pathology in the Contursi kindred.* Acta Neuropathol, 2002. **104**(1): p. 7-11.
356. Ishizawa, T., et al., *Colocalization of tau and alpha-synuclein epitopes in Lewy bodies.* J Neuropathol Exp Neurol, 2003. **62**(4): p. 389-97.
357. Kotzbauer, P.T., et al., *Fibrillization of alpha-synuclein and tau in familial Parkinson's disease caused by the A53T alpha-synuclein mutation.* Exp Neurol, 2004. **187**(2): p. 279-88.
358. Halliday, G.M., et al., *Neuropathology underlying clinical variability in patients with synucleinopathies.* Acta Neuropathol, 2011. **122**(2): p. 187-204.
359. Watts, J.C., et al., *Serial propagation of distinct strains of Abeta prions from Alzheimer's disease patients.* Proc Natl Acad Sci U S A, 2014.
360. Clavaguera, F., et al., *"Prion-like" templated misfolding in tauopathies.* Brain Pathol, 2013. **23**(3): p. 342-9.
361. Frost, B. and M.I. Diamond, *Prion-like mechanisms in neurodegenerative diseases.* Nat Rev Neurosci, 2010. **11**(3): p. 155-9.

362. Crowther, R.A. and M. Goedert, *Abnormal tau-containing filaments in neurodegenerative diseases.* J Struct Biol, 2000. **130**(2-3): p. 271-9.
363. Prusiner, S.B., *Some speculations about prions, amyloid, and Alzheimer's disease.* N Engl J Med, 1984. **310**(10): p. 661-3.
364. Prusiner, S.B., *Shattuck lecture--neurodegenerative diseases and prions.* N Engl J Med, 2001. **344**(20): p. 1516-26.
365. Aguzzi, A. and A.M. Calella, *Prions: protein aggregation and infectious diseases.* Physiol Rev, 2009. **89**(4): p. 1105-52.
366. Dunning, C.J., S. George, and P. Brundin, *What's to like about the prion-like hypothesis for the spreading of aggregated alpha-synuclein in Parkinson disease?* Prion, 2013. **7**(1): p. 92-7.
367. Bloch, A., et al., *Alpha-synuclein pathology of the spinal and peripheral autonomic nervous system in neurologically unimpaired elderly subjects.* Neuropathol Appl Neurobiol, 2006. **32**(3): p. 284-95.
368. Halliday, G., H. McCann, and C. Shepherd, *Evaluation of the Braak hypothesis: how far can it explain the pathogenesis of Parkinson's disease?* Expert Rev Neurother, 2012. **12**(6): p. 673-86.
369. Dickson, D.W., et al., *Evidence in favor of Braak staging of Parkinson's disease.* Mov Disord, 2010. **25 Suppl 1**: p. S78-82.
370. Burke, R.E., W.T. Dauer, and J.P. Vonsattel, *A critical evaluation of the Braak staging scheme for Parkinson's disease.* Ann Neurol, 2008. **64**(5): p. 485-91.
371. Alafuzoff, I., et al., *Staging/typing of Lewy body related alpha-synuclein pathology: a study of the BrainNet Europe Consortium.* Acta Neuropathol, 2009. **117**(6): p. 635-52.
372. Danzer, K.M., et al., *Different species of alpha-synuclein oligomers induce calcium influx and seeding.* J Neurosci, 2007. **27**(34): p. 9220-32.
373. Sung, J.Y., et al., *Induction of neuronal cell death by Rab5A-dependent endocytosis of alpha-synuclein.* J Biol Chem, 2001. **276**(29): p. 27441-8.
374. Zhang, W., et al., *Aggregated alpha-synuclein activates microglia: a process leading to disease progression in Parkinson's disease.* FASEB J, 2005. **19**(6): p. 533-42.
375. Hansen, C., et al., *alpha-Synuclein propagates from mouse brain to grafted dopaminergic neurons and seeds aggregation in cultured human cells.* J Clin Invest, 2011. **121**(2): p. 715-25.
376. Waxman, E.A. and B.I. Giasson, *A novel, high-efficiency cellular model of fibrillar alpha-synuclein inclusions and the examination of mutations that inhibit amyloid formation.* J Neurochem, 2010. **113**(2): p. 374-88.
377. Colby, D.W., et al., *Design and construction of diverse mammalian prion strains.* Proc Natl Acad Sci U S A, 2009. **106**(48): p. 20417-22.
378. Makarava, N., et al., *Recombinant prion protein induces a new transmissible prion disease in wild-type animals.* Acta Neuropathol, 2010. **119**(2): p. 177-87.
379. Borghi, R., et al., *Full length alpha-synuclein is present in cerebrospinal fluid from Parkinson's disease and normal subjects.* Neurosci Lett, 2000. **287**(1): p. 65-7.
380. El-Agnaf, O.M., et al., *Alpha-synuclein implicated in Parkinson's disease is present in extracellular biological fluids, including human plasma.* FASEB J, 2003. **17**(13): p. 1945-7.
381. Lee, H.J., S. Patel, and S.J. Lee, *Intravesicular localization and exocytosis of alpha-synuclein and its aggregates.* J Neurosci, 2005. **25**(25): p. 6016-24.
382. Nickel, W. and C. Rabouille, *Mechanisms of regulated unconventional protein secretion.* Nat Rev Mol Cell Biol, 2009. **10**(2): p. 148-55.
383. Emmanouilidou, E., et al., *Cell-produced alpha-synuclein is secreted in a calcium-dependent manner by exosomes and impacts neuronal survival.* J Neurosci, 2010. **30**(20): p. 6838-51.
384. Tsigelny, I.F., et al., *Mechanisms of hybrid oligomer formation in the pathogenesis of combined Alzheimer's and Parkinson's diseases.* PLoS One, 2008. **3**(9): p. e3135.
385. Lee, H.J., et al., *Assembly-dependent endocytosis and clearance of extracellular alpha-synuclein.* Int J Biochem Cell Biol, 2008. **40**(9): p. 1835-49.

386. Vella, L.J., et al., *Packaging of prions into exosomes is associated with a novel pathway of PrP processing.* J Pathol, 2007. **211**(5): p. 582-90.
387. Kayed, R., et al., *Permeabilization of lipid bilayers is a common conformation-dependent activity of soluble amyloid oligomers in protein misfolding diseases.* J Biol Chem, 2004. **279**(45): p. 46363-6.
388. Park, J.Y., et al., *On the mechanism of internalization of alpha-synuclein into microglia: roles of ganglioside GM1 and lipid raft.* J Neurochem, 2009. **110**(1): p. 400-11.
389. Hu, X., et al., *Amyloid seeds formed by cellular uptake, concentration, and aggregation of the amyloid-beta peptide.* Proc Natl Acad Sci U S A, 2009. **106**(48): p. 20324-9.
390. Krammer, C., H.M. Schatzl, and I. Vorberg, *Prion-like propagation of cytosolic protein aggregates: insights from cell culture models.* Prion, 2009. **3**(4): p. 206-12.
391. Kfoury, N., et al., *Trans-cellular propagation of Tau aggregation by fibrillar species.* J Biol Chem, 2012. **287**(23): p. 19440-51.
392. Ren, P.H., et al., *Cytoplasmic penetration and persistent infection of mammalian cells by polyglutamine aggregates.* Nat Cell Biol, 2009. **11**(2): p. 219-25.
393. Wu, J.W., et al., *Small misfolded Tau species are internalized via bulk endocytosis and anterogradely and retrogradely transported in neurons.* J Biol Chem, 2013. **288**(3): p. 1856-70.
394. Holmes, B.B., et al., *Heparan sulfate proteoglycans mediate internalization and propagation of specific proteopathic seeds.* Proc Natl Acad Sci U S A, 2013. **110**(33): p. E3138-47.
395. Gousset, K., et al., *Prions hijack tunnelling nanotubes for intercellular spread.* Nat Cell Biol, 2009. **11**(3): p. 328-36.
396. Wang, Y., et al., *Tunneling-nanotube development in astrocytes depends on p53 activation.* Cell Death Differ, 2011. **18**(4): p. 732-42.
397. Ulusoy, A., et al., *Caudo-rostral brain spreading of alpha-synuclein through vagal connections.* EMBO Mol Med, 2013. **5**(7): p. 1051-9.
398. Eisele, Y.S., et al., *Peripherally applied Abeta-containing inoculates induce cerebral beta-amyloidosis.* Science, 2010. **330**(6006): p. 980-2.
399. Kimberlin, R.H. and C.A. Walker, *Pathogenesis of mouse scrapie: effect of route of inoculation on infectivity titres and dose-response curves.* J Comp Pathol, 1978. **88**(1): p. 39-47.
400. Braak, H. and K. Del Tredici, *Neuroanatomy and pathology of sporadic Parkinson's disease.* Adv Anat Embryol Cell Biol, 2009. **201**: p. 1-119.
401. Resenberger, U.K., et al., *The cellular prion protein mediates neurotoxic signalling of beta-sheet-rich conformers independent of prion replication.* EMBO J, 2011. **30**(10): p. 2057-70.
402. Resenberger, U.K., K.F. Winklhofer, and J. Tatzelt, *Cellular prion protein mediates toxic signaling of amyloid beta.* Neurodegener Dis, 2012. **10**(1-4): p. 298-300.
403. Biasini, E. and D.A. Harris, *Targeting the cellular prion protein to treat neurodegeneration.* Future Med Chem, 2012. **4**(13): p. 1655-8.
404. Barry, A.E., et al., *Alzheimer's disease brain-derived amyloid-beta-mediated inhibition of LTP in vivo is prevented by immunotargeting cellular prion protein.* J Neurosci, 2011. **31**(20): p. 7259-63.
405. Chung, E., et al., *Anti-PrPC monoclonal antibody infusion as a novel treatment for cognitive deficits in an Alzheimer's disease model mouse.* BMC Neurosci, 2010. **11**: p. 130.
406. Klyubin, I., et al., *Peripheral administration of a humanized anti-PrP antibody blocks Alzheimer's disease Abeta synaptotoxicity.* J Neurosci, 2014. **34**(18): p. 6140-5.
407. Um, J.W., et al., *Alzheimer amyloid-beta oligomer bound to postsynaptic prion protein activates Fyn to impair neurons.* Nat Neurosci, 2012. **15**(9): p. 1227-35.
408. Balducci, C., et al., *Synthetic amyloid-beta oligomers impair long-term memory independently of cellular prion protein.* Proc Natl Acad Sci U S A, 2010. **107**(5): p. 2295-300.
409. Dohler, F., et al., *High molecular mass assemblies of amyloid-beta oligomers bind prion protein in patients with Alzheimer's disease.* Brain, 2014. **137**(Pt 3): p. 873-86.

410. Beland, M., et al., *Abeta induces its own prion protein N-terminal fragment (PrPN1)-mediated neutralization in amorphous aggregates.* Neurobiol Aging, 2014. **35**(7): p. 1537-48.
411. Chen, S., S.P. Yadav, and W.K. Surewicz, *Interaction between human prion protein and amyloid-beta (Abeta) oligomers: role OF N-terminal residues.* J Biol Chem, 2010. **285**(34): p. 26377-83.
412. Fluharty, B.R., et al., *An N-terminal fragment of the prion protein binds to amyloid-beta oligomers and inhibits their neurotoxicity in vivo.* J Biol Chem, 2013. **288**(11): p. 7857-66.
413. Nicoll, A.J., et al., *Amyloid-beta nanotubes are associated with prion protein-dependent synaptotoxicity.* Nat Commun, 2013. **4**: p. 2416.
414. Nieznanski, K., et al., *Soluble prion protein inhibits amyloid-beta (Abeta) fibrillization and toxicity.* J Biol Chem, 2012. **287**(40): p. 33104-8.
415. Nieznanski, K., et al., *Interaction between prion protein and Abeta amyloid fibrils revisited.* ACS Chem Neurosci, 2014. **5**(5): p. 340-5.
416. Calella, A.M., et al., *Prion protein and Abeta-related synaptic toxicity impairment.* EMBO Mol Med, 2010. **2**(8): p. 306-14.
417. Cisse, M., et al., *Ablation of cellular prion protein does not ameliorate abnormal neural network activity or cognitive dysfunction in the J20 line of human amyloid precursor protein transgenic mice.* J Neurosci, 2011. **31**(29): p. 10427-31.
418. Legname, G., G. Giachin, and F. Benetti, *Structural Studies of Prion Proteins and Prions*, in *Non-fibrillar Amyloidogenic Protein Assemblies - Common Cytotoxins Underlying Degenerative Diseases*, F. Rahimi and G. Bitan, Editors. 2012, Springer Netherlands. p. 289-317.
419. Finder, V.H. and R. Glockshuber, *Amyloid-beta aggregation.* Neurodegener Dis, 2007. **4**(1): p. 13-27.
420. Iraci, N., et al., *DECODING THE FUNCTION OF THE N-TERMINAL TAIL OF THE CELLULAR PRION PROTEIN TO INSPIRE NOVEL THERAPEUTIC AVENUES FOR NEURODEGENERATIVE DISEASES.* Virus Res, 2014.
421. Moroncini, G., et al., *Motif-grafted antibodies containing the replicative interface of cellular PrP are specific for PrPSc.* Proc Natl Acad Sci U S A, 2004. **101**(28): p. 10404-9.
422. Solforosi, L., et al., *Toward molecular dissection of PrPC-PrPSc interactions.* J Biol Chem, 2007. **282**(10): p. 7465-71.
423. Khosravani, H., et al., *Prion protein attenuates excitotoxicity by inhibiting NMDA receptors.* J Cell Biol, 2008. **181**(3): p. 551-65.
424. Wadia, J.S., et al., *Pathologic prion protein infects cells by lipid-raft dependent macropinocytosis.* PLoS One, 2008. **3**(10): p. e3314.
425. Pasupuleti, M., et al., *Antimicrobial activity of human prion protein is mediated by its N-terminal region.* PLoS One, 2009. **4**(10): p. e7358.
426. Sunyach, C., et al., *The mechanism of internalization of glycosylphosphatidylinositol-anchored prion protein.* EMBO J, 2003. **22**(14): p. 3591-601.
427. Taylor, D.R., et al., *Assigning functions to distinct regions of the N-terminus of the prion protein that are involved in its copper-stimulated, clathrin-dependent endocytosis.* J Cell Sci, 2005. **118**(Pt 21): p. 5141-53.
428. Engelender, S., et al., *Synphilin-1 associates with alpha-synuclein and promotes the formation of cytosolic inclusions.* Nat Genet, 1999. **22**(1): p. 110-4.
429. Opazo, F., et al., *Accumulation and clearance of alpha-synuclein aggregates demonstrated by time-lapse imaging.* J Neurochem, 2008. **106**(2): p. 529-40.
430. Tabrizi, S.J., et al., *Expression of mutant alpha-synuclein causes increased susceptibility to dopamine toxicity.* Hum Mol Genet, 2000. **9**(18): p. 2683-9.
431. Danzer, K.M., et al., *Seeding induced by alpha-synuclein oligomers provides evidence for spreading of alpha-synuclein pathology.* J Neurochem, 2009. **111**(1): p. 192-203.
432. Huang, C., et al., *A new method for purification of recombinant human alpha-synuclein in Escherichia coli.* Protein Expr Purif, 2005. **42**(1): p. 173-7.

433. Mellon, P.L., et al., *Immortalization of hypothalamic GnRH neurons by genetically targeted tumorigenesis.* Neuron, 1990. **5**(1): p. 1-10.
434. Biedler, J.L., L. Helson, and B.A. Spengler, *Morphology and growth, tumorigenicity, and cytogenetics of human neuroblastoma cells in continuous culture.* Cancer Res, 1973. **33**(11): p. 2643-52.
435. Latawiec, D., et al., *Modulation of alpha-synuclein aggregation by dopamine analogs.* PLoS One, 2010. **5**(2): p. e9234.
436. Nečas, D. and P. Klapetek, *Gwyddion: An open-source software for SPM data analysis.* Central European Journal of Physics, 2012. **10**(1): p. 181-188.
437. Butler, D.A., et al., *Scrapie-infected murine neuroblastoma cells produce protease-resistant prion proteins.* J Virol, 1988. **62**(5): p. 1558-64.
438. Livak, K.J. and T.D. Schmittgen, *Analysis of relative gene expression data using real-time quantitative PCR and the 2(-Delta Delta C(T)) Method.* Methods, 2001. **25**(4): p. 402-8.
439. Winer, J., et al., *Development and validation of real-time quantitative reverse transcriptase-polymerase chain reaction for monitoring gene expression in cardiac myocytes in vitro.* Anal Biochem, 1999. **270**(1): p. 41-9.
440. Taraboulos, A., D. Serban, and S.B. Prusiner, *Scrapie prion proteins accumulate in the cytoplasm of persistently infected cultured cells.* J Cell Biol, 1990. **110**(6): p. 2117-32.
441. Veith, N.M., et al., *Immunolocalisation of PrPSc in scrapie-infected N2a mouse neuroblastoma cells by light and electron microscopy.* Eur J Cell Biol, 2009. **88**(1): p. 45-63.
442. Morales, R., et al., *Protein misfolding cyclic amplification of infectious prions.* Nat Protoc, 2012. **7**(7): p. 1397-409.
443. Newman, A.J., D. Selkoe, and U. Dettmer, *A new method for quantitative immunoblotting of endogenous alpha-synuclein.* PLoS One, 2013. **8**(11): p. e81314.
444. Aelvoet, S.A., et al., *Noninvasive bioluminescence imaging of alpha-synuclein oligomerization in mouse brain using split firefly luciferase reporters.* J Neurosci, 2014. **34**(49): p. 16518-32.
445. Lee, B.R. and T. Kamitani, *Improved immunodetection of endogenous alpha-synuclein.* PLoS One, 2011. **6**(8): p. e23939.
446. Lledo, P.M., et al., *Mice deficient for prion protein exhibit normal neuronal excitability and synaptic transmission in the hippocampus.* Proc Natl Acad Sci U S A, 1996. **93**(6): p. 2403-7.
447. Schuffler, P.J., et al., *TMARKER: A free software toolkit for histopathological cell counting and staining estimation.* J Pathol Inform, 2013. **4**(Suppl): p. S2.
448. Nazor, K.E., T. Seward, and G.C. Telling, *Motor behavioral and neuropathological deficits in mice deficient for normal prion protein expression.* Biochim Biophys Acta, 2007. **1772**(6): p. 645-53.
449. Cole, N.B. and D.D. Murphy, *The cell biology of alpha-synuclein: a sticky problem?* Neuromolecular Med, 2002. **1**(2): p. 95-109.
450. Sacino, A.N., et al., *Conformational templating of alpha-synuclein aggregates in neuronal-glial cultures.* Mol Neurodegener, 2013. **8**: p. 17.
451. Caughey, B. and P.T. Lansbury, *Protofibrils, pores, fibrils, and neurodegeneration: separating the responsible protein aggregates from the innocent bystanders.* Annu Rev Neurosci, 2003. **26**: p. 267-98.
452. Winner, B., et al., *In vivo demonstration that alpha-synuclein oligomers are toxic.* Proc Natl Acad Sci U S A, 2011. **108**(10): p. 4194-9.
453. Puchtler, H., F.S. Waldrop, and S.N. Meloan, *A review of light, polarization and fluorescence microscopic methods for amyloid.* Appl Pathol, 1985. **3**(1-2): p. 5-17.
454. Schell, H., et al., *Nuclear and neuritic distribution of serine-129 phosphorylated alpha-synuclein in transgenic mice.* Neuroscience, 2009. **160**(4): p. 796-804.
455. Wakamatsu, M., et al., *Accumulation of phosphorylated alpha-synuclein in dopaminergic neurons of transgenic mice that express human alpha-synuclein.* J Neurosci Res, 2007. **85**(8): p. 1819-25.

456. Masuda-Suzukake, M., et al., *Pathological alpha-synuclein propagates through neural networks.* Acta Neuropathol Commun, 2014. **2**: p. 88.
457. Kim, C., et al., *Neuron-released oligomeric alpha-synuclein is an endogenous agonist of TLR2 for paracrine activation of microglia.* Nat Commun, 2013. **4**: p. 1562.
458. Hirsch, E.C. and S. Hunot, *Neuroinflammation in Parkinson's disease: a target for neuroprotection?* Lancet Neurol, 2009. **8**(4): p. 382-97.
459. Graeber, M.B. and W.J. Streit, *Microglia: biology and pathology.* Acta Neuropathol, 2010. **119**(1): p. 89-105.
460. Prusiner, S.B., *Genetic and infectious prion diseases.* Arch Neurol, 1993. **50**(11): p. 1129-53.
461. Dlakic, W.M., E. Grigg, and R.A. Bessen, *Prion infection of muscle cells in vitro.* J Virol, 2007. **81**(9): p. 4615-24.
462. Schmitt-Ulms, G., et al., *Binding of neural cell adhesion molecules (N-CAMs) to the cellular prion protein.* J Mol Biol, 2001. **314**(5): p. 1209-25.
463. Altmeppen, H.C., et al., *Proteolytic processing of the prion protein in health and disease.* Am J Neurodegener Dis, 2012. **1**(1): p. 15-31.
464. Harris, D.A., et al., *Processing of a cellular prion protein: identification of N- and C-terminal cleavage sites.* Biochemistry, 1993. **32**(4): p. 1009-16.
465. Shyng, S.L., M.T. Huber, and D.A. Harris, *A prion protein cycles between the cell surface and an endocytic compartment in cultured neuroblastoma cells.* J Biol Chem, 1993. **268**(21): p. 15922-8.
466. Gasset, M., et al., *Predicted alpha-helical regions of the prion protein when synthesized as peptides form amyloid.* Proc Natl Acad Sci U S A, 1992. **89**(22): p. 10940-4.
467. Tagliavini, F., et al., *Synthetic peptides homologous to prion protein residues 106-147 form amyloid-like fibrils in vitro.* Proc Natl Acad Sci U S A, 1993. **90**(20): p. 9678-82.
468. Westergard, L., J.A. Turnbaugh, and D.A. Harris, *A naturally occurring C-terminal fragment of the prion protein (PrP) delays disease and acts as a dominant-negative inhibitor of PrPSc formation.* J Biol Chem, 2011. **286**(51): p. 44234-42.